nato

RTD TDR-63-3056

RTD
TDR
63-3056

SHOCK-WAVE ATTENUATION IN ELASTIC-RIGID FOAMS

October 1963

TECHNICAL DOCUMENTARY REPORT NO. RTD TDR-63-3056

Research and Technology Division
AIR FORCE WEAPONS LABORATORY
Air Force Systems Command
Kirtland Air Force Base
New Mexico

Project No. 5776, Task No. 577601

(Prepared under Contract AF 29(601)-4363
by John R. Rempel, Poulter Laboratories,
Stanford Research Institute, Menlo Park,
California)

Research and Technology Division
Air Force Systems Command
AIR FORCE WEAPONS LABORATORY
Kirtland Air Force Base
New Mexico

FOREWORD

This report covers work done between 1 July, 1962, and 1 July, 1963, at the Poulter Laboratories, Stanford Research Institute, under the supervision of Dr. G. R. Fowles, as the Institute's Project PGU-3581. Other major contributors were Betty B. Bain, J. G. Berke, J. O. Erkman, Mary M. Grathwol, W. M. Isbell, J. R. Rempel, D. N. Schmidt, and A. C. Wheeler, all of the Poulter Laboratories.

ABSTRACT

Described are experimental techniques for the study of the response of foamed or distended materials to impact loading and the results of applying these techniques to four different kinds of foam -- polyurethane, aluminum, silica, and graphite. An approximate theory for calculating the behavior of elastic-rigid locking solids is developed and applied to the materials tested. Within certain limits agreement with experiment is good, and at least for some materials within a range of impact momenta the internal pressure history can be logically related to measurements of quasi-static compression, although better agreement is possible when certain parameters are measured dynamically.

PUBLICATION REVIEW

This report has been reviewed and is approved.

Winfred E. Mauldin

WINFORD E. MAULDIN
Lt USAF
Project Officer

John J. Neuer

JOHN J. NEUER
Lt Colonel USAF
Chief, Physics Branch

Perry L. Huie

PERRY L. HUIE
Colonel USAF
Chief, Research Division

CONTENTS

ILLUSTRATIONS

ILLUSTRATIONS

ILLUSTRATIONS

TABLES

I INTRODUCTION

A casing of light-weight distended material may be a means of protecting structures from shock waves produced by impacts. Because momentum is conserved, a layer placed in the path of this wave can not reduce the total momentum delivered to the structure, but it may spread delivery over a period of time and thus reduce peak pressure induced in a structure by an impact. For a certain range of impulse the amount of damage to a structure is determined by peak pressure. A distended, expanded, or foamed material contains voids or pores which must be collapsed in the transmission of strong pressures through it. Since this crushing takes time, shock waves moving through a foamed layer are slowed, allowing rarefactions from the impacted surface, travelling relatively rapidly through compacted or "locked" material, to overtake the front during a relatively long interval before collision of wave and structure. This gradual erosion of the shock front has the effect of distributing the impact momentum over the entire thickness of countermeasure and prevents rapid momentum transfer to the vehicle. In contrast, a pressure pulse in a metal layer would tend to remain narrow since the unshocked and shocked materials are very similar, and the shock and the following rarefactions move at nearly equal speeds.

Workers at Poulter Laboratories during a previous program[1] discovered another important mechanism of peak pressure reduction by locking solids: the elastic forerunning wave. For wave pressures between certain limits, the single shock front in some foams is unstable, and a fast-moving, low-pressure front (0.2 to 5 kb) appears ahead of the main shock. The forerunner does not collapse the pores of the foam and the region between it and the main shock is one of nearly constant pressure, density, and particle speed. However, on collision with a rigid wall this elastic wave starts pore collapse, but again, because of the large specific volume change as a result of collapse, the accumulation of condensed foam at the wall is slow and the pressure induced in the wall is low. This pressure is also constant in time so that it is easily possible for the entire impact momentum to be delivered to the wall through the elastic wave when countermeasure foam thickness is large enough.

There are features of the static stress-strain curve of a foam that foretell the existence of an elastic forerunning shock, specifically a large region in strain where the rate of change of stress with strain is very low compared to its value for other ranges of strain. The stress value in the plateau represents a yield magnitude and may be the stress behind the forerunner. The slope of the static stress-strain curve for low stress (below yield point) may be related to forerunner speed in the same way the slope of the Rayleigh line in a shock Hugoniot diagram indicates shock speed.[2] Strain-rate effects are undoubtedly important in the high compression of foams and these relationships can only be loose but they may nevertheless be useful for gauging the effectiveness of a material as a counter measure.

II SUMMARY

During the past year we have demonstrated through experiment the two-wave structure of impact waves in three foams (polyurethane, aluminum, and silica), have measured the strength of the forerunner and in some cases its speed, have timed the interval between the forerunner and main waves and have observed the strength of the main wave, in some cases. We have compared these results with predictions of a simple theory based on static compression observations and have found considerable agreement, although there are obvious areas where improvement in the theory is needed. The behavior of aluminum, particularly, stands outside the range of expectation.

Impacts were produced by explosively-spalled, aluminum plates 0.012 to 0.040 inch thick, which carried 0.6 to 2×10^4 dyne-sec cm^{-2} of momentum and which struck foam slabs broadside. Initial distention* in these foams varied from 2:1 to about 4:1. We passed the induced waves into a steel anvil or witness plate and observed with a smear or streak camera their effect on the images of luminous light sources reflected in a polished free surface. Two different methods of spalling the flyer plates were tried: simultaneous and progressive. In the first, all parts of the flying plate's free surface leave the mother slab simultaneously; in the second, the flyer emerges at some small angle to the mother or driver. We found that both methods were satisfactory for our purposes; i.e., sufficient flatness and speed of the flyer could be easily obtained by either method, but because the impact with the target foam must take place in a partial vacuum, simultaneous spall is more convenient. We made all our flying plate experiments using that technique. The area of the flyer plate and shape of the anvil were chosen so that reflections from the edges did not enter the observational area of the mirror for a certain period, the "clear" time of the mirror, which in our experiments was about 8 μsec after the arrival of first wave at the mirror.

The calculational simulation of these experiments, based on the elastic-rigid model described earlier,[1] employed the assumptions that

* Defined as the ratio of expanded to solid density.

material speed behind the second or locking wave (including the flyer) was uniform, that the first wave was truly elastic, and that the only independent variables were time and distance perpendicular to the flyer. An expression of conservation of total momentum in flyer and foam was written, along with statements of conservation of momentum and mass across the two shock fronts. First estimates of numerical values of yield stress, elastic speed, and final or locked density were the results of quasi-static stress-strain measurements made on a confined cylinder of the foam. That in many cases the elastic speed calculated from the portion of the compression curve below yield was markedly lower than sound speed led us to try to measure first wave speed in a foam. One such successful attempt yielded a value less than sound speed but greater than the speed inferred from the static compression curve.

Using the method of artificial viscosity we have also written a calculational code for the Burroughs 7090 computer to find the pressure history at any point in a foam struck by a flying plate. Preliminary tests show the code is effective and we expect it will, in the future, produce more sophisticated simulation of foam behavior than the faster but more approximate method mentioned in the preceding paragraph.

Table I summarizes our findings concerning the first, forerunning or elastic wave. The third and fourth columns contain the values of forerunner stress measured at the anvil mirror and the numbers of the experiments from which each value stems. The error limits quoted are not standard deviations but a subjective estimate of the valid range of data points. The fifth and sixth columns have only one entry each, since in only one material (39 lb/ft^3 polyurethane) was the forerunner speed measured directly. The seventh through ninth columns show data taken from static measurements on the foams. The forerunner strengths in the foam entered in the final column are estimates based on the best values (Table II) we have now of the quantities V_1 and U_e, final locked specific volume and elastic wave speed, respectively. Excepting the entry for 42 lb/ft^3 these values of wave strength may be considerably in error. We derived the formula for wave strength P_e appearing in the table from the locking solid model and the assumption that the foam is brought to rest at the anvil.

Observed time intervals between first (A-) and second (B-) waves, and between first and driver (E-) waves passing from various thicknesses of several foams into the anvil appear in Table III. (The driver also is

Table I

STRENGTH AND SPEED OF FORERUNNER (A-WAVE) IN SEVERAL FOAMS

MATERIAL	NOMINAL ORIGINAL DENSITY AND DISTENTION	FIRST (A-) WAVE STRENGTH IN ANVIL (kb)	SHOT NOS.	MEASURED A-WAVE SPEED (mm/μsec)	SHOT NOS.	SOUND SPEED (mm/μsec)	PREDICTED ELASTIC SPEED FROM COMPRESSION CURVE (mm/μsec)	YIELD ZONE ON COMPRESSION CURVE (kb)	ESTIMATED FIRST WAVE STRENGTH IN FOAM (kb)
Polyurethane*	20 lb/ft^3, 3.6:1	0.15 ± 0.03	9227 9228			1.43	0.93	0.085-0.13, Fig. 66	0.145
	39 lb/ft^3, 1.8:1	0.82 ± 0.17	9431	1.60 ± 0.03	9341 9342				
	40 lb/ft^3, 1.8:1	0.95 ± 0.15	8773 8775 8863			1.73			
	42 lb/ft^3, 1.7:1	1.0 ± 0.10	9155 9180 9217				1.23	0.55-0.92, Fig. 65	0.88
	42	1.35 ± 0.05	9216[△]						
Silica†	1.1 g/cm^3, 2.0:1	0.65 ± 0.05	9345			1.35	0.624	0.31-0.61, Fig. 70	0.50
Aluminum§ open cell	0.75 g/cm^3, 3.7:1	0.55 ± 0.05[#]	9329			1.63	~1.6	0.051-0.17, Fig. 68	0.53
	1.4 g/cm^3, 2.0:1					4.7	<<4.7	Fig. 69	
Graphite♦	1.04 g/cm^3, 2.1:1						0.41×10^5	0.10-0.17, Fig. 71	

* Supplied by Peterson Products, Belmont, Calif.

† Eccofoam-Si, trade name, Emerson-Cummings, Inc., Gardena, Calif.

§ MD-40, trade name, Emerson-Cummings, Inc., Gardena, Calif.

△ Flyer was twice as thick during this experiment as during other shots with this material.

Actually B-wave. See page 49.

♦ Supplied by National Carbon Co. Lawrenceburg, Tenn.

□ Computed from formula:

$$P_a = \frac{P_a(V_0 - V_1)}{V_0 - V_1 + P_a(V_0/U_e)^2}$$

where

P_a = pressure in anvil

V_0 = original foam specific volume

V_1 = fully compacted foam specific volume

and

U_e = elastic wave speed in foam.

Values of P_a are from column (3); other parameters from Table II.

Table II

NUMERICAL VALUES OF FOAM PARAMETERS USED IN TABLE I

MATERIAL		P_e (mm/μsec)	V_0 (cm^3/gm)	V_1 (cm^3/gm)
Polyurethane	20 lb/ft^3	1.43	3.12	0.96
	30 lb/ft^3	1.60	1.60	0.90
	42 lb/ft^3	1.65	1.48	0.90
	60 lb/ft^3	2.0	1.04	0.90
Silica	1.1 g/cm^3	0.624	0.90	0.455
Aluminum open cell	0.75 g/cm^3	1.63	1.33	0.36

Mass per unit area in flyer μ_0 and surface density of momentum in flyer I_0 computed from: $\mu_0 = 6.99t$ (in gm/cm^2) where t = flyer thickness in inches; $I_0 = 8.2\mu_0\ 10^4$ (in dyne sec cm^{-2}).

Table III

TIME INTERVALS BETWEEN WAVES IN VARIOUS THICKNESSES OF SEVERAL FOAMS

TARGET MATERIAL	TARGET ORIGINAL DENSITY	TARGET THICKNESS (mm)	SHOT NOS.	MEASURED TIME INTERVAL BETWEEN FOREHUNNER (A) AND MAIN WAVE (B) (μsec)	MEASURED TIME INTERVAL BETWEEN FOREHUNNER (A) AND DRIVER WAVE (E) (μsec)	MEASURED TIME INTERVAL BETWEEN MAIN (B) AND DRIVER WAVE (E) (μsec)
Polyurethane	20 lb/ft^3	3.0	9296	1.5	5.1	
		10.0	9228	B-wave not seen	6.05	
		12.5	9227	B-wave not seen	6.9	
	42 lb/ft^3	5.0	9155	1.7 to 2.6	8.0	
		6.5	9217	3.0 to 4.9	8.65	
		10.0	9180	B-wave not seen	9.5	
		10.0	9216*	2.6 to 4.9	3.6	
	60 lb/ft^3	3.0	9297	A-wave not seen		4.1
Silica	1.1 g/cm^3	4.25	9325	A-wave not seen		3.4
		4.6	9345†	4.8 to 5.7	3.3	
Aluminum open cell	0.75 g/cm^3	3.5	9329	1.2§	-0.34	
		4.5	9344	B-wave not seen	0.82	
	1.4 g/cm^3	2.0	9324	A-wave not seen		3.7
Graphite	1.5 g/cm^3	6.0	9328	A-wave not seen		2.9

NOTE: Flyer thickness = 0.020 inch and $I_0 = 1.15 \times 10^4$ dyne sec cm^{-2} in all cases except:

* Shot 9216, flyer thickness = 0.040 inch, $I_0 = 2.30 \times 10^4$ dyne sec cm^{-2}.

† Shot 9345, flyer thickness = 0.012 inch, $I_0 = 0.69 \times 10^4$ dyne sec cm^{-2}.

§ Actually interval M-I, see page 49.

thrown into the target by the explosive and since we know the interval between arrivals of driver and flyer at the original foam face, driver impact arrival at the mirror gives us information on the speeds of flyer impact waves in the foam.) We discuss in Section VI-B some computations of these intervals from the simple theory of elastic locking solids. (No estimates from the Q-code are available yet.) Computed values are, in most cases, extremely sensitive to values of certain foam parameters: elastic wave pressure (P_e), elastic wave speed (U_e), original and locked specific volumes (V_0 and V_1, respectively), flyer surface density (μ_0) and flyer surface density of momentum (I_0). We have no reliable, independent measurements of any of these quantities except, of course, V_0, μ_0, and I_0.* Elastic wave speed U_e is susceptible to independent observation and we have made one such measurement, as indicated in columns five and six of Table I.

In many cases also the calculated interval is quite sensitive to the existence of the locking wave reflected off the anvil; for this reason we made some effort to find its shadow on a flash X-ray photograph but without success. We do not, however, consider that these experiments conclusively prove the absence of the reflected locked wave and we continue to assume its presence.

Measurements of wave intervals at different thicknesses of the same material, *e.g.*, the three thicknesses of polyurethane in Table III, make the best available test of the simple theory. It is obvious that any theory of shock behavior of foam must meet such a test if it is to serve in evaluating countermeasures; the duration of the elastic pulse at the vehicle surface is a direct measure of the proportion of the total momentum delivered at the yield stress, and of the input momentum remaining to be delivered at a higher pressure.

We would like to know the value of this higher stress as well. If for the compacted foam (specific volume V_1) we supply shock characteristics, *e.g.*, a complete Hugoniot pressure-specific volume curve or merely an approximate value of shock speed over a wide range of shock pressure, the simple theory will predict the pressure behind the second impact wave in the rigid wall of the vehicle. Because the foam layer will bounce off the relatively rigid wall, this pressure in general will be higher than the

*We know original flyer or input momentum (I_0) from separate measurements of flyer speed and also from a few measurements made concurrently with the shock observations in the anvil.

ratio of the undelivered part of the input momentum (I_0) to twice the transit time of a shock through the now locked foam. In Table IV we collect observed values of pressures induced in the anvil by the main impact wave in several foams of various thicknesses. In some cases the main wave either does not reach the wall at all or is not able to get there before the E-wave: the words "B-wave not seen" are placed in the fourth column to show this. We do not as yet have satisfactory values of computed main wave pressures to compare with these observations. (Further discussion is on page 104.)

Table IV

PRESSURE JUMPS IN MAIN (B-) WAVE FOR DIFFERENT THICKNESSES OF VARIOUS FOAMS

TARGET MATERIAL	TARGET ORIGINAL DENSITY	TARGET THICKNESS (mm)	SHOT NO.	OBSERVED MAIN (B-) WAVE PRESSURE IN ANVIL (kb)	ORIGINAL FLYER MOMENTUM I_0 $\frac{\text{dyne-sec}}{\text{cm}^2} \times 10^4$	OBSERVED TOTAL MOMENTUM IN ANVIL $\frac{\text{dyne-sec}}{\text{cm}^2} \times 10^4$
Polyurethane	20 lb/ft^3	3.0	9296	>8	1.15	film unreadable
		10.0	9228	B-wave not seen	1.15	0.10
	42 lb/ft^3	5.0	9155	2.25 ± 0.25	1.15	1.50
		6.5	9217	1.0 ± 0.15	1.15	1.44
		10.0	9180	B-wave not seen	1.15	1.08
		10.0	9216	3.0 ± 0.5	2.30	
	60 lb/ft^3	3.0	9297	5.0 ± 1.0	1.15	
Silica	1.1 g/cm^3	4.25	9325	$7.0 \begin{smallmatrix} +1.0 \\ -0.2 \end{smallmatrix}$	1.15	
		4.6	9345	1.6 ± 0.3	0.690	
Aluminum open cell	0.74 g/cm^3	3.5	9329	I-wave: 2.6 ± 0.3 J-wave: 1.3 ± 0.2	1.15	
	0.75 g/cm^3	4.5	9344	B-wave not seen	1.15	
	1.4 g/cm^3	2.0	9324	film unreadable; see page 49	1.15	
Graphite	1.5 g/cm^3	5.6	9328	film unreadable	1.15	

Prediction by the simple theory of total momentum given to the anvil during our experiments is complicated by the presence of the flyer layer outside the foam; since such a layer may not be present on a vehicle, we have not made this calculation but report in Table IV the flyer or input momentum (I_0) and the maximum momentum seen in the anvil before arrival of driver impact (or E-) wave. In most cases the latter is not the full momentum delivered by the flyer because of the interruption of the record by the E-wave. In only one case does the record appear complete (Shot 9155), that is, there appear to be contributions to maximum observed momentum from bounce-off of both flyer and foam.

Our flyer-plate experiments provide another, less reliable test of the simple theory. We have measured the speed of the driver plate which follows the flyer into the foam target and we know the time interval between driver and flyer arrival at the plane of the original foam free surface. If we assume a value for the average speed of the driver impact shock in the foam, we can calculate the time interval between its arrival at the anvil and either the forerunner or main wave arrival. The actual interval is easily measured. The final two columns of Table III contain this comparison.

There appears to be a change in shape of both forerunning and main waves as they progress through the foam; that is, the rise-time of both waves becomes greater as distance travelled increases. There is also some inconclusive evidence that the supposedly constant pressure in the forerunner may decay with distance travelled. If sound speed is greater than forerunner speed, acoustic rarefactions from either the edges or the rear impacted surface could overtake and weaken the forerunner. The simple theory predicts the radiation of rarefactions into the elastically strained region behind the forerunner, but because of the assumption of perfect elasticity (or linear stress-strain curve) in theory these travel forward at the same speed as the forerunner and never overtake it. We have some experimental evidence elastic or forerunner speed may be slightly less than sound speed in 40 lb ft^3 polyurethane.

Table V chronologically lists all the major experiments done as a part of the present effort. The text of Section III is a description of the performance and purpose of each of these experiments. Results, where not already given in this Summary, are stated.

Section IV presents certain special methods of data analysis Static compression tests and density measurements of foams are described and results are shown in Section V. In Section VI we derive the formulas used in the computational simulation of shocked foams. Finally, Section VII contains our conclusions and recommendations for further study.

Table V

CHRONOLOGICAL LIST OF MAJOR EXPERIMENTS

SHOT NO.	INSTRUMENT	PURPOSE	DESCRIPTION
8773	Smear camera	Observe two wave system in foam; test recording	Material: 0.64 g/cm³ polyurethane, 0.50 in. thick; impact: FL-506D explosive, 0.020 in. thick; normal atmosphere. Figs. 4, 5, and 54
8775	Smear camera	Test constancy of forerunner	Material: 0.64 g/cm³ polyurethane, 0.50 in. thick; impact: FL-506D explosive, 0.020 in. thick; normal atmosphere. Figs. 4, 6, 55, and 60
8863	Smear camera	Increase magnification in recording system	Material: 0.64 g/cm³ polyurethane, 0.50 in. thick; impact: FL-506D explosive, 0.020 in. thick; normal atmosphere. Figs. 4, 7, and 56
8966 8967 8977 8978 8979 8980	Flash X ray	Develop progressive spall technique	See Figs. 10 and 11
8984	Framing camera	Develop simultaneous spall technique	Two views of 0.01 in.-Al flyer spalled off 1 in.-steel driver
8996	Flash X ray	Develop progressive spall technique	See Figs. 10 and 11
8997	Flash X ray	Search for reflected locked wave in 2-D geometry	Material: 0.64 g/cm³ polyurethane, 0.50 in. thick; impact: FL-506D explosive, 0.020 in. thick; normal atmosphere. Figs. 23 and 24
9038	Flash X ray	Search for reflected locked wave in 2-D geometry	Material: 0.64 g/cm³ polyurethane, 0.50 in. thick; impact: FL-506D explosive, 0.050 in. thick; normal atmosphere. Figs. 23, 24, and 25
9039	Flash X ray	Develop progressive spall technique	See Figs. 10 and 11
9046	Smear camera	Develop progressive spall technique	See Fig. 12. Crossed grids
9093	Smear camera	Observe duration of explosive argon source	Detected grid line blooming on film
9094	Smear camera	Develop simultaneous spall technique	Steel driver only. See Fig. 13
9097	Smear camera	Develop simultaneous spall technique	See Figs. 13 and 15
9098	Smear camera	Develop simultaneous spall technique	See Figs. 13 and 16
9155	Smear camera	Observe waves in foam with simultaneous spall technique	Material: 0.67 g/cm³ polyurethane, 0.50 cm thick; impact: Al flyer, 0.020 in. thick; vacuum. Figs. 2, 18, 19, 26, 47, and 61
9180	Smear camera	Observe waves in foam	Material: 0.67 g/cm³ polyurethane, 1.00 cm thick; impact: Al flyer, 0.020 in. thick; vacuum. Figs. 2, 18, 19, 27, and 48

Table V *Continued*

SHOT NO.	INSTRUMENT	PURPOSE	DESCRIPTION
9181	Smear camera	Observe effect of atmosphere on waves in foam	Material: 0.67 g/cm³ polyurethane, 0.50 cm thick; impact: Al flyer, 0.020 in. thick; normal atmosphere. Fig. 28
9216	Smear camera	Observe effect of different flyer thickness on waves in foam	Material: 0.67 g/cm³ polyurethane, 1.00 cm thick; impact: Al flyer, 0.040 in. thick; vacuum. Figs. 2, 18, 19, 29, and 49
9217	Smear camera	Observe waves in foam	Material: 0.67 g/cm³ polyurethane, 0.65 cm thick; impact: Al flyer, 0.020 in. thick; vacuum. Figs. 2, 18, 19, 30, 50, and 62
9227	Smear camera	Observe effect of different distention on waves in foam	Material: 0.32 g/cm³ polyurethane, 1.25 cm thick; impact: Al flyer, 0.020 in. thick; vacuum. Figs. 2, 18, 19, 31, and 51
9228	Smear camera	Observe waves in foam	Material: 0.32 g/cm³ polyurethane, 1.00 cm thick; impact: Al flyer, 0.020 in. thick; vacuum. Figs. 2, 18, 19, 32, and 52
9244	Smear camera	Observe waves in foam	Material: 0.32 g/cm³ polyurethane, 0.60 cm thick impact: Al flyer, 0.020 in. thick; vacuum. Figs. 2, 18, and 19
9245	Smear camera	Test effect of 4 inches added Baratol upon flyer speed and planarity and driver speed	0.020 in. Al flyer, polished and holed; 1 in.-(1020) steel driver; 2 mirror targets; vacuum. Figs. 13 and 39
9296	Smear camera, raster oscilloscope	Observe effect of thickness on waves in foam	Material: 0.32 g/cm³ polyurethane, 0.30 cm thick; impact: Al flyer, 0.020 in. thick; vacuum. Figs. 2, 18, 19, 33, 40, and 42
9297	Smear camera, raster oscilloscope	Observe effect of distention on waves in foam	Material: 0.96 g/cm³ polyurethane, 0.30 cm thick; impact: Al flyer, 0.020 in. thick; vacuum. Figs. 2, 18, 19, 34, 50, 51, and 63
9324	Smear camera, raster oscilloscope	Observe waves in foam	Material: 1.40 g/cm³ Al-foam*, 0.20 cm thick; impact: Al flyer, 0.020-in. thick; vacuum. Figs. 2, 18, 19, 37, and 40
9325	Smear camera, raster oscilloscope	Observe waves in foam	Material: 1.10 g/cm³ Si-foam,† 0.42 cm thick; impact: Al flyer, 0.020 in. thick; vacuum. Figs. 2, 18, 19, 35, 40, and 64
9328	Smear camera, raster oscilloscope	Observe waves in foam	Material: 1.50 g/cm³ graphite,§ 0.56 cm thick; impact: Al flyer, 0.020 in. thick; vacuum. Figs. 2, 18, 19, and 40
9329	Smear camera, raster oscilloscope	Observe waves in foam	Material: 0.74 g/cm³ target, 0.35 cm Al-foam;* impact: Al flyer, 0.020 in. thick; vacuum. Figs. 2, 18, 19, 38, 40, and 59

Table V *Concluded*

SHOT NO.	INSTRUMENT	PURPOSE	DESCRIPTION
9344	Smear camera	Observe waves in foam	Material: 0.75 g/cm³ target, 0.45 cm Al-foam;* impact: Al flyer, 0.020 in. thick; vacuum. Figs. 2, 18, and 19
9345	Smear camera, raster oscilloscope	Observe effect of lowering input momentum	Material: 1.10 g/cm³ Si-foam† target, 0.45 cm thick; impact: Al flyer, 0.012 in. thick; vacuum. Figs. 2, 18, 19, 36, 40, and 53
9431	Smear camera, raster oscilloscope	Measure forerunner speed	0.62 g/cm³ polyurethane wedge at 17°10′ loaded with 0.02-in. FL-506D explosive; normal atmosphere. Figs. 43, 45, and 57
9432	Smear camera, raster oscilloscope	Measure forerunner speed	0.62 g/cm³ polyurethane wedge at 24°10′ loaded with 0.02-in. FL-506D explosive; normal atmosphere. Figs. 43, 44, 46, and 58

* MD-AO trade name, Emerson & Cumings Inc., Gardena, Calif.

† Eccofoam Si, trade name of Emerson & Cumings Inc., Gardena, Calif.

§ Supplied by National Carbon Co., Lawrenceburg, Tenn.

III MAJOR EXPERIMENTS

A. THE OPTICAL LEVER WITH THE SMEAR CAMERA [3,4]

Slight movement of a mirror surface can produce large displacement of an image formed in it; a compressional or rarefactional wave in reflecting at a free surface sets the surface in motion outward or inward, respectively, and can thus leave a film record of the wave strength and time of arrival at a certain point, as shown in Figs. 1 and 2. Angles α and α' (Fig. 1) are directly proportional to the free surface speeds left by the compressional and rarefactional waves, respectively, and inversely proportional to the speed of these waves along the mirror surface, called the apparent speed in this report. The magnitude of turning angle α falls in the range 10^{-5} to 10^{-3} radians in our experiments.

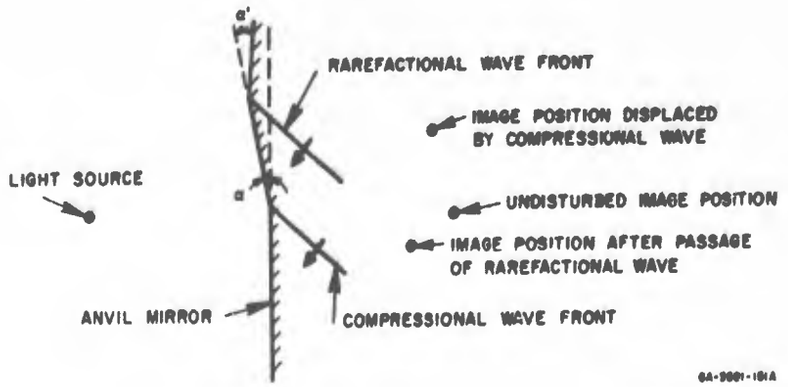

FIG. 1 DISPLACEMENT OF AN IMAGE IN THE ANVIL MIRROR BY COMPRESSIONAL AND RAREFACTIONAL WAVES (U)

Figure 2 shows how we measure amounts and times of reflected image displacement in an anvil mirror. Refracted images of the reflected images are formed on the opaque screen within the smear camera. The narrow vertical slit in this screen permits a section of the refracted image at any time to be refocussed onto the film along a certain vertical line whose position depends on the momentary position of the rotating

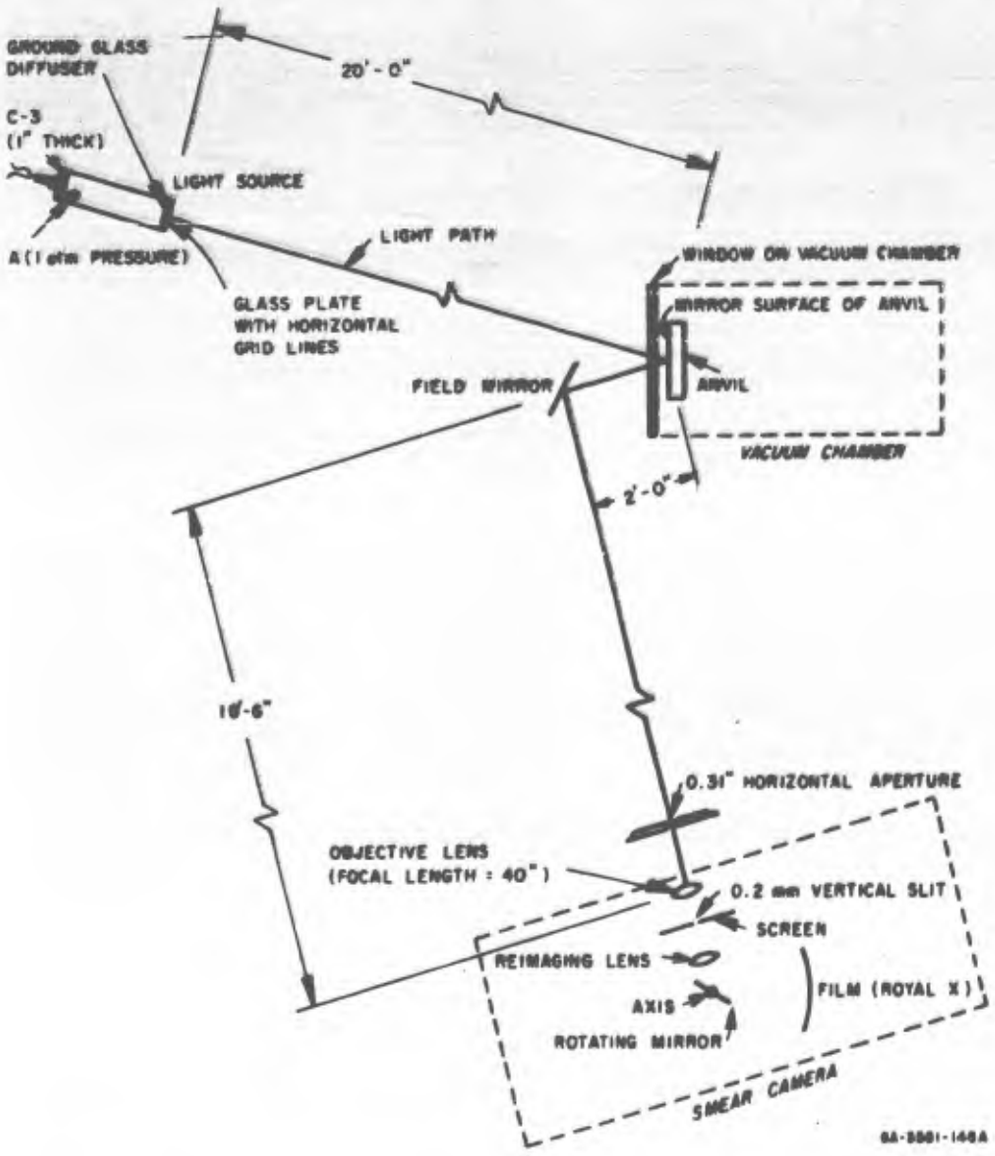

FIG. 2 APPLICATION OF METHOD OF THE OPTICAL LEVER TO THE STUDY OF FOAMS (U)

mirror. Rotation speed is carefully measured and lies in the range 500 to 2000 rps; thus we can achieve maximum image (horizontal) speeds along the film of 0.150 inch/μsec. Time coverage from about 26 to about 500 μsec is available.

The horizontal aperture ahead of the objective limits the vertical breadth on the anvil mirror of the reflection zone which can be used by light emerging from a single point of the object (called "light source"

in Fig. 2) to reach the objective lens; that is, when the reflected image of a point light source is disturbed we know all, or part, of the mirror surface within a certain narrow horizontal band has been displaced. (For the arrangement sketched in Fig. 2 this band is about 3.8 mm wide; the method of calculation of this width is made clear in Fig. 3.)

The objects reflected in the mirror are always shock-luminescent light sources.[5] These are boxes generally 4 × 8 × 12 inches or 4 × 8 × 24 inches filled with argon gas at one atmosphere pressure closed at one end (4 × 8 inches) by a one-inch-thick pad of C-3 explosive, and at the other end by two glass plates placed over one another. One glass plate is a translucent light diffuser and the other carries an emulsion surface on which carefully spaced horizontal lines 0.2 mm wide have been etched. When the explosive is initiated the shock stimulates nearly white luminescence in the gas, and the horizontal grid on the face of the box shines into the mirror whose motion is under study. The vertical slit in the smear camera passes light from only one small area of each grid line; thus the light source functions as a series of luminous points arranged at known distances along a vertical line. The reflection zones of these points in the mirror do not overlap and lie in a vertical line. A disturbance moving up or down the mirror passes from one zone to the next and displaces images in succession; the rate of displacement, hence the apparent speed of the wave, is readily calculated from the film record and the speed of the rotating mirror.

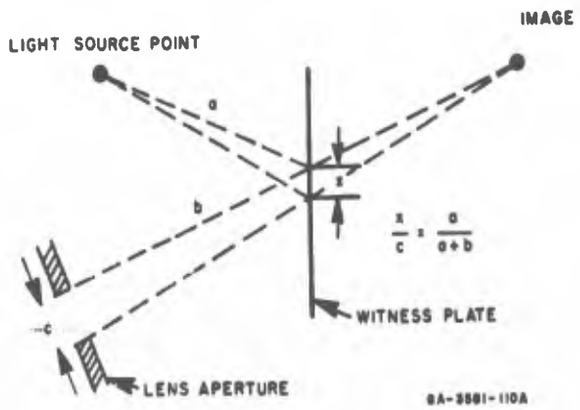

FIG. 3 AREA OF REFLECTOR USED IN REFLECTING A SPOT OF LIGHT INTO APERTURE OF STREAK CAMERA (U)

Free surface speed of the mirror is a measure of wave strength. In present experiments all mirrors are polished, hardened steel in which elastic limits are in the range 10 - 17 kb. Because the waves of interest are sufficiently weak we can analyze free surface motion by the theory of elasticity. Section IV explains the method of analysis.

B. EXPLORATORY TWO-DIMENSIONAL SHOTS

Figure 4 illustrates an arrangement employing the optical lever for a rapid, inexpensive exploration of the wave structure in shocked foam (in this case 42 lb/ft^3 polyurethane). The detonation front in a sheet of explosive drags waves up the 4 × 6-inch face of the anvil mirror, which is a simple slab of steel one inch thick. The method has the disadvantages of reverberations in the anvil, which must be distinguished from the primary phenomena, and two-dimensional flow in the foam, which complicates the deduction of wave parameters in the foam from observations at the anvil free surface.

The three experiments done in this way (Shots 8773, 8775, and 8863) were identical except for the thickness of explosive (Table V) and distances of light source and mirror from objective. Smear records (Figs. 5, 6, and 7) show in each case a succession of four compression waves pushing the mirror surface outward as they travel up the anvil at apparent speeds equal to the detonation speed of the explosive used. There are also reflections of each wave from the top edges moving downward at apparent speeds less than detonation speed. Analysis shows the first waves in all three experiments carried nearly the same pressure (Table VI). (Because Shot 8863

Table VI

CHARACTERISTICS AND RESULTS OF 2-D EXPERIMENTS

SHOT NO.	HE THICKNESS (inches)	APPROXIMATE IMPULSE (10^4 dyne-sec/cm^2)	APPARENT WAVE SPEED (mm/μsec)	PRESSURES PRODUCED IN ANVIL (kb)	
				Forerunner (A-Wave)	Main (B-Wave)
8773	0.020	1.3	7.18 ± 0.72*	0.87 ± 0.10*	Stops short
8775	0.050	3.2	7.51 ± 1.075	0.97 ± 0.09	5.73 ± 0.21
8863	0.050	3.2	8.04 ± 1.88	1.12 ± 0.07	5.95 ± 0.10
		Average	7.78 ± 2.25	0.99 ± 0.15	

* Standard deviation of a single measurement.

NOTE: (a) Foam tested was 0.66 g/cm^3 polyurethane 0.50 inch thick.
(b) Speed of all waves in anvil assumed to be 6.08 mm/μsec.

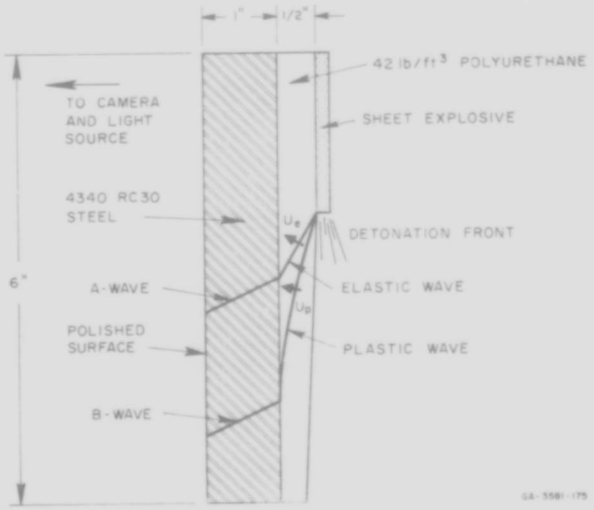

FIG. 4 TWO-DIMENSIONAL STUDY OF WAVES IN FOAM (U)

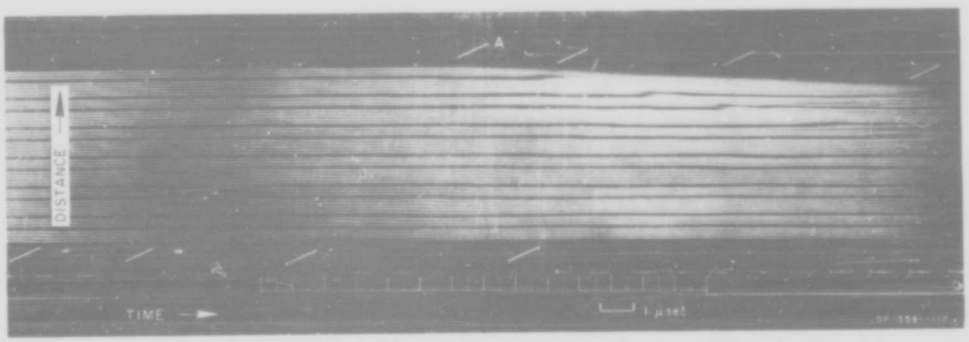

FIG. 5 SMEAR CAMERA RECORD FROM SHOT 8773 (U)

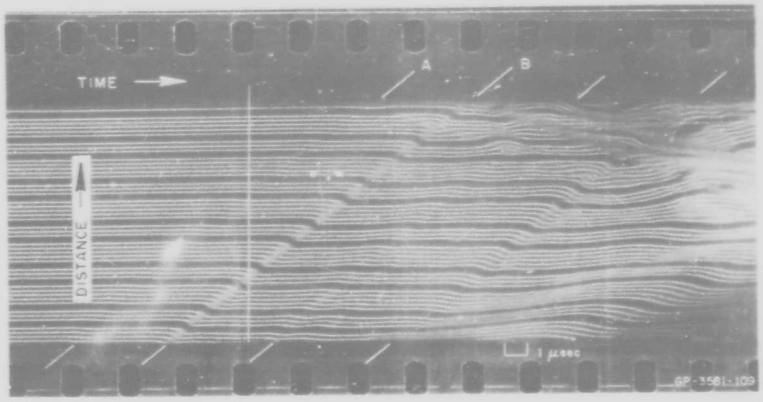

FIG. 6 SMEAR CAMERA RECORD FROM SHOT 8775 (U)

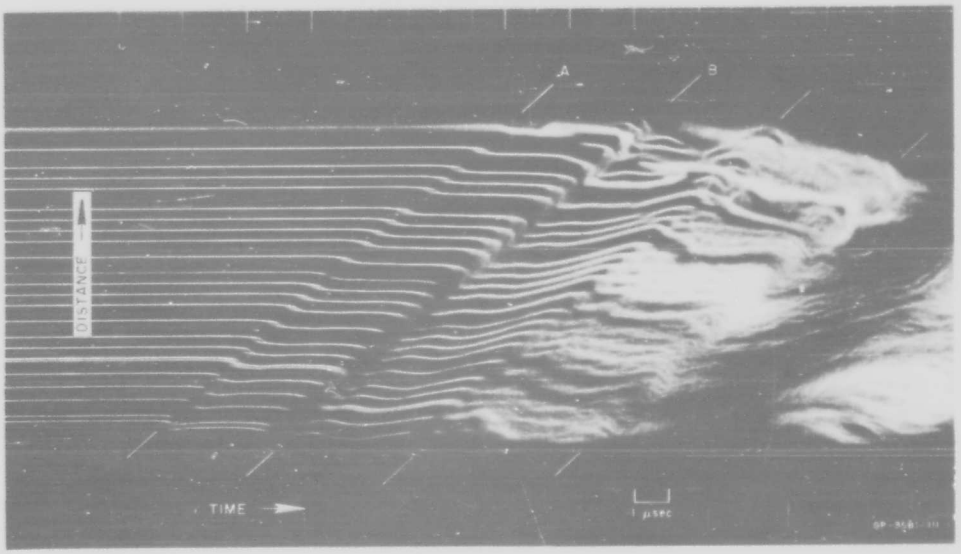

FIG. 7 SMEAR CAMERA RECORD FROM SHOT 8863 (U)

was an attempt to get maximum magnification of image displacement, the trace jumps in Fig. 7 are larger than in Figs. 5 and 6.) In making this analysis we assumed the shock speed in the anvil was always 6.08 mm/μsec, Poisson's ratio was 0.29, and applied the theory of oblique impact of an elastic wave at a free surface (as discussed further in Section IV). From Figs. 5, 6, and 7 we conclude:

(1) The first wave in all three shots is clearly the wave transmitted to the anvil by foreforerunner in the foam.

(2) Because the second waves in Shots 8775 (Fig. 6) and 8863 (Fig. 7) are markedly larger than the first, they must be transmissions from the main waves in the foam and their intensities are also entered in Table VI.

(3) However, there are no entries in Table VI for the main wave in Shot 8773 because we do not believe it reached the anvil; the second wave in Fig. 5 is thought, on the basis of later experiments, to be a reverberation of the first.

(4) Higher order reverberations and perhaps primary shear waves are also seen in the three figures.

Elastic potential theory applied to the interaction of forerunner and the foam-steel interface yields a ratio between normal stresses in the incident and transmitted dilatational waves of 0.465. However, we do not believe the foam at the interface remains elastic after the impact of the forerunner; therefore we have not used this value to compute forerunner stress in the foam. The one-dimensional experiments to be discussed later provide less ambiguous measurements of this quantity.

These two-dimensional experiments established the two-wave response of foamed polyurethane to impulsive loads of 1 to 4 $\times$ 10^4 dyne-sec/cm^{-2} and the approximately constant amplitude of the forerunner under variation of this load within the stated limits.

C. DEVELOPMENT OF ONE-DIMENSIONAL TECHNIQUE

Calculations involving plane waves moving normally to plane interfaces are simpler than those made for oblique interactions and the application of the results is less ambiguous. In order to match such one-dimensional calculations with experiments we sought ways to throw thin metal plates broadside into foam slabs. The momentum in a thin plate striking a plane barrier simultaneously is rapidly transferred to the

barrier and subjects it to an impulse of approximately the same duration and spatial distribution as might an X-ray burst from a nuclear weapon. We set aluminum plates (0.012- to 0.040-inch thick) in motion by explosively spalling them from carefully machined slabs of brass or steel to which they had been glued under high pressure. When the spalling shock front lay in a plane parallel to the flyer, the spall was simultaneous, and the flying plate was more or less parallel to the driver as it moved off. In this case the target was aligned with its large plane face parallel to the driver. When the spalling shock collided obliquely with the flyer the spall was progressive, and the target was placed at a small angle (0.7 to 7.0°) to the driver. Explosive for simultaneous spall was a point-initiated plane-wave generator* eight inches in diameter; for the tests of the progressive spall method, a block of Du Pont EL-5061 or Composition B3 3 inches wide and 15 inches long was initiated simultaneously along a line parallel to the width. The driver used with the plane-wave generator was 1020 steel 12 inches in diameter and one inch thick; but for progressive spall we used brass 3 inches wide and 9 inches long. Figures 8 and 9 illustrate the two plate-throwing techniques.

We fired 13 developmental shots without foam targets. All but one of the progressive spall tests were observed with flash X-ray shadowgraphs, one of which is reproduced in Fig. 10. The exposure was made by passing an X-ray beam through the driver, explosive, and spall in a direction parallel to the detonation front and perpendicular to the direction of propagation of detonation. With detonation speed known, the angles α and α' become measures of flyer and brass-spall speed, respectively. Figure 11 and Table VII summarize all observations of progressive spall except Shot 9046. The thickness of the shadow of the flyer is reported in Table VII as a rough indication of flyer planarity. In Shot 9046, sketched in Fig. 12, we sought unsuccessfully to use two optical levers on the same shot in order to observe flyer planarity along both length and breadth. The levers were used in this experiment merely to record arrival times, specifically, arrivals of various parts of the flyer at a mirror placed more or less parallel to the flyer in flight. A dove prism rotated one of the two fields of view, and both were superimposed on the same smear camera screen. The record was unclear, probably because of air shock ahead of the flyer and/or insufficient parallelism between flyer and target mirror.

* A two-component explosive lens, trade name P-80, Mason and Hanger, Inc., Amarillo, Texas.

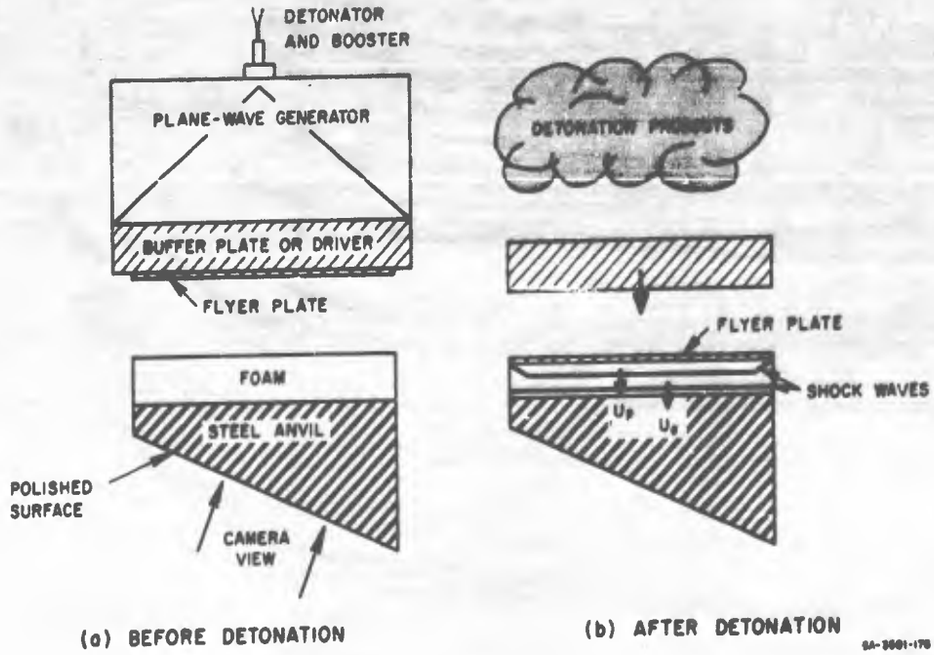

FIG. 8 CROSS SECTIONAL VIEW: SIMULTANEOUS SPALL TECHNIQUE (U)

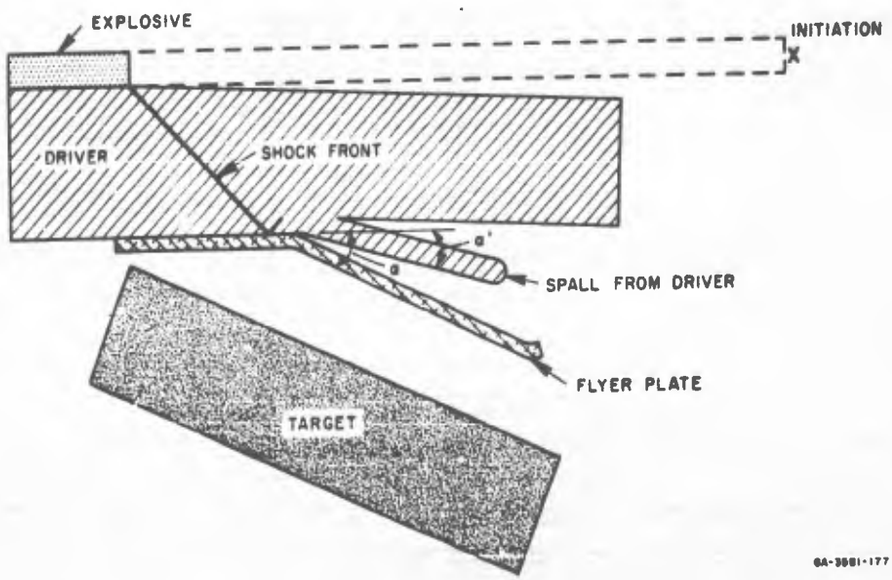

FIG. 9 CROSS SECTIONAL VIEW: PROGRESSIVE SPALL TECHNIQUE (U)

FIG. 10 X-RAY OBSERVATION OF PROGRESSIVE SPALL, SHOT 8979 (U)

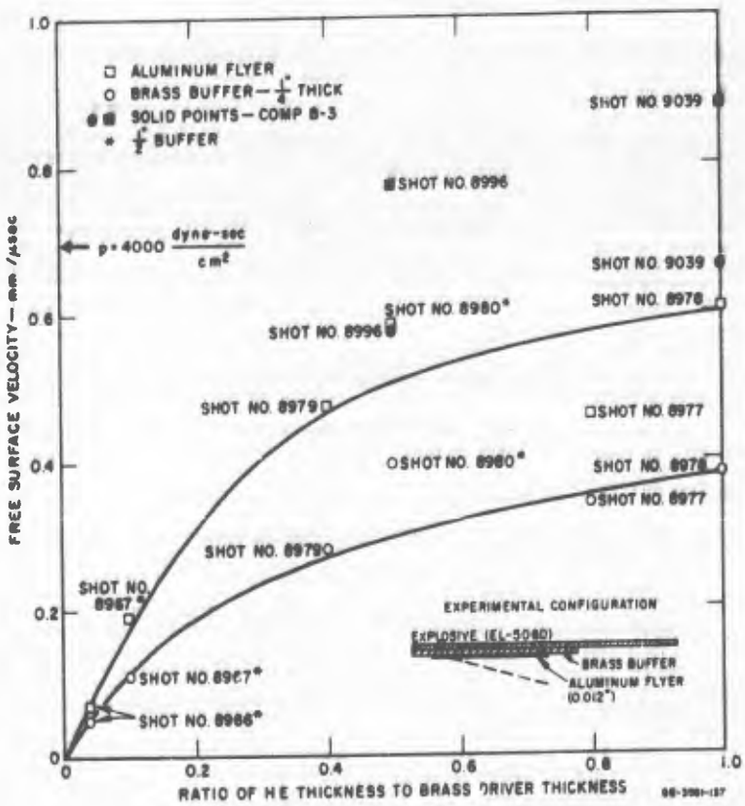

FIG. 11 SUMMARY OF X-RAY OBSERVATIONS OF PROGRESSIVE SPALLS (U)

Table VII

MEASUREMENT OF SPALL ANGLES IN PROGRESSIVE SPALL EXPERIMENTS

SHOT NO.	DIMENSIONS OF Al FLYER PLATE (inches)	KIND OF EXPLO-SIVE	DIMENSIONS OF BRASS DRIVER PLATE (inches)	DIMENSIONS OF EXPLOSIVE PAD (inches)	THICKNESS RATIO (EXPLOSIVE/ BRASS)	ANGLE α (°)	ANGLE α' (°)	APPARENT FLYER PLATE THICKNESS (inches)	SPEED OF FLYER (mm/μsec)	SPEED OF BRASS SPALL (mm/μsec)	MOMENTUM IN FLYER $\times 10^3$ (dyne sec/cm^2)
8966	1 x 6 x 0.012	EL-506D	3 x 9 x 0.5	3 x 15 x 0.020	0.040	0.04	0.2	1 to 2(mm) = 1/16 in.	0.05	0.02	0.4
8967	1 x 6 x 0.012	EL-506D	3 x 9 x 0.5	3 x 15 x 0.050	0.10	1.5	1.7		0.19	0.11	1.5
8979	1 x 6 x 0.012	EL-506D	3 x 9 x 0.25	3 x 15 x 0.10	0.40	3.8	2.3		0.475	0.28	3.8
8980	1 x 6 x 0.012	EL-506D	3 x 9 x 0.50	3 x 15 x 0.25	0.50	4.7	3.2		0.585	0.395	4.7
8977	1 x 6 x 0.012	EL-506D	3 x 9 x 0.25	3 x 15 x 0.20	0.80	3.7	2.7		0.46	0.34	3.7
8978	1 x 6 x 0.012	EL-506D	3 x 9 x 0.25	3 x 15 x 0.25	1.00	4.8	3.0		0.605	0.38	4.8
8996	1 x 6 x 0.012	Comp B-3	3 x 9 x 0.50	3 x 12 x 0.25	0.50	5.75	4.3		0.775	0.575	5.75
9039	1 x 6 x 0.020	Comp B-3	3 x 9 x 0.50	3 x 12 x 0.50	1.00	≈6.5	≈4.8		≈0.88	≈0.66	≈12.0

NOTE: Detonation speed in EL-506D assumed to be 7.3 mm/μsec, and in Comp B-3, 7.8 mm/μsec.

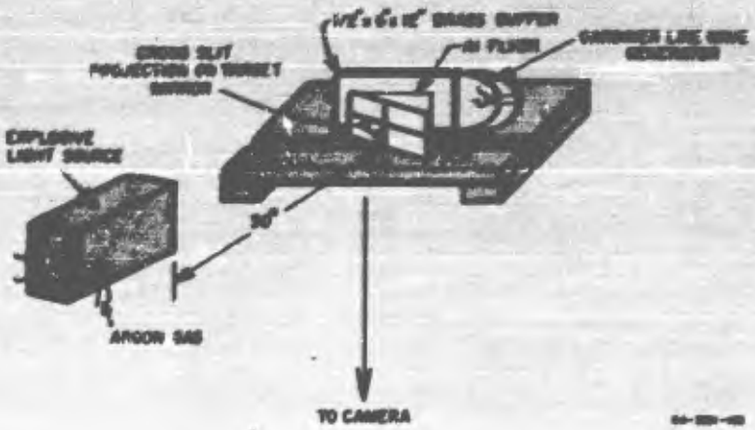

FIG. 12 EXPERIMENTAL ARRANGEMENT FOR PROGRESSIVE SPALL, SHOT 9046 (U)

The four developmental experiments with the simultaneous spall showed it had no advantage over the progressive technique except perhaps greater compactness, but Bancroft, Peterson and Minshall [6] had shown the existence of a stable train of three characteristic shocks which may be induced in steels by explosions of plane-wave lenses or generators. In order to guarantee ourselves a fairly reproducible plate speed, we followed their experimental scheme in all our tests of distended material.

We believe the operation of the one-dimensional plate throwing system is as follows:

Detonation of a P-80 explosive plane-wave generator produces a train of three shock waves in a one-inch-thick machined slab of 1020 steel in contact with the generator. The first wave, with relatively weak pressure of 10-12 kb, pushes or spalls from the steel an aluminum disc glued to the steel face opposite the P-80; but the second wave, of 130 kb pressure, reaches the now free steel-surface and drives it into the flying plate. The second interaction is the source of most of the flyer speed. The third wave, of strength greater than 130 kb, does not affect the flyer motion but brings the surface of the steel up to its final speed behind the flyer.

In Shots 9097 and 9098 (Fig. 13), this flyer impacted in low vacuum of 5 to 10 μ a flat piece of glass striped with reflecting gold. The glass

was aligned parallel to the spalling surface of the driver and again we used the optical lever to note the degree of simultaneity with which the various parts of the flyer struck the glass. Through the clear strips on the mirror between the gold we reflected the grid light source off the flyer itself. Figure 14 reproduces the resulting smear camera film from Shot 9097. The record of Shot 9098 is similar. The heavy lines represent points reflected in the gold; the light lines, those coming by way of the flyer surface. Careful study of the original record show times A and B in the traces reflected in the flyer surface, marking, we believe, the response of the flyer to the first two waves of the characteristic three-shock train in the driver. Times C are flyer arrivals at the glass; signals indicated with D show impact shock wave emergence from the far side of the glass. We measured these times C on a film reader* and have plotted our readings in Figs. 15 and 16. Arrival is simultaneous to within 0.5 μsec over an area about 6 inches in diameter. Because of the recording method, this represents the state of affairs only along one diameter of the flyer, of course, but we assume it is typical in this regard.

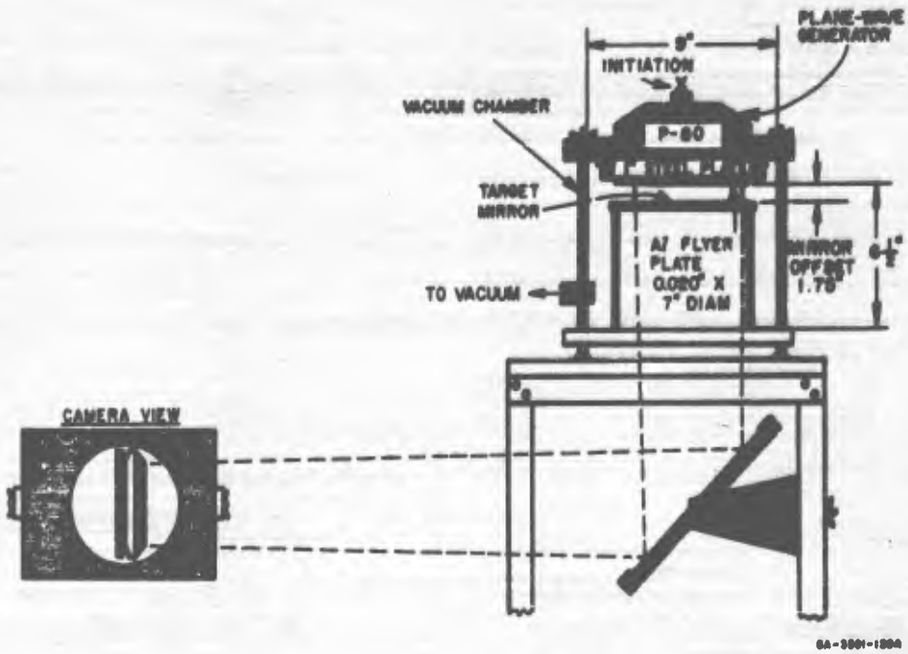

FIG. 13 EXPERIMENTAL ARRANGEMENT FOR SMEAR CAMERA OBSERVATION OF SIMULTANEOUS SPALL, SHOTS 9097 AND 9098 (U)

* Vanguard Instrument Corp., New York, N.Y., model 71/4. Magnification is about 5X.

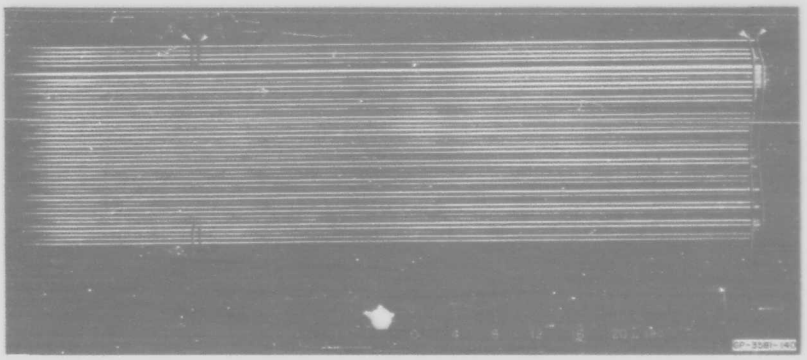

FIG. 14 SMEAR CAMERA RECORD, SHOT 9097 (U)

Repeating the experiment without a flyer glued to the driver we made the record shown in Fig. 17 (Shot 9094). Here signals *C* and *D* result from the impact of the central portion of the driver at the glass, and the increase in the time *A* to *C* over that same interval in Shots 9097 and 9098 is approximately the time we have at a target to observe the waves produced by the flyer before they are overridden by a stronger shock from the steel driver, which of course must also strike the target. The increase is about 8 μsec.

Average speeds for central areas of flyer (as indicated by the intervals *B* to *C*) are: 0.823 mm/μsec in Shot 9097 and 0.817 mm/μsec in Shot 9098; in Shot 9094, the driver has a maximum average speed of 0.70 mm/μsec.

The foregoing describes how we produce the controlled shock train in a foam target; we observe this train by the optical lever in an anvil of 4340 steel hardened to Rockwell C 30 to which the foam slab is glued. Opposite the ground and lapped surface carrying the foam target is a polished mirror surface bevelled at an angle of 30° with the receiving or target plane. The mirror plane is placed parallel to the glass cover on the light source and the foam-covered surface is made as nearly parallel as is easily possible to the grid lines on the glass cover. A perfectly plane wave from the foam will reach the mirror simultaneously at all points of a line parallel to the grid lines, and both the undisturbed and deflected mirror surfaces represented in Fig. 1 will be very nearly normal to the plane

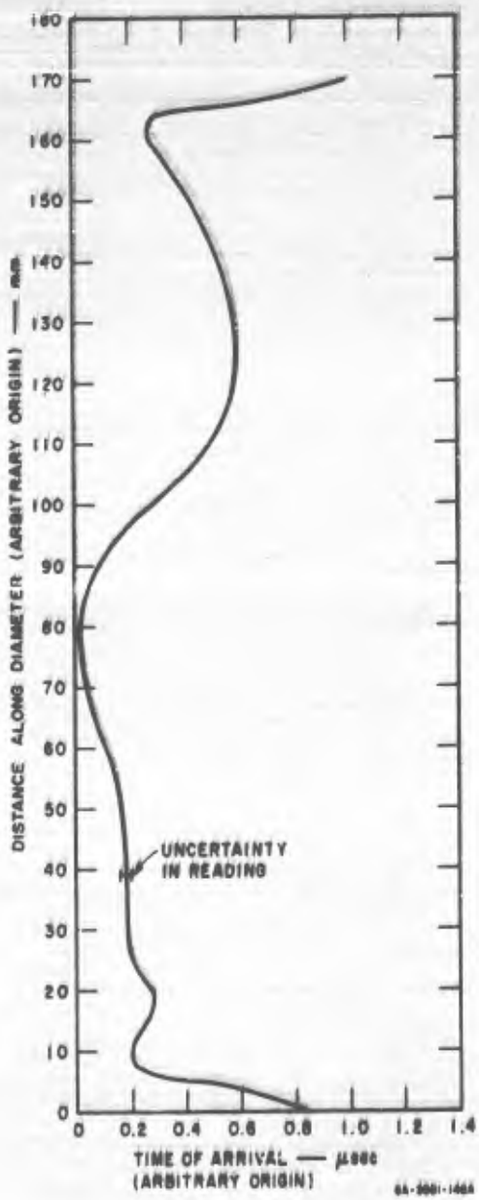

FIG. 15 TIMES OF ARRIVAL OF FLYER AT TARGET MIRROR, SHOT 9097 (U)

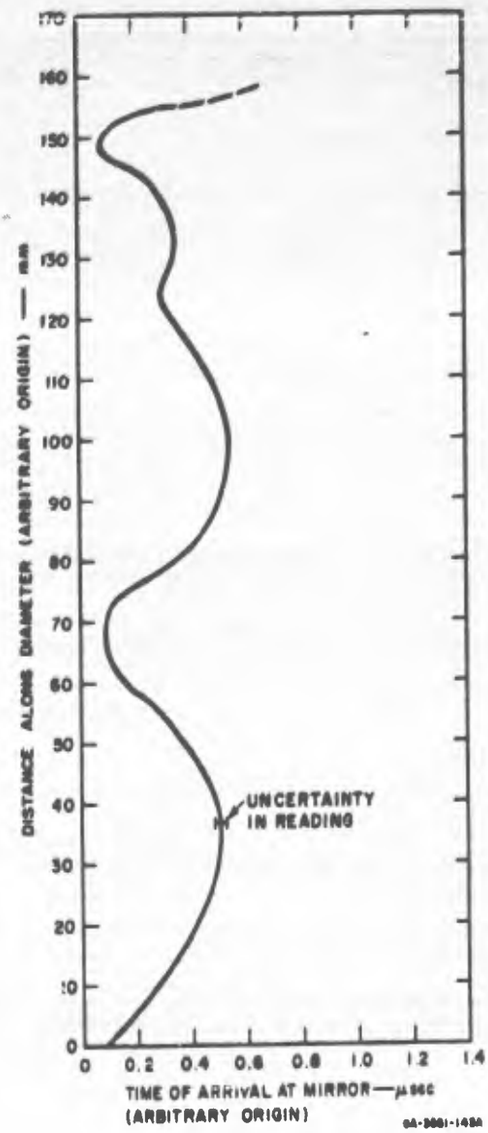

FIG. 16 TIMES OF ARRIVAL OF FLYER AT TARGET MIRROR, SHOT 9098 (U)

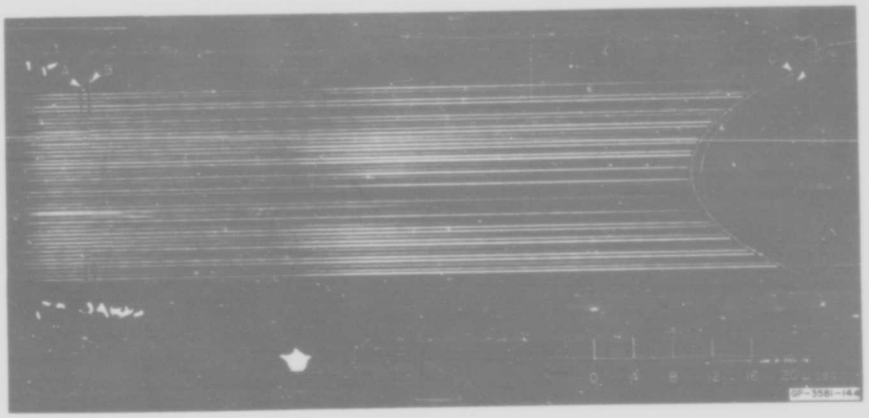

FIG. 17 SMEAR CAMERA RECORD, SHOT 9094 (U)

of the drawing. Because the anvil steel has a high elastic yield stress (18 to 20 kb), in our experiments all waves in the anvil stemming from the flyer impact behave elastically; propagation speed of waves from receiving to mirror surfaces is independent of wave strength and waves are unaffected by passage through the track of earlier waves reflected at the mirror.

Figures 2 and 18 are sketches of the system for one-dimensional study of shocks by the method of simultaneous spall. Figure 18 is a central section through a cylindrical tank except the supporting bolts shown in the figure are actually outside and on both sides of that plane. We attach the explosive lens to the outside surface of the driver plate opposite the flyer. Dimensions in Fig. 2 are typical. Figure 19 is a photograph of the system in the field just before one experiment.

The two-wave response of foam requires us to watch a foam target for a period of ten or more μsec. We have mentioned the limitation on the length of observation time imposed by the driver impact; another may arise from the reflection into the mirror surface of the first wave at the sides or edges of foam and anvil. Reflection at the foam-anvil interface is a very nearly one-dimensional problem and its effects can be easily calculated (if we want to know the reaction to the flyer of the foam layer alone). Edge effect is neither one-dimensional nor steady in time and introduces complexities into the analysis of phenomena ariving

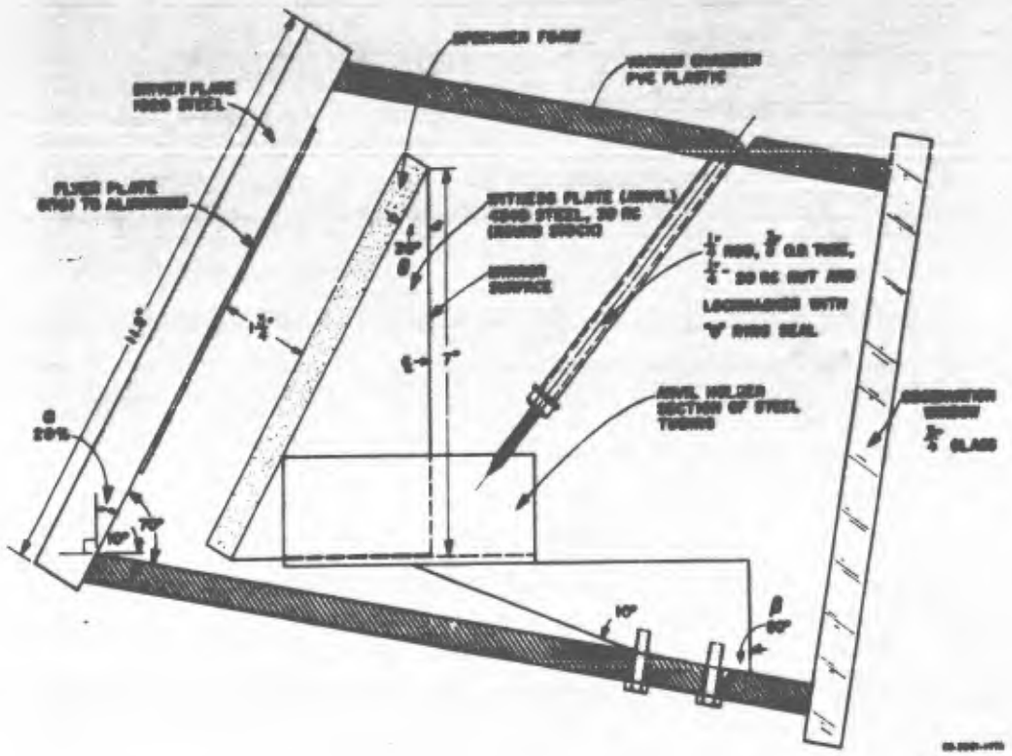

FIG. 18 PLATE-THROWING APPARATUS WITH WEDGE WITNESS ANVIL IN VACUUM (U)

at the mirror after these effects are felt there—even if the record remains clear. (Reflection at the bevelled mirror surface can not be treated one-dimensionally, either; however, all parts of the second wave pass through the same mirror-reflected wave into a region of zero compressive stress, and behind the "clear area" of the mirror this collision of reflection from first wave and of the second wave takes place in the steel anvil. If the time interval between first and second waves is greater than about 15 μsec this may not be true, and we would have to consider the effect of the reflection upon the foam.) Since the reflection zones of the points of light used to make the smear record lie in a central vertical band across the mirror face, the most critical edge effects in the anvil will be disturbances sent from the upper and lower extremities of this band; these will be the first to affect the mirror. If Fig. 20 represents a cross section through the anvil at the reflection zone, then the surface BC is the mirror; and the face AB is the site of the foam layer. If U is sound speed (= elastic wave speed) in the anvil, all points of the mirror between F and G are free or clear of edge effects stemming from reaction of first wave

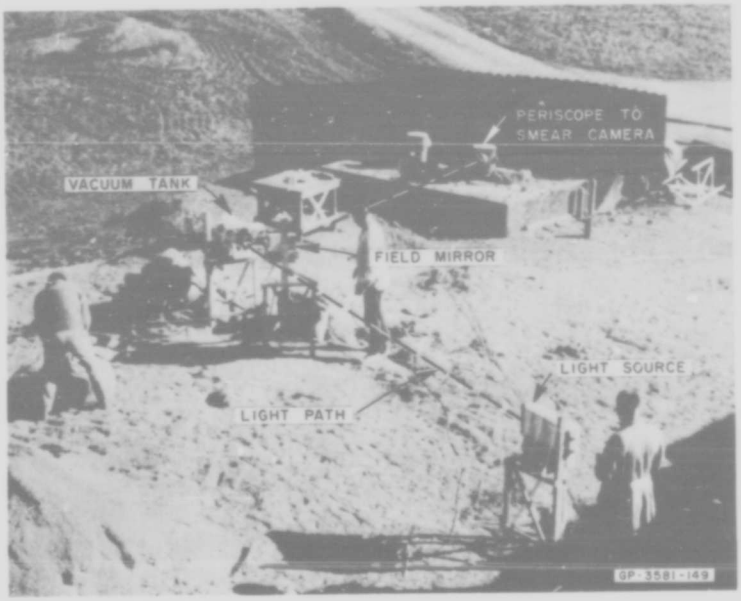

FIG. 19 ARRANGEMENT OF APPARATUS AT SMEAR CAMERA SITE FOR SHOT 9155 (U)

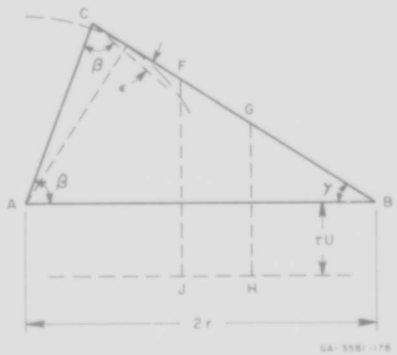

FIG. 20 GRAPHICAL DISCOVERY OF CLEAR AREA OF ANVIL MIRROR (U)

at points A and B for an interval τ after first wave arrival—provided angle $AFB > \pi/2$. In other words, the clear area is defined such that $\overline{AF} = \overline{FJ}$ and $\overline{BG} = \overline{GI}$. From a few sketches of this kind it is readily seen that for a given value of τ the clear area FG increases monotonically with increasing wedge diameter ($2r$), and decreases monotonically with increasing wedge angle γ. For given values of r and γ the clear area decreases monotonically with increasing τ. It is also readily apparent when there is no clear area at all.

Since angular displacement of the mirror image increases with increasing angle between wave and mirror surface, the requirements of large clear area on the mirror and large deflection on the film tend to conflict. The relation between refractive image displacement δ and wedge angle γ is:

$$\left(\frac{2}{\frac{d_0}{f} - 1}\right)\left(\frac{d}{f}\right)\left(\frac{u_n}{U}\right)\sin\gamma = \frac{\delta}{f}$$

where:

d_0 = optical distance from lens to mirror image

d = perpendicular distance from mirror image to mirror surface

u_n = normal component of mirror free-surface speed

U = speed of shock front in steel anvil in direction normal to itself (or dilatational wave speed)

f = objective lens focal length.

If, as an application of the above design criteria, we choose wedge angle $\gamma = 30°$ when wave interval $\tau = 8$ μsec, we compute the size $\overline{FG}$ and location $\overline{BG}$ of the clear area to be: $\overline{FG} = 3.5$ cm, $\overline{BG} = 9.2$ cm. If $d_0 = 20$ ft, $d = 20$ ft, and $f = 40$ inches, the same wedge will under a 1-kb wave produce a refractive image displacement $\delta = 0.029$ inch. To be measurable a displacement must be at least 0.004 inch (0.020 inch after magnification by five on the film reader) so an experiment with the values of d, d_0, f, and γ chosen in this example will not quite reveal a 0.1-kb wave clearly.*

* As will be explained in Section IV we calibrate observed film displacements δ by means of the known grid spacing in the light source, and do not use the focal length of the camera or assume that the refracted image is in perfect focus.

When shocks (or dilatational waves) are weak in the anvil their reflection from free surfaces will be nearly specular.* For certain anvil geometries a free-surface specular reflection will reach the clear area, as defined above, before the last wave which is to be observed. Using the terminology of Fig. 20 the condition for this can be written:

$$\overline{BC} \sin \gamma + \overline{CF} \sin \epsilon < \overline{BG} + \overline{FG} \sin \gamma$$

where

$$\epsilon = \pi - \gamma - 2\beta \quad .$$

This condition is due to the fact that the first wave drags a reflection up the face AC which reaches F before the sonic disturbance centered at A.

The specular reflection from the back face of the anvil can never precede the last wave to be observed in the clear area (as defined above). It is obvious it cannot if $\gamma > \pi/6$, for then the specular reflection from AB cannot possibly reach the mirror ahead of the sonic disturbance centered at B. (Fig. 21) For the case $0 < \gamma \leq \pi/6$ it can be shown that the breakout point K on the mirror surface of the double specular reflection of the first wave will always arrive at the edge of the clear area (point G in Fig. 20) behind the last wave from the foam to be observed. The calculation is as follows and the nomenclature is illustrated in Fig. 22:

$$\alpha = 2\gamma$$

$$\beta = 3\gamma \quad .$$

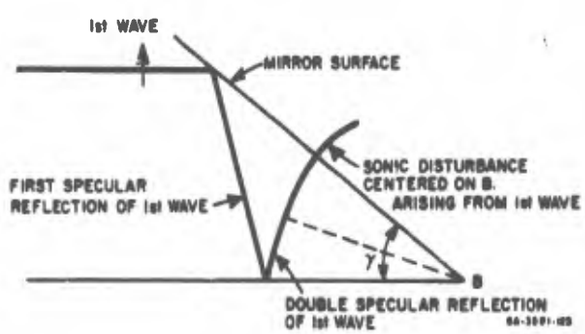

FIG. 21 SPECULAR REFLECTION FROM BACK SURFACE OF ANVIL FOR CASE OF $\pi/4 > \gamma > \pi/6$ (U)

* Angle of incidence = angle of reflectance.

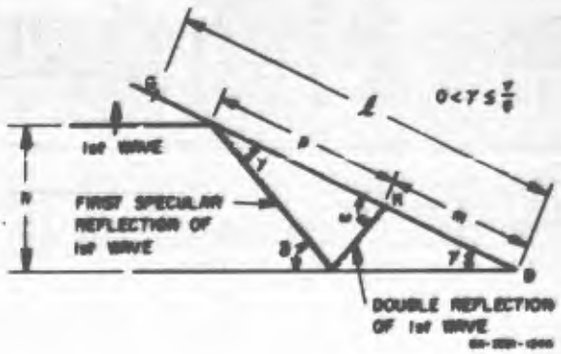

FIG. 22 NOMENCLATURE FOR CALCULATION OF SPEED OF DOUBLE SPECULAR REFLECTION IN WEDGE ANVIL FOR CASE $0 < \gamma \leq \pi/6$ (U)

From the law of sines,

$$\frac{p}{\sin(\pi - 2\gamma)} = \frac{h}{\sin\gamma \sin\pi}$$

Also,

$$m + p = \frac{h}{\sin\gamma}$$

so that

$$m = \frac{h}{\sin\gamma} - \frac{h \sin 4\gamma}{\sin 2\gamma \sin 3\gamma}$$

or, differentiating both sides with respect to time and simplifying,

$$\frac{dm}{dt} = \frac{U}{\sin\gamma(3 - 4\sin^2\gamma)} \quad . \tag{1}$$

If the point K is to reach G after the last wave from the foam, then

$$\frac{l}{dm/dt} \leq \frac{l \sin\gamma}{U} + \tau$$

where

$$l = \frac{\tau U}{1 - \sin \gamma} .$$

Hence the condition becomes: $\sin \gamma(3 - 4 \sin^2 \gamma) \leq 1$ which is always true for $0 < \gamma \leq \pi/6$.

Equation (1) above can provide an estimate of the arrival time of the double specular reflection in the clear area of the mirror.

D. SEARCH FOR REFLECTED LOCKING WAVE

Fowles and Curran reported seeing the two wave system in impacted polyurethane foam (40 lb/ft^3) directly in X-ray shadowgrams made during

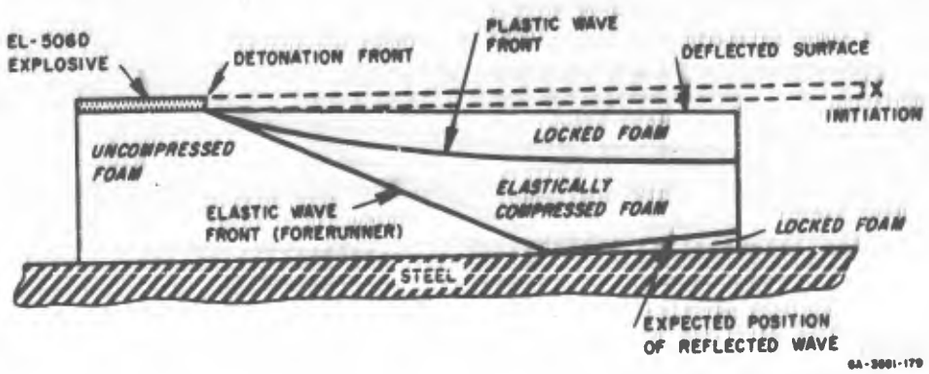

FIG. 23 CROSS SECTION: EXPECTED WAVE CONFIGURATION DURING X-RAY SEARCH FOR REFLECTED LOCKED WAVE (U)

experiments similar to those just described.[7] We repeated their experiment with one improvement: we cut the foam layer thinner and rested it on a steel plate in order to stimulate production of a reflected locking wave. (See Figs. 23 and 24.) The slight change in density behind the forerunning elastic wave was seen by Fowles and Curran with great difficulty after several unsuccessful attempts; but the dense material behind the locked wave makes itself very plain on almost any shadowgram. Our two experiments, Shots 8997 and 9038 (Fig. 25), showed neither elastic wave nor reflected locking wave (although the locked foam directly under

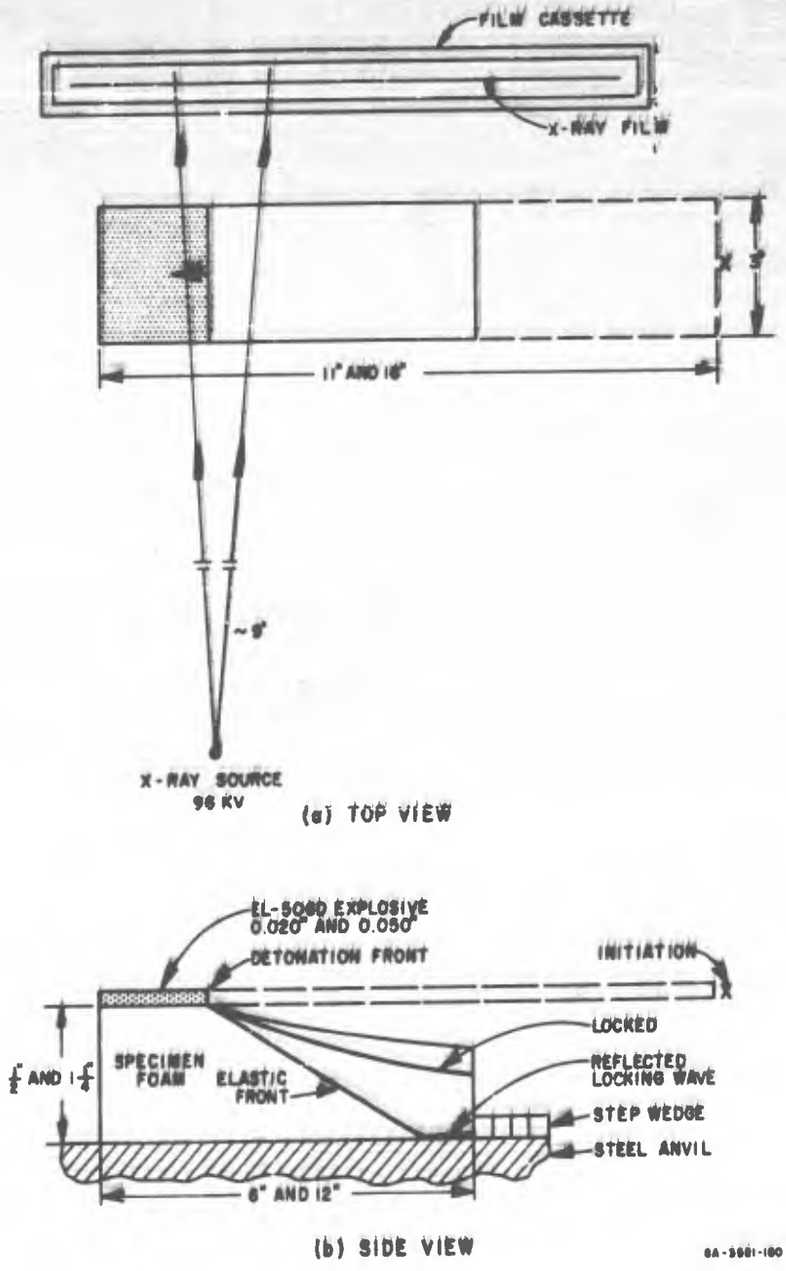

FIG. 24 FLASH X-RAY STUDY OF WAVES IN FOAM (U)

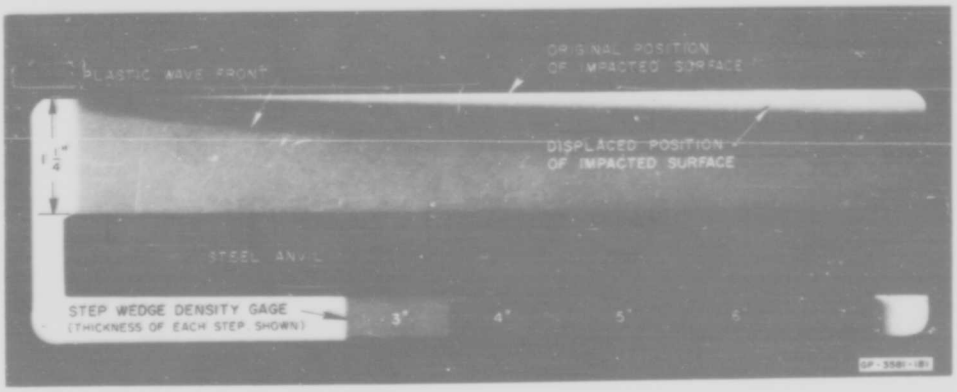

FIG. 25 FLASH X-RAY PHOTOGRAPH, SHOT 9038 (U)

the explosive stood out clearly). The X-ray beam was not collimated and the interface between foam and steel was put on a line to the X-ray source by eye only. We do not think, therefore, the negative results of this search prove the absence of a locked reflection, although it is probably evident the reflected wave is weaker or extends less far back into the foam than anticipated. We based our anticipation on one-dimensional considerations which will be set forth later; these do not take account of the two-dimensional interactions at the two interfaces, nor do they recognize the edge effects.

The failure to locate an elastic wave in these experiments is also not significant.

E. FLYER-PLATE EXPERIMENTS

Figure 26 shows the smear camera record made by the optical lever when a flying plate carried 1.15×10^4 dyne sec cm^{-2} of momentum into a 0.5-cm-thick slab of 0.674 g/cm^3 (42 lb/ft^3) polyurethane foam (Shot 9155). The trace marked ℄ was reflected in a horizontal strip of the anvil mirror about 3.8 mm wide located near the center; a similar strip about 3.4 inches below the center of the mirror on the thick part of the anvil reflected the light of the bottom trace (Fig. 18). The vertical scale in the figure measures distances between reflection zones of the traces. In making the photograph the rotating mirror in the smear camera turned at very nearly 1000 rps, and the time scale marks the horizontal distance equivalent to 2 μsec.

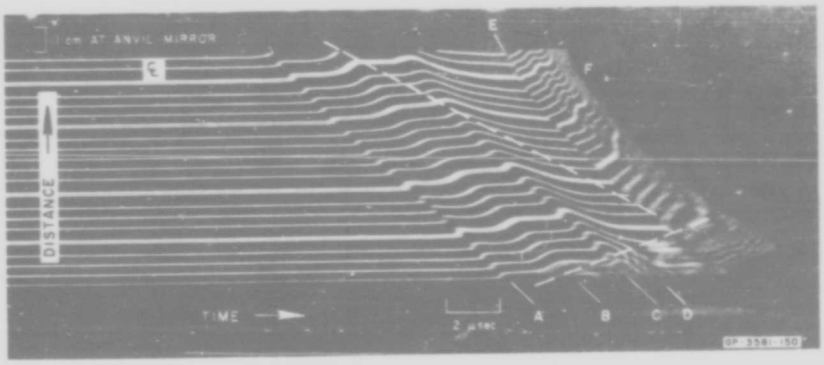

FIG. 26 SMEAR CAMERA RECORD, SHOT 9155 (U)

Waves move out of the target material at the back of the wedge anvil toward the mirror surface where a compressional wave pushes the surface outward and a rarefactional wave pulls it inward. Because of the wedge shape of the anvil, this motion is not simultaneous all over the surface but appears to travel downward; as a result an image reflected in it will be moved upward by a compression, and downward by a rarefaction. This behavior is illustrated in Fig. 1.

Thus the first wave in Fig. 26 is the transmitted elastic wave (hereafter termed the A-wave) from the foam. The traces break upward sharply; and the amount of displacement and the slope of the locus of breaks indicate a wave strength of about 1 kb in steel. The second or plastic wave (B-wave) is also compressional but appears much more gradual. The additional displacement indicates a wave strength of about 2.5 kb in the anvil. Between the two waves the traces are straight, but not always level or parallel to their former undisturbed positions. The same condition prevails between second and third (or C-wave). Over the bottom half of the film the traces in the third wave show a sharp upward displacement. We think this wave is a double reflection of the preceding one in the foam; *i.e.*, we believe the second or plastic wave in the foam reflects from the anvil into the now locked foam slab, reflects again from the aluminum flyer at the rear foam surface, and passes forward through the foam and is transmitted into the anvil. Since the flyer is thin, the reflection of a compressional pulse from the foam-aluminum interface should be followed by rarefactions (labelled D) reducing the

pressure to zero. These rarefactions show very clearly in the photograph but the mirror surface has not, in the case of every grid line, returned to its original alignment before the arrival of the fourth compressional wave (marked E).

The fourth shock is extremely sharp and moves the images upward about five times as far as the second. It stems from impact of the steel driver and probably represents a wave at the elastic stress limit in the anvil. The impact also produces waves of stress above the elastic limit and speed slower than elastic in the anvil. The effect of one of these later disturbances is seen also in the photograph when the images are finally thrown out of the field of view by such a plastic wave (marked F) carrying a very high stress in the anvil.

The train of two waves, E and F, is evidence of the first two of the three waves in steel and iron discussed earlier (page 24). The magnitude of trace displacements and apparent speed in the E-wave correspond to a stress of about 15 kb (which is in the region of the elastic limit of 4340 steel), but the disappearance of the traces in the F-wave removes all evidence of the value of pressure in it. The second wave in the three wave train is thought to carry a stress near 130 kb.[6] We believe the driver impact raises the pressure in the steel anvil to a value between 50 and 100 kb, and that from this unstable wave the elastic forerunner splits off to become our E-wave; both the E and F disturbances, then, stem from the driver impact. We do not understand the trace movements in our records between the E and F jumps, but presume they come from the interaction of the reflection of the 15 kb elastic wave at the bevelled free surface and the main driver shock. (We think the most important intermediate movement represents simply the arrival of a compression at the free surface even though in some places of some of the records this compression seems to be followed by a relaxation, *e.g.*, the upper traces in Fig. 26. The seeming relaxation is probably attributable to distortion in the nonuniformly bent mirror caused by the very strong warping of the driver (Fig. 17). We could expect also that this warping might conceivably lead to a diverging and weakening elastic wave in the anvil even though the elastic front must be followed by a strong plastic shock. Disturbances then may be able to pass through the plastic shock front and into the elastically strained region ahead of it, if pressure there has been lowered below the elastic limit by divergence.)

The results of Bancroft, Peterson, and Minshall indicate that our driver impact wave in the anvil is always double, that is, the elastic forerunner (at about 15 kb) is in existence at the foam-anvil interface. Such a wave always moves at the same speed as the earlier, weaker waves stemming from flyer impact. The speed of the main driver shock or F-wave, however, may not be fixed; its average speed through the anvil may vary from experiment to experiment, depending upon the thickness and kind of material in the foam layer.

The third wave (C) in Fig. 26 is rounded in the traces at the top of the photograph and becomes sharp only near the middle. We consider this shows weakening of the wave by a rarefaction arising from the interaction of the first wave with the top of the wedge. We can not trace the exact course of the onset of this weakening in the photograph, but the dotted line in Fig. 26 is an estimate. The apparent speed of this rarefaction down the mirror face is markedly less than the apparent speed of the previously described waves; in fact, as expected from the analysis of edge effects above, the traces near the wedge bottom seem to be completely unaffected by this disturbance. We can see the predicted rarefaction from the interaction of first wave and bottom edge of the wedge disturbing the first four traces from the bottom of Fig. 26. It appears that the fifth, sixth, and seventh traces may be free of these two rarefactions for about 8 μsec after the arrival of first wave.

The record from Shot 9180 (Fig. 27) shows a new feature, the double reflection of the first wave from the front and rear wedge surfaces. The approximate course of this reflection (marked R) is dotted in the figure. The first wave is not sharp and the second and third waves are missing. The foam target was 42 lb/ft^3 polyurethane, as in Shot 9155, but in this case we used a slab twice as thick, *i.e.*, 1.0 cm. The plastic wave does not reach the anvil under the influence of the flyer alone; it waits for the driver impact. There is considerable unsteadiness in the traces between wave arrivals; the apparent speeds down the wedge face of these slight hills and valleys in the traces seem similar to that of the first wave.

Apparent wave speeds and the magnitude of trace displacements in Shot 9180 are very similar to their counterparts in Shot 9155.

Shot 9181 was virtually a duplicate of Shot 9155 except we used no vacuum tank—the flying plate travelled through normal atmosphere. In contrast to the record of Shot 9155, the smear photograph from Shot 9181 (Fig. 28) shows a gradual first or A-wave, a late and sharp second or

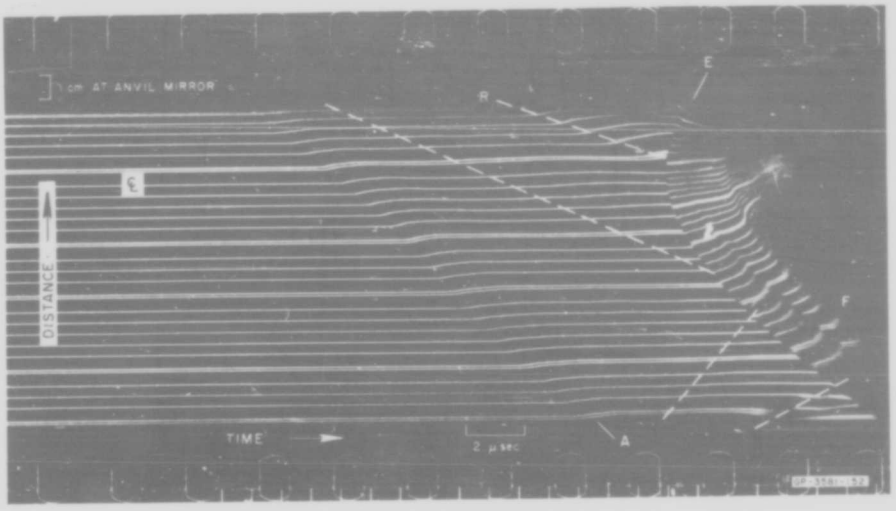

FIG. 27 SMEAR CAMERA RECORD, SHOT 9180 (U)

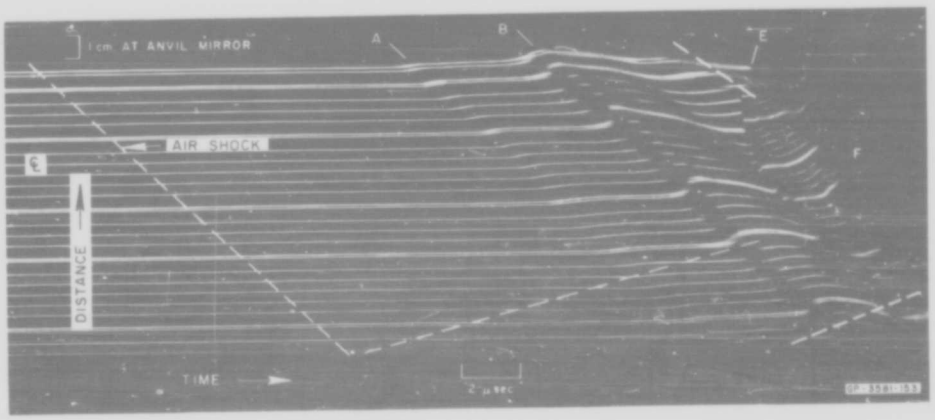

FIG. 28 SMEAR CAMERA RECORD, SHOT 9181 (U)

B-wave, a strong rarefaction but no third compressional wave. Some unsteadiness in the traces is seen between the first and second waves. We think we see also the arrival of a very small compressional wave due to an air shock ahead of the flyer, and a rarefaction arising from the interaction of this wave and the bottom edge of the anvil. Deflections due to these disturbances are dotted in Fig. 28. The air shock induces a shock in the witness plate about one-tenth the strength of that stemming from the first wave.* Because of the long time interval over which the air shock acts upon the target it must transfer a significant portion of the flyer momentum to the target. We can see something like the sought for third wave in the traces of Shot 9181 immediately following the very large, sharp breaks due to driver impact; perhaps this wave comes in later than it did during Shot 9155. Certainly the second wave is later, so the third is also. If our identification of the third wave is right, the strong rarefactions following the second wave in Shot 9181 (Fig. 28) and following the third wave in Shot 9155 (Fig. 26) must be primarily the rarefactions which arise at the designated time t^* in earlier theoretical discussions.†

As a result of Shot 9181 we think the flying plate experiments must be done in vacuum.

In Shot 9216, we doubled the thickness of the flyer plate, and repeated Shot 9180. If, as we expect, the flyer received its momentum from waves in the 1020 steel of the driver which are constant in amplitude with time, the thicker flyer will move at the same speed as the thinner and the thicker will therefore carry twice the momentum of the thinner. The flyer momentum per unit weight of target foam was expected to be the same in Shot 9216 as in Shot 9155.

Figure 29 is the record made for Shot 9216. The first wave is sharp and has very nearly the same strength as in Shots 9155 and 9180, *i.e.*, 1 kb. The second wave does appear (in contrast to Shot 9180), but it is very gradual and follows the first wave by a greater length of time than it did in Shot 9155.

We do not understand the disturbance (shown by dotted lines in Fig. 29) that starts at the first wave just above the center of the

---

* This wave is, of course, not first in time of arrival when an air shock is present.

† Figure 6 of AFSWC-TDR-62-22, p. 32.

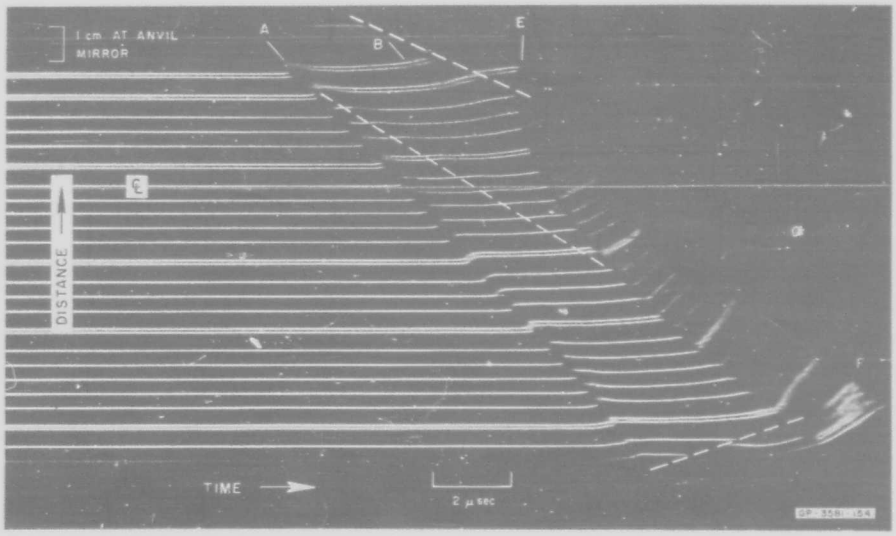

FIG. 29 SMEAR CAMERA RECORD, SHOT 9216 (U)

mirror but it apparently originates outside the vertical reflection zone of the mirror.

Foam thickness in Shot 9217 (Fig. 30) was 0.65 cm, intermediate to the thicknesses used in Shots 9155 and 9180. The first wave is still sharp, as in Shot 9155, and has approximately the same strength. The second wave appears but is later, weaker, (~1 kb) and more gradual than in Shot 9155. A trough follows the second wave. This may mean that rarefactions from the flyer begin to arrive before the double reflection of the second wave.

Four following experiments, Shots 9227, 9228, 9244, and 9296 (Figs. 31, 32, and 33), demonstrate the much different response of 20 lb/ft^3 polyurethane foam to an impact of 1.15×10^4 dyne-sec cm^{-2}. Foam thickness is 1.25 cm in Shot 9227, 1.0 cm in Shot 9228, 0.60 cm in Shot 9244 and 0.3 cm in Shot 9296.

There are only two waves in the records of Shots 9227 and 9228: the first or elastic wave, and the rarefaction from the bottom edge. Other waves were either not present in the anvil or the deflections produced by them were too small to be distingushed. We expected the elastic

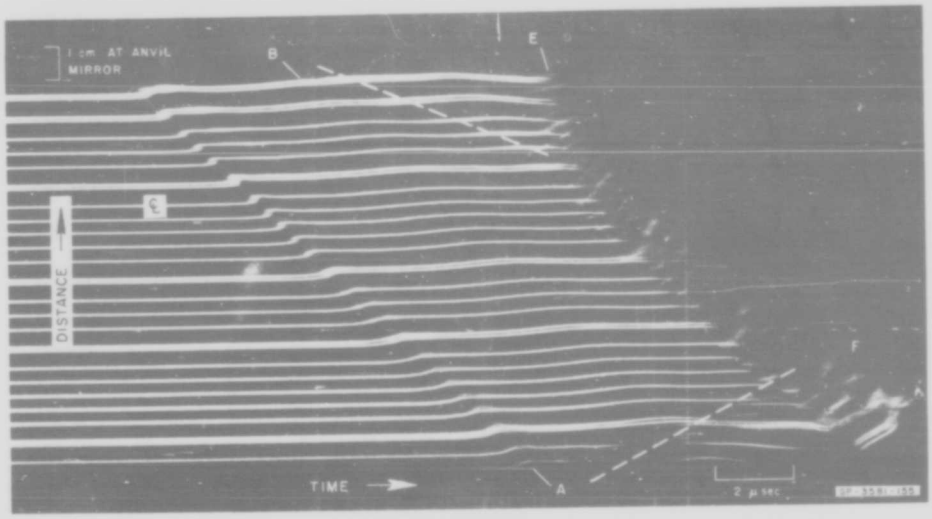

FIG. 30 SMEAR CAMERA RECORD, SHOT 9217 (U)

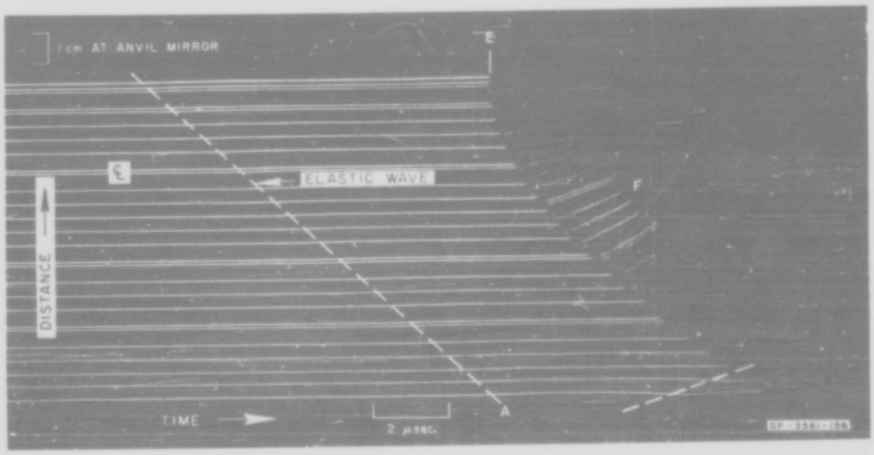

FIG. 31 SMEAR CAMERA RECORD, SHOT 9227 (U)

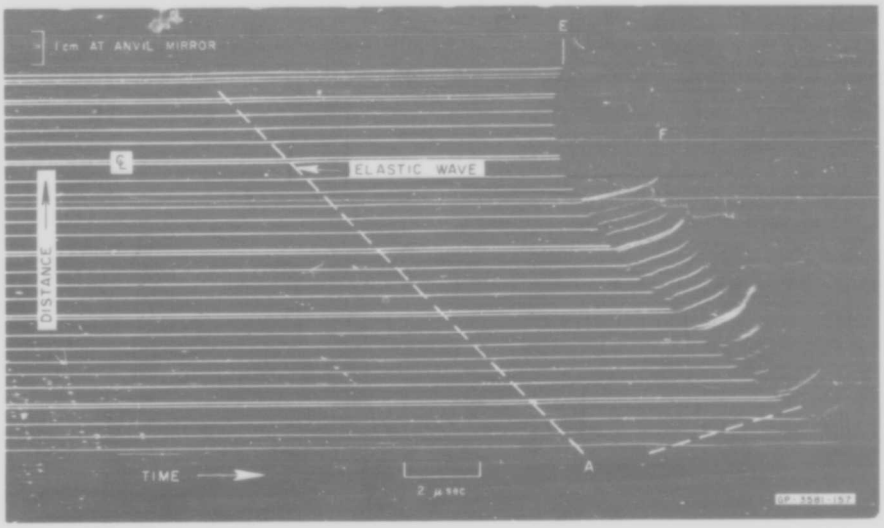

FIG. 32 SMEAR CAMERA RECORD, SHOT 9228 (U)

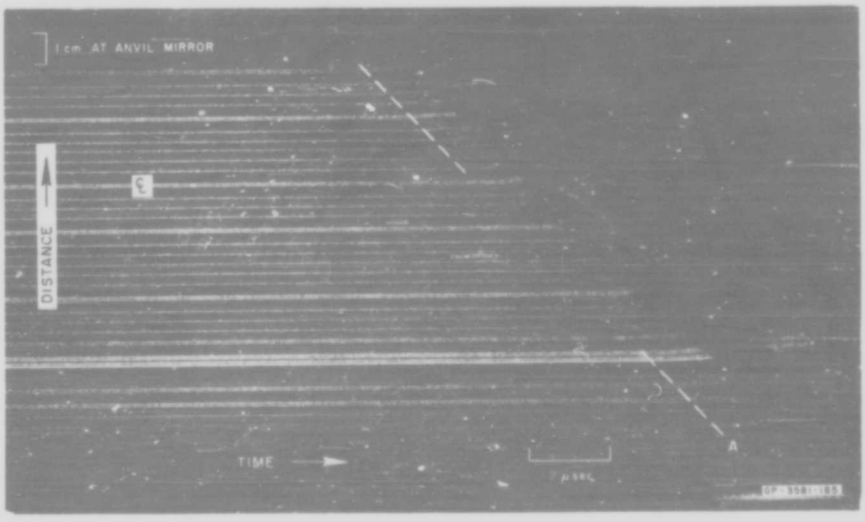

FIG. 33 SMEAR CAMERA RECORD, SHOT 9296 (U)

wave to be weaker and slower in the more distended foam than in the 40 lb/ft^3 foam,* and the records of Shots 9227 and 9228, reproduced in Figs. 31 and 32, show a first wave in the anvil between 0.1 and 0.2 kb in strength.

In Shot 9244 the target was thinner to allow the locking wave to reach the anvil, and we gained about 30% greater magnification of the image displacement by increasing the distance between anvil mirror and light source above the values shown in Fig. 2. (This required a field mirror between anvil and source, not shown in Fig. 2.) The experiment was only marginally successful because the film was improperly exposed and we have not attempted to reproduce the record here. We saw some indication however of the start of a second, or locking wave, about 3.6 μsec behind the first; the full deflection in the second wave never appeared, either because of poor film exposure or because the driver wave overran it.

To see more of the second wave, we cut the target for Shot 9296 only 0.30 cm thick. We were again not entirely successful with film exposure in the smear camera, but the record (Fig. 33) is better than that for Shot 9244. The first wave is again about 0.1 kb in strength. The second wave did appear and it may be stronger than any second wave seen before. There is a small region below the center line of the mirror where the first wave disappears from the grid lines reflected in that region; first motion there appears to be a part of the second wave. We think this is related to the manner in which a timing transducer was attached to the foam-anvil interface (see Section IV). Quantitative interpretation of the traces in the second wave is impossible because of instability in the mirror response and poor photographic exposure. The record shows plainly, though, that the duration of the second wave was short, about 1.4 μsec, after which period the traces appear to have returned to near their undeflected positions. Glimpses of the disturbed traces seem to indicate a steady fall preceding this return. If we assume, therefore, that the full momentum, less an allowance of 10 percent for the momentum in the first wave, appears in a triangular shaped second wave, we estimate the peak pressure to be:

$$p = \frac{1.0 \times 10^4}{1.4 \times 10^{-6}} \times 2 = 14.3 \text{ kb} .$$

* Acoustic speeds generally decline with distention. Table III, p. 66, AFSWC-TDR-62-22. Elastic yield stress also decreases with distention.

This is about the stress in the first driver impact (or E) wave, which is easily analyzed in most of our smear photographs.

Our system is probably incapable of recording on the same record two waves as different in strength as the first and second of Shot 9296.

Shot 9297, our only experiment with 60 lb/ft^3 polyurethane foam, produced an unusual smear camera record (Fig. 34). There is a strong, sharp, first wave of strength 4 to 5 kb followed by rarefactions (shown dotted) which have slightly less apparent speeds than the first wave and which we consider an edge effect. There is a strong, second compressional wave but the photograph is hard to read in that region. The second wave is everywhere followed by a sharp rarefaction which returns traces to near their original levels. The letter identifications of the waves in Fig. 34 are tentative. It is entirely possible the wave marked B is actually an elastic forerunner (A-wave) and that the wave designated C is not a reflection of the preceding off the flyer, but is a second, plastic or B-wave. The magnitude of the impulse in the first wave (marked B), approximately 1.5×10^4 dyne-sec cm^{-2}, favors the interpretation shown in the figure.*

Our first experiment with foamed silica (Shot 9325) showed that an impact of 1.15×10^4 dyne-sec cm^{-2} produced no forerunner in 4.25 mm of the material. The B-wave in the anvil was between 7 and 8 kb (Fig. 35). (The G-wave shown in the figure is regarded as spurious because it has a markedly lower apparent speed than expected for a wave front parallel to the rear anvil surface.) About 2 μsec after B-arrival pressure in the foam has returned to zero and delivered momentum about equals input, suggesting that rebound of flyer or foam, if it was present, carried little momentum. In Shot 9345 we impacted the same material, cut to about the same thickness, with 60% of the impulse.† The two waves are plain (Fig. 36). The first (A) is about 0.65 kb in the anvil; the second (B), about 1.6 kb strong, follows 4.2 μsec behind. There is some minor trace motion moving with the same apparent speed between the two waves. The E-wave ended observation before any relaxation of the foam was possible.

Our experiments with aluminum foam were not so successful as those described above, due to unfortunate choices of target thicknesses. The

---

* Impulse is estimated as time interval between loci of B- and C-waves times pressure represented by jump in B-wave. The rarefaction front (dotted in figure) is not regarded as a feature of the one-dimensional behavior of the foam.

† Achieved by reducing flyer thickness to 0.012 inch.

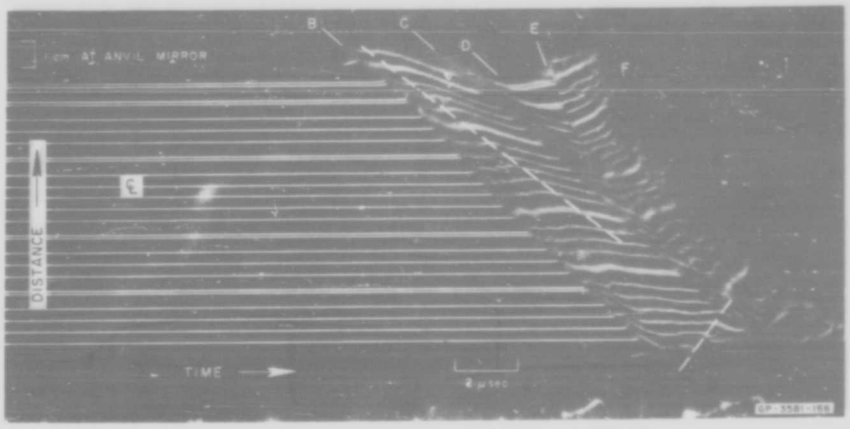

FIG. 34 SMEAR CAMERA RECORD, SHOT 9297 (U)

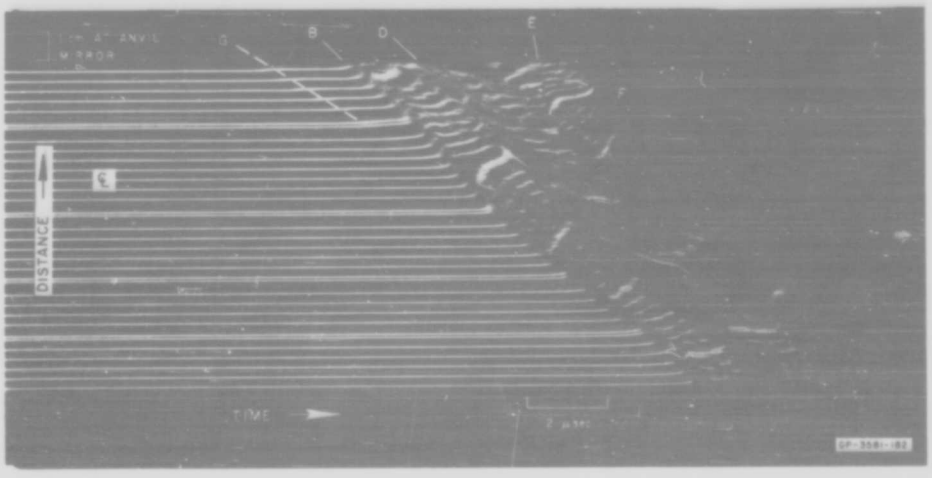

FIG. 35 SMEAR CAMERA RECORD, SHOT 9325 (U)

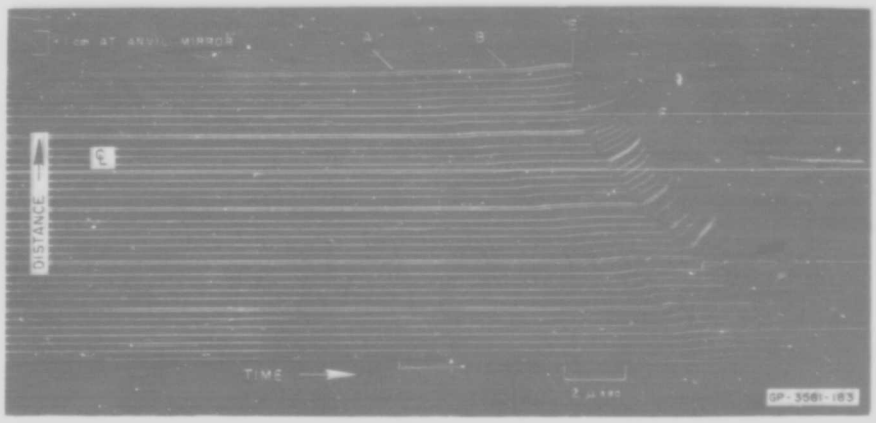

FIG. 36 SMEAR CAMERA RECORD, SHOT 9345 (U)

first, in 1.4 g cm open cell foam 2 mm thick struck by a 1.15×10^4 dyne-sec cm^{-2} impulse (Shot 9324) showed an apparently very strong, very brief B-wave. The photograph is blurred (Fig. 37) and only certain time intervals can be measured accurately. There are ambiguous signs of a two wave structure, probably B- and C-waves. Assuming a single triangular pulse between the B- and D-disturbances (which are about 2 μsec apart) we calculate a peak pressure due to the input impulse of about 10 kb. If the two waves are present, this is a serious underestimate.* A thicker slab (3.5 mm) of lighter material (0.75 g cm^3) impacted with the same flyer (Shot 9329) gave the peculiar smear record seen in Fig. 38 where we have not attempted to assign the customary letter designations to the several waves, but, for the time being, have called them G-, H-, I-, and J-waves. The H-, I-, and J-structures have the same apparent speed; possibly the H-wave is a gradual A-front between 0.5 and 0.6 kb strength; but we can not identify the sharp I-wave (~2.3 kb) nor the gradual J-disturbance (~1.5 kb). The G-wave with an apparent speed of about 2/3 that of H, I, and J has the appearance of an edge effect originating off a vertical line on the mirror drawn through the reflection zone, but its strength is unusually large. The E-wave overruns all its predecessors in a region just below mirror center; however the G- and I-waves connect smoothly with waves between the E- and F-breaks and seem

* The blurring of the traces in Fig. 37 may be due to permanent impairment of the reflecting surface of the anvil by a very strong shock. If this is so, the B-wave in this experiment must be considerably stronger than 15 kb since the E-wave in other shots does not cause similar impairment.

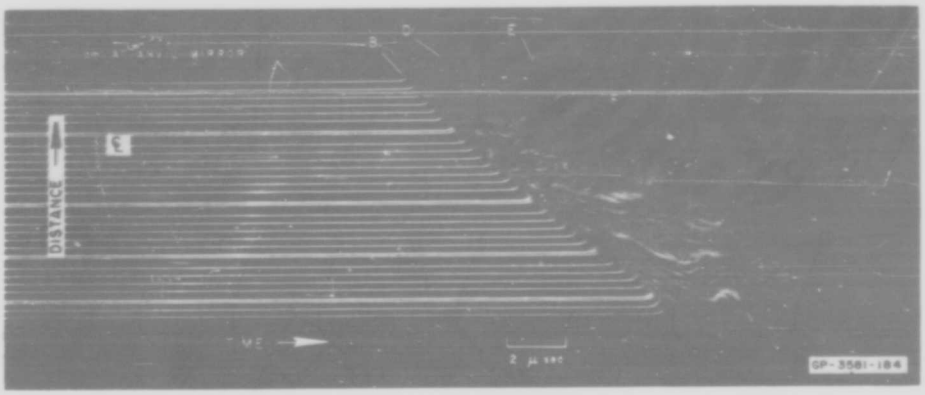

FIG. 37 SMEAR CAMERA RECORD, SHOT 9324 (U)

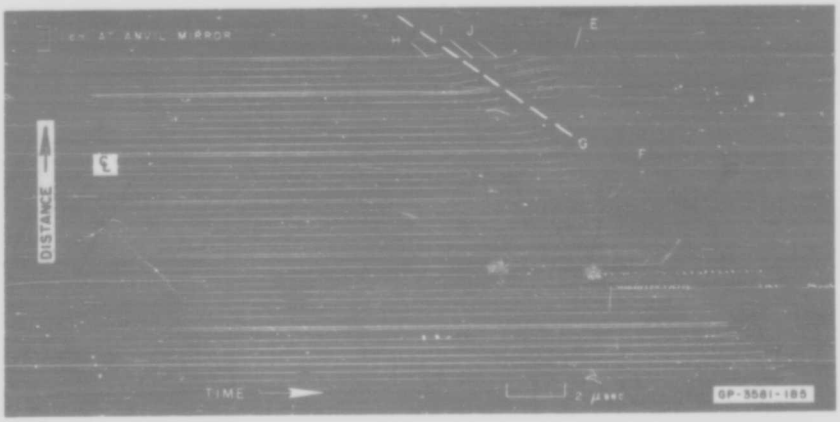

FIG. 38 SMEAR CAMERA RECORD, SHOT 9329 (U)

to go on at their previous apparent speed in that area of the record. We compare this phenomenon with the appearance of small waves between the E- and F-loci of Fig. 26, Shot 9155.

A second impact (Shot 9344) of the same foam cut 30% thicker (4.5 mm) produced an incomplete film record because of faulty exposure, but the photograph does show a slightly larger time interval between the E- and E-waves in the mirror area below the center. The first wave is approximately the same strength as in Shot 9329. Traces above the center were lost.

In Shot 9328 we applied an impulse of 1.15×10^4 dyne-sec cm^{-2} to 6.0 mm of foamed graphite about 1.5 g/cm^3 dense. There are two waves, an F and probably a B. The latter blurred the record beyond reading in the region following it.

The intelligibility of these experiments depends upon a reproducible, known flyer speed. If flyer acceleration stems from the impact of two waves characteristic of the driver material, any explosive charge large enough to induce the two characteristic waves ought to lead to the same flyer speed. (And, as mentioned earlier, this speed will be independent of flyer thickness.) Any charge smaller than this minimum would not induce the stronger of the two characteristic waves in the driver; flyer speed would be less than expected and may vary from shot to shot because of small differences in the explosive. Although two earlier experiments, Shots 9097 and 9098, yielded flyer speeds consistent with each other, we fired Shot 9245 to be sure the explosive charge used in the preceding experiments was above the minimum. We put two slabs of Baratol, each 2 inches thick, between the P-80 plane-wave generator and the driver, and observed the impact of the 0.020-inch-thick aluminum flyer on a glass plate coated with stripes of reflecting gold. The experiment was generally similar to Shots 9094, 9097, and 9098 described in Section D above.

We did hope in the new experiment, however, to observe reflections in the surfaces of both the flyer and driver during flight and to record separately arrivals of flyer and driver at two offset mirrors.* The smear camera record (Fig. 39) is puzzling for it seems to show the driver overtaking the flyer. We see the steel elastic wave arrival at the driver surface (marked B in the figure) and at the flyer surface (G), first motion of the flyer (A), driver impact at its target mirror (C), and flyer arrival at its target (D). But there are changes in the reflection off the flyer during flight (F) and an apparent spread of shock disturbance (E)

* There was a hole in the flyer to allow it to pass over the first, or driver, mirror without disturbing it.

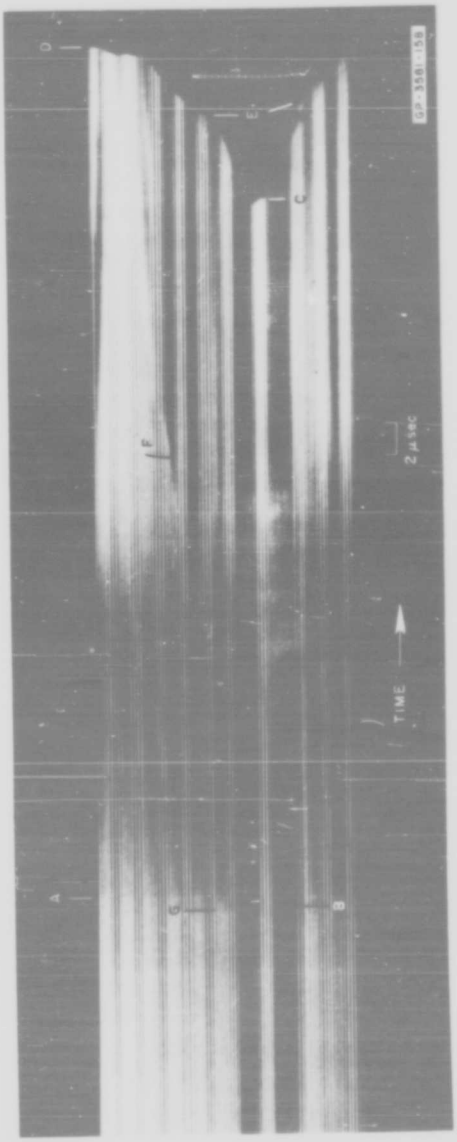

FIG. 39 SMEAR CAMERA RECORD, SHOT 9245 (U)

from the first to the second target. Impact at the two targets would have been simultaneous had the driver and flyer behaved as previously (when no Baratol was used). The cut-off in reflections at driver target (C) and and the changes (marked F) both seem to show the influence of the strong curvature of the driver.

Average driver speed across the gap was 0.728 mm/μsec—about the same as in Shot 9094 when no Baratol was used—and as reported by Bancroft *et al.*[6] when Baratol was used with the P-80. Flyer speed was seemingly less than this in contradiction of our earlier results. (Bancroft *et al.* did not observe the speed of a spalled flyer.) Although we doubted the validity of such a perplexing record, the outcome of this experiment led us to make special measurements during succeeding flying-plate, foam-impact experiments which showed that when Baratol was not added flyer speed was almost constant at the expected value. We will discuss these measurements in subsection F. If the shock wave induced in the driver by the Baratol has and retains an unusually* long rise-time, the peak pressure may not be able to influence flyer motion; that is, flyer and driver may finally separate before pressure rises fully to that in the second characteristic wave in steel (~130 kb).

F. MEASUREMENT OF FLYER AND WAVE SPEEDS

During some of our flying-plate experiments we tried by means of electrical signals placed on a raster oscilloscope to observe flyer flight time and first wave transit time in the foam. The signals for these purposes came from switches and from a PZT transducer arranged in the vacuum tank as sketched in Fig. 40. Trigger to start the raster sweep came from the firing circuit; the PZT sensed the motion of the driver free surface about 30 μsec later; the flyer completed the electrical circuit containing the first switch and allowed a capacitor to discharge through a resistor; and when the foam moved into the anvil the contacts of the second were closed. A typical sequence of signals appears in Fig. 41.

Flyer speeds measured in this way were fairly consistent (Table VIII). Their average was about 5% higher than the average result of Shots 9097 and 9098. A number of apparently extraneous signals appeared in the

* Compared to that of the wave induced in the driver by the explosive lens without the Baratol layer, i.e., by Composition B, which forms the terminal element of the P-80. The slope in front must persist during the one-inch-long transit of the driver.

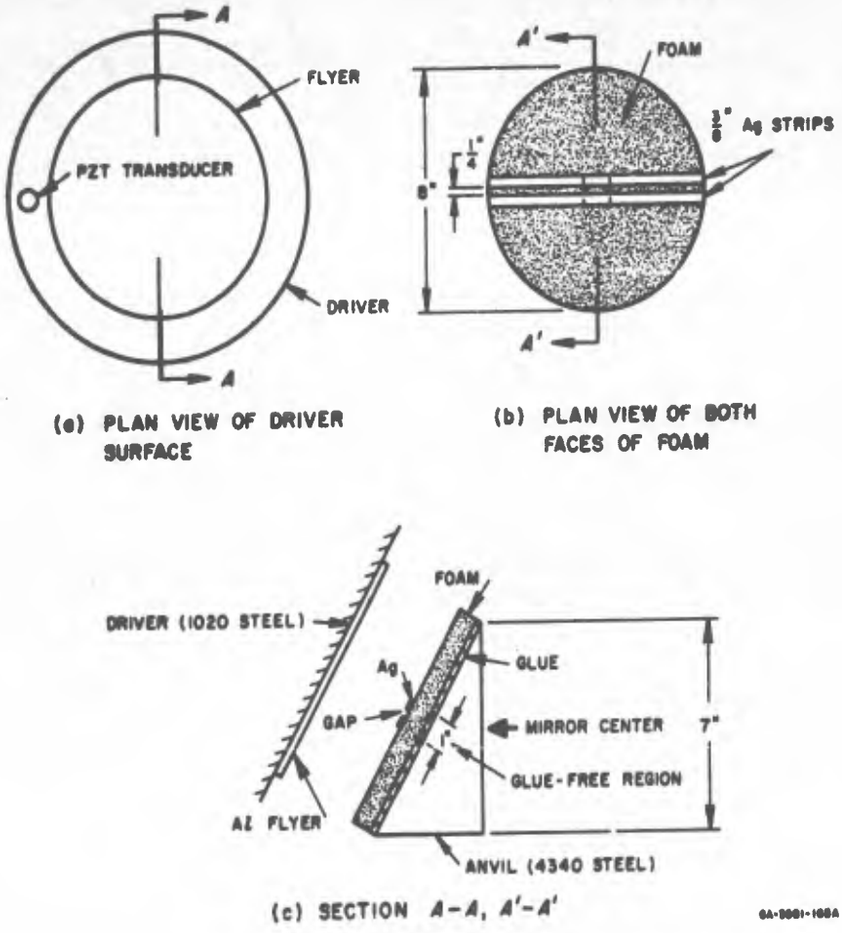

(a) PLAN VIEW OF DRIVER SURFACE

(b) PLAN VIEW OF BOTH FACES OF FOAM

(c) SECTION $A-A$, $A'-A'$

FIG. 40 SCHEMATIC DRAWING OF DEVICES FOR OBSERVING ARRIVAL TIMES, SHOTS 9296 AND 9297 (U)

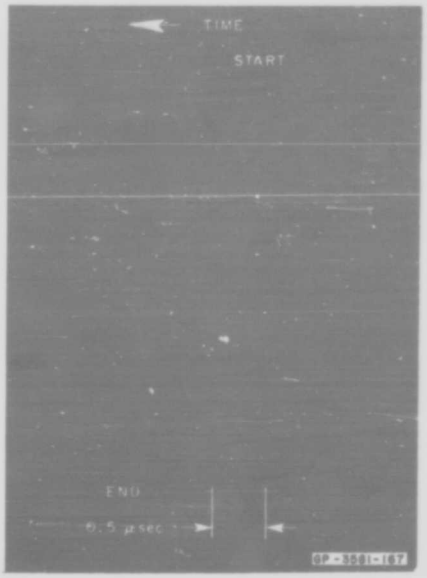

FIG. 41 RASTER OSCILLOSCOPE TRACE, SHOT 9297 (U)

Table VIII

FLYER AND WAVE SPEEDS MEASURED BY RASTER OSCILLOSCOPE

SHOT NO.	TARGET MATERIAL	DISTANCE FLYER TO FOAM (mm)	FLYER TIME OF FLIGHT (μsec)	FLYER SPEED (mm/μsec)	THICKNESS OF FOAM (mm)	WAVE TRANSIT TIME (μsec)	AVERAGE WAVE SPEED IN FOAM (mm/μsec)	PRESUMED IDENTITY† OF WAVE CLOSING SECOND SWITCH
9296	Polyurethane 20 lb/ft^3	44.12 ± 0.10	52.45	0.841	3.02 ± 0.05	1.59	1.87	*A*
9297	Polyurethane 60 lb/ft^3	43.99 ± 0.10	52.35	0.840	3.05 ± 0.05	1.9	1.60	*B*
9324	MD-AO 1.4 g/cm^3	44.48	51.31	0.867	1.98	2.58	0.767	*B*
9325	Eccofoam Si 1.1 g/cm^3	44.73	53.40	0.838	4.14	2.37	1.745	*B*
9328	Graphite 1.5 g/cm^3	44.09	50.35	0.876	5.66	0.96	5.90	*B*
9329	MD-AO 0.74 g/cm^3	44.32	52.79	0.840	3.43	signal lost*	--	*E**§
9345	Eccofoam-Si 1.1 g/cm^3	44.20	49.13	0.900	4.56	2.94	1.55	*A*
				Average 0.857 ± 0.022				

* Driver-wave overtook flyer-wave in the foam; failure of second switch may be due to unusually high strength of activating wave.

† See classification scheme on pages 38-39.

§ First switch in all cases presumably closed by flyer.

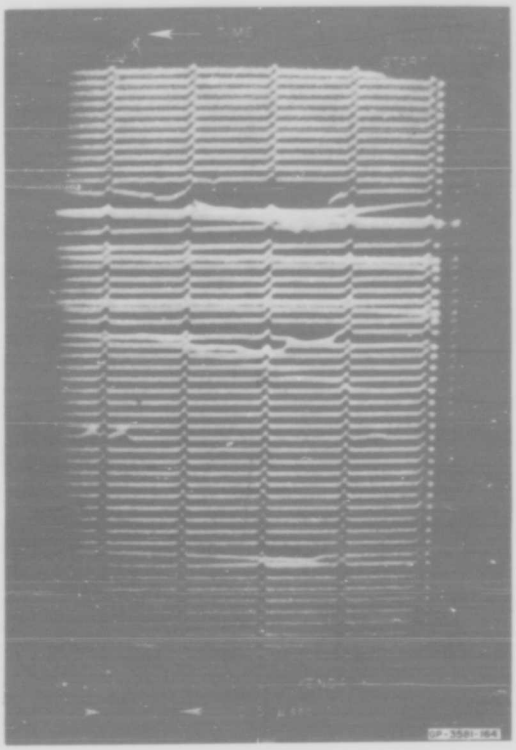

FIG. 42 RASTER OSCILLOSCOPE TRACE,
SHOT 9296 (U)

raster traces, as may be seen, for example, by contrasting Figs. 41 and 42; nearly all the signals last a significant length of time. For these reasons we hold optical measurements more reliable and use their result, *i.e.*, 0.82 mm/μsec, in calculations of impulse.

The average wave speeds based on the electrical measurements, which are also entered in Table VIII, are probably even less reliable than flyer speeds because the transit time is short compared to signal length. Only two entries relate to the elastic forerunner (A-wave); the first, in 20 lb/ft^3 polyurethane (Shot 9296), is considerably higher than sound speed (1.30 mm/μsec)[8] which is unusual; the second, in silica-foam

(Shot 9345), is also higher than sound speed in that material (1.35 mm/μsec)[6] but less so than the first. The assumptions are implicit in these two cases that the A- and B-fronts separated at the foam-flyer interface and that the second switch closed as soon as the wave had passed through the foam. As will be seen in Section VI, the first assumption is generally good only if A-wave speed is near sound speed; if it is considerably lower, separation does not occur immediately and the entries in Table VIII, column 8, may be considerably higher than true A-wave speed. The second assumption may lead to an overestimate of transit time of at most a few tenths of a μsec, which will lead to an underestimate of wave speed of 10 to 20%.

Table VIII shows a value of 1.60 mm/μsec for B-wave[4] speed in 60 lb/ft^3 polyurethane (Shot 9297); sound speed in this material is 2.0 mm/μsec.[6]

We do not at present put much value on these measurements of wave speeds in foam.

In sharp contrast to the dubious method of wave speed observation presented above, an optical technique has produced quite satisfying measurements of elastic wave speed in 39 lb/ft^3 polyurethane. Here we used the usual optical lever with the smear camera but the mirror was a flat, thin plate of hardened steel glued to the oblique face of a wedge of foam (Fig. 43). We established a plane wave front in the foam with sheet explosive and photographed the movement of images in the mirror after the wave entered in the steel slab. Figure 44, a cross-section through the apparatus, shows the elastic wave reverberating in the steel layer. We read the speed of point P from the smear record and assumed this to be the speed of Q, which, combined with the detonation speed provided by the pin switches in the explosive and the carefully measured value of the angle θ, yielded wave speed in the foam. For our first trial (Shot 9431) we used sheet explosive 0.020 inch thick and a wedge angle θ of 17° 10′; we repeated the measurement with 0.050 inch of explosive and an angle of 24° 10′. Figures 45 and 46 reproduce the smear photographs. The traces marked ℄ are reflections from the mirror area near the fiducial mark (Fig. 43) where the wave had passed

[4] Tentative identification. See page 47 .

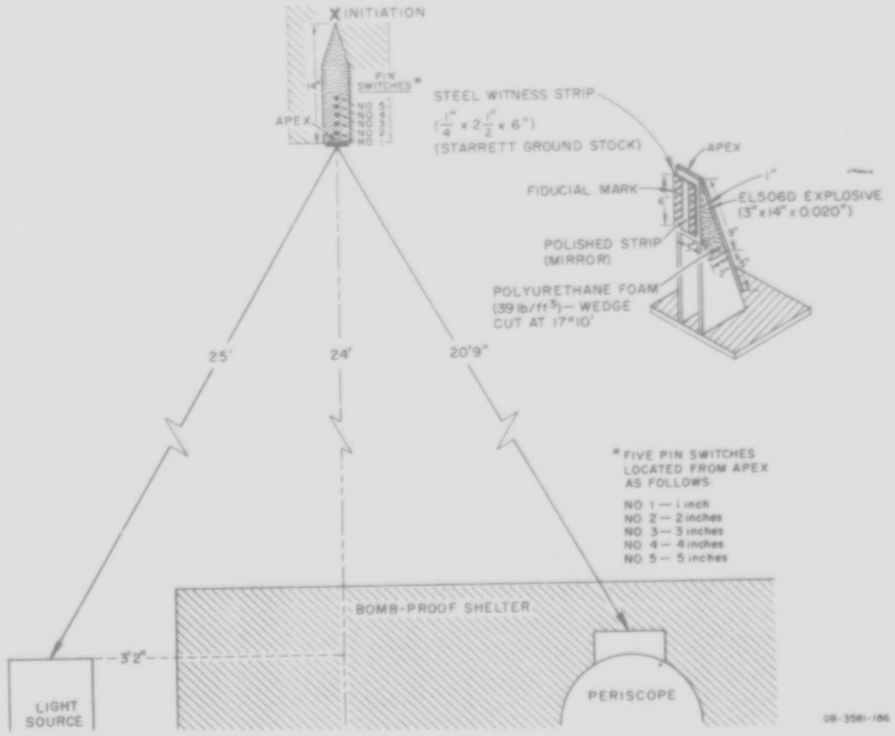

FIG. 43 EXPERIMENTAL ARRANGEMENT FOR MEASUREMENT OF WAVE SPEED IN A WEDGE BY THE OPTICAL LEVER (U)

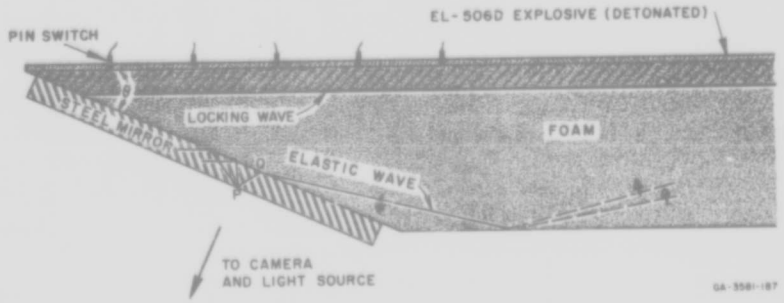

FIG. 44 MEASUREMENT OF WAVE SPEED IN A FOAM WEDGE (Cross Section), SHOT 9432 (U)

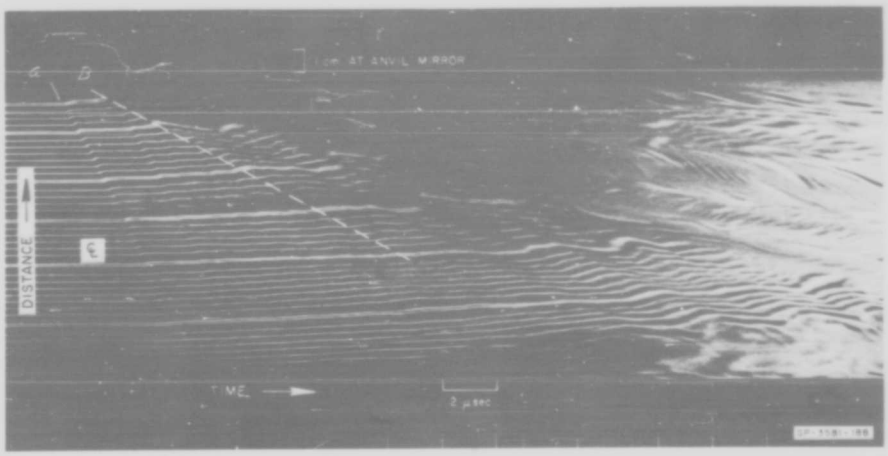

FIG. 45 SMEAR CAMERA RECORD, SHOT 9431 (U)

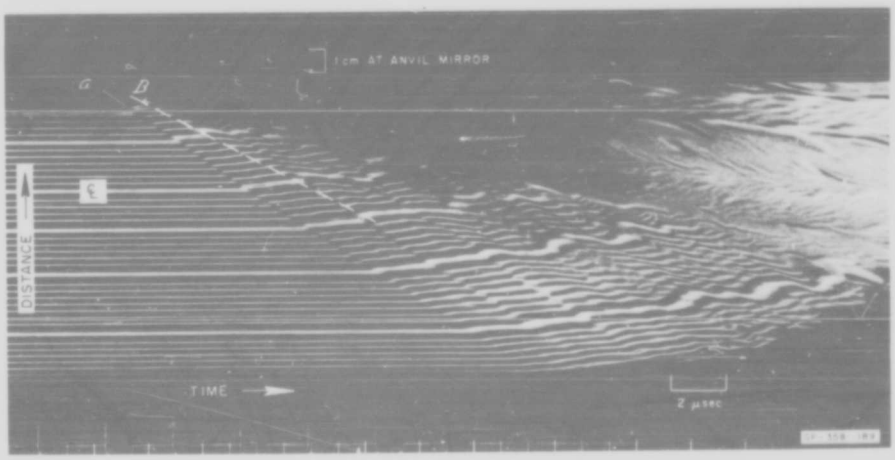

FIG. 46 SMEAR CAMERA RECORD, SHOT 9432 (U)

through approximately one inch of foam. The locus A marks the arrival of the elastic wave and the following loci of similar slope are due to reverberations of this wave in the steel. Sound signals or edge effects from the top of the mirror travel more slowly down the face and leave traces such as B. Most of the slower disturbances (as contrasted to reverberations) seem to die out before reaching the bottom of the photographed region. The locking wave probably does not strike this part of the steel but its effects are undoubtedly transmitted down the mirror and seen in the record long after the passage of wave A.

In both figures the slope of the first locus is nearly constant over almost 5.0 cm of the mirror near the top. Apparent speeds here are 26.6 mm/μsec (Shot 9431) and 7.96 mm/μsec (Shot 9432). Using the average values of detonation speed measured by the pin switches, 7.25 mm/μsec and 7.23 mm/μsec, respectively, we compute elastic wave speeds of 1.63 and 1.585 mm/μsec, respectively, or an average of 1.60 ± 0.02 mm/μsec.

The detonation speed in any one shot is unsteady by less than 2%.

In both Figs. 45 and 46 the trace displacements become markedly less sharp and more gradual as the reflection zone becomes lower, i.e., as the wave travels through more foam. In Fig. 46 (Shot 9432) this gradualness is manifested at first as less overlap of original and displaced trace instead of as a gentle rise to the displaced level as in Fig. 45 (Shot 9431). When mirror object and its reflection zone are in a plane with the line of sight to the camera, as in these two experiments, a pressure wave of step-like profile will cause the same amount of overlap regardless of its strength. We concluded there is a change in wave shape during our observations. We saw the same effect in one-dimensional impacts (Shots 9155 and 9180), but there were no indications there of an accompanying change in peak pressure in the wave. However, Shots 9431 and 9432 do show a gradual pressure fall as the A-wave moves through more and more foam. We report on this behavior on page 74.

IV ANALYSIS OF FREE SURFACE MOTION

A. THEORETICAL BACKGROUND

Fowles[3] has calculated the normal stress P in a dilatational elastic wave from the turning angle of an oblique free surface. If we apply his results to waves induced in our wedge anvil and observed by the optical lever, we find the following formulas:

$$\sin \theta = \frac{U_s}{U_e}$$

$$\cos \delta = 1 - \frac{2\nu - 1}{\nu - 1} \sin^2 \theta$$

$$\psi = \frac{\sin \delta \cos \theta + \cos \delta \sin (\theta - \delta)}{\sin 2\theta}$$

$$P = \rho_0 U_s U_e \frac{s}{2d_\perp} \psi \sec \delta \quad .$$

In these expressions U_s = dilatational elastic velocity in witness plate (6.06 mm/μsec), ν = Poisson's ratio for the anvil (0.29), U_e = apparent speed of wave along mirror surface, ρ_0 = original density of anvil (7.8 gm/cm^3), s = displacement of image of light source in anvil mirror, and $d_\perp$ = perpendicular distance from light source to mirror. The quantity U_e is the slope of the locus of first motion of the traces in the film multiplied by

$$f_g \left(\frac{l_w}{l_w + l_g} \right) \frac{1}{f_t}$$

where f_g is the ratio of distance on the grid light source to vertical distance on the film reader screen; f_t, the ratio between elapsed time and horizontal distance on the screen; l_w and l_g are distances from objective lens to wedge and from wedge to grid light source, respectively. The quantity s is the trace displacement on the screen multiplied by f_g.

Angle θ_n, the (acute) angle between the wave front and the free surface, will, of course, vary during an experiment if the wave front is not perfectly flat. We can find the approximate shape of the wave (assuming it does not change greatly during its interaction with the surface) by measuring angle of incidence θ_n at each of many distances z_n along the reflection zone of the mirror. Thus, if z' is distance perpendicular to the back face of the wedge (whose angle is 30°) coordinates of successive points (z'_n, z'_n) in the front will be given by:

$$z'_N = \sum_{n=1}^{N} (z_n - z_{n-1}) \tan\left(\frac{\pi}{6} - \theta_n\right) \cos\frac{\pi}{6}, \qquad \begin{matrix} n = 1,2,\ldots,N \\ N = 1,2,\ldots \end{matrix}$$

$$z'_N = z_n \cos(\pi/6)$$

Here obviously z' is a distance parallel to the back face of the wedge. In all our one-dimensional experiments we measured the wedge angle and used the exact value in the formulas above even though it never differed from 30° by more than 30'.

In the analysis of two-dimensional experiments we arbitrarily define "wedge angle" to be

$$\sin^{-1}\frac{U_s}{U_d} .$$

In our one-dimensional experiments wave divergence and convergence may affect the observed stresses significantly. Flyer curvature is severe enough (Figs. 15 and 16) to cause its impact wave in the anvil to have a curvature of radius about 200 mm. Since diminution or increase of strength in a spherically diverging or converging wave goes in the near region approximately as reciprocal distance squared,* we might expect weakening or strengthening of the wave in the clear area of the wedge to be more than 30%.

* Bolsg, Jardetsky and Press,[9] show a solution for elastic displacement due to a disturbance in a spherical cavity of radius R_0. Differentiating this with respect to radius R we find two terms for stress, one depending on $1/R^3$ and one on $[3(1+\sqrt{3})/8R_0]$. If we take the radius of curvature of the flying plate impact wave as R_0 we see that the dependence of stress on distance is more nearly $1/R^2$ than $1/R$ in the region of the mirror face of the anvil.

B. PRESSURE DISTRIBUTIONS IN THE ANVIL DUE TO FIRST OR A-WAVE

With every trace motion in a wave we associate three numbers*: horizontal and vertical coordinates, and displacement. The coordinates are replaced by an eighth degree polynomial fit by the method of least squares; displacement is similarly reduced to a function of position on the mirror. From these two curves we derive the quantities necessary in the calculation set forth in subsection A above.

We applied this analysis to all our foam impact experiments except Shots: 9181 (flyer in air), 9244 (0.6 cm of 20 lb/ft^3 polyurethane), 9296 (0.3 cm of 20 lb/ft^3 polyurethane), 9324 (1.4 g/cm^3 Al), 9238 (1.5 g/cm^3 graphite), and 9344 (0.45 cm of 0.75 g/cm^3 Al). In all these cases except the first, the photograph was unsuitable.

Figures 47 through 64 present the distributions and configurations we were able to find. The arrow in each figure along the z'-axis marks the approximate location of the foot of a perpendicular to the back face of the wedge which passes through the center of the reflection zone of the mirror.

For two-dimensional experiments we present a fictitious "wave configuration" found by attributing the surface motion to a wave moving obliquely into the mirror from a steel half-space. There are arrows along the z' axes in only two cases, Figs. 57 and 58; these mark the approximate location of the point on the rear surface of the mirror reached by a wave after travelling through one inch of foam.

Between the points ABC along the configuration curve in Fig. 47, the average radius of curvature is between 150 and 250 mm, and the departure from simultaneity of arrival of such a wave at a plane parallel to the back face would amount to about 0.5 μsec in steel. We may reasonably suppose that the flyer configuration shown in Figs. 15 and 16 is responsible for such a wave shape. Consequently, we read the true pressure in the wave (in steel) represented in Fig. 47 as very close to 1.0 kb; that is, we believe the section of the pressure distribution curve $B'C'$ stems from a part of the wave having slight curvature.

*Read from the image of the 35-mm film negative projected by a Vanguard model 7½-inch wide-angle screen film reader. Magnification in the reader is about 5x.

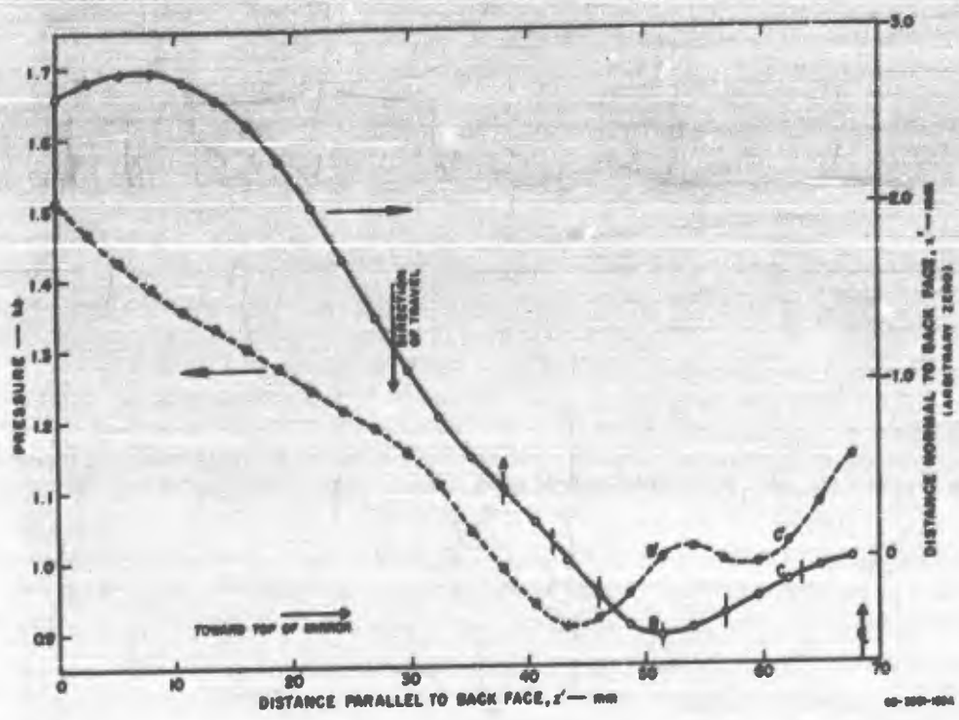

FIG. 47 STRESS DISTRIBUTION AND WAVE CONFIGURATION OF ELASTIC WAVE IN ANVIL, SHOT 9155 (U)

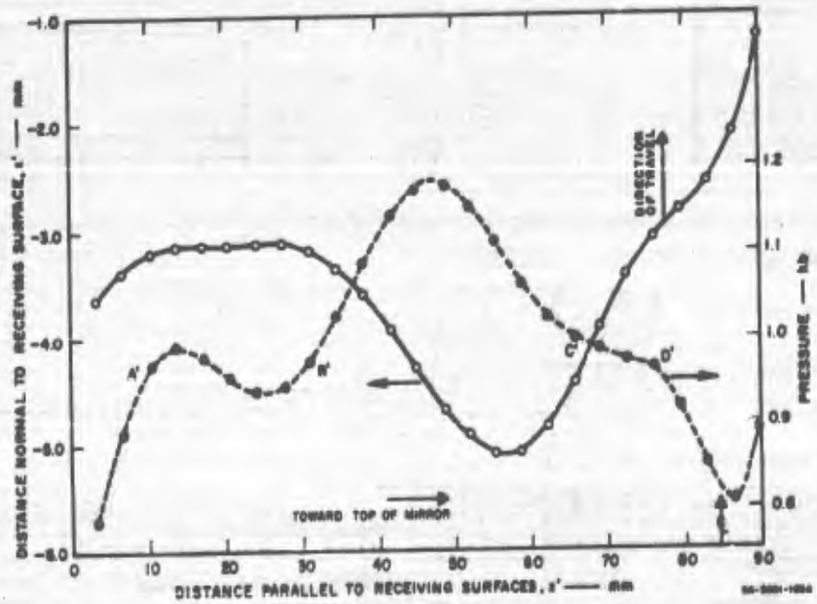

FIG. 48 PRESSURE DISTRIBUTION AND WAVE CONFIGURATION, ELASTIC WAVE IN ANVIL, SHOT 9180 (U)

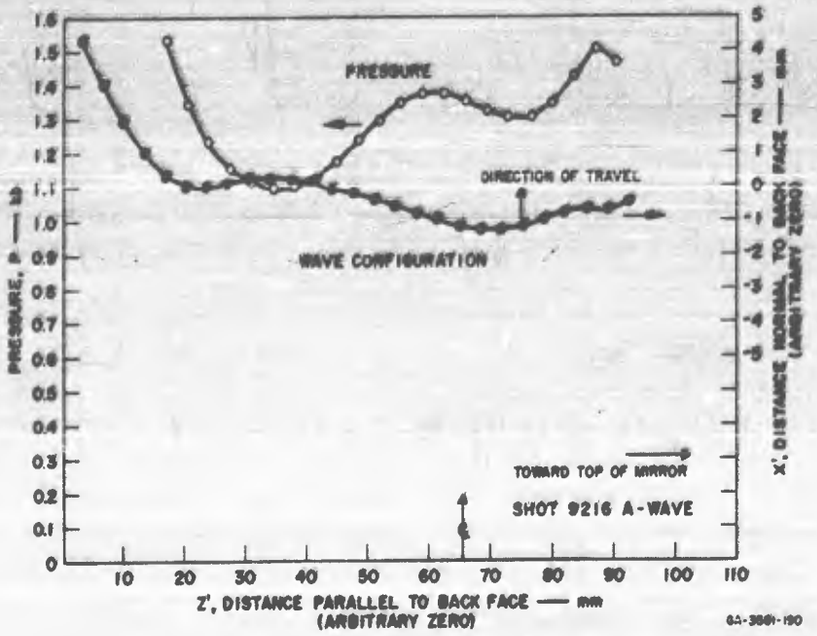

FIG. 49 PRESSURE DISTRIBUTION AND WAVE CONFIGURATION, ELASTIC WAVE IN ANVIL, SHOT 9216 (U)

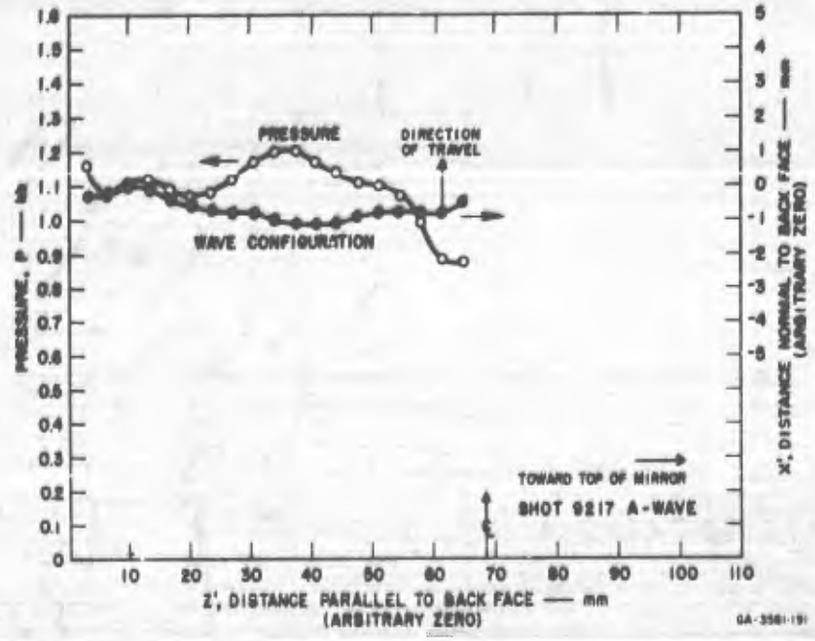

FIG. 50 PRESSURE DISTRIBUTION AND WAVE CONFIGURATION, ELASTIC WAVE IN ANVIL, SHOT 9217 (U)

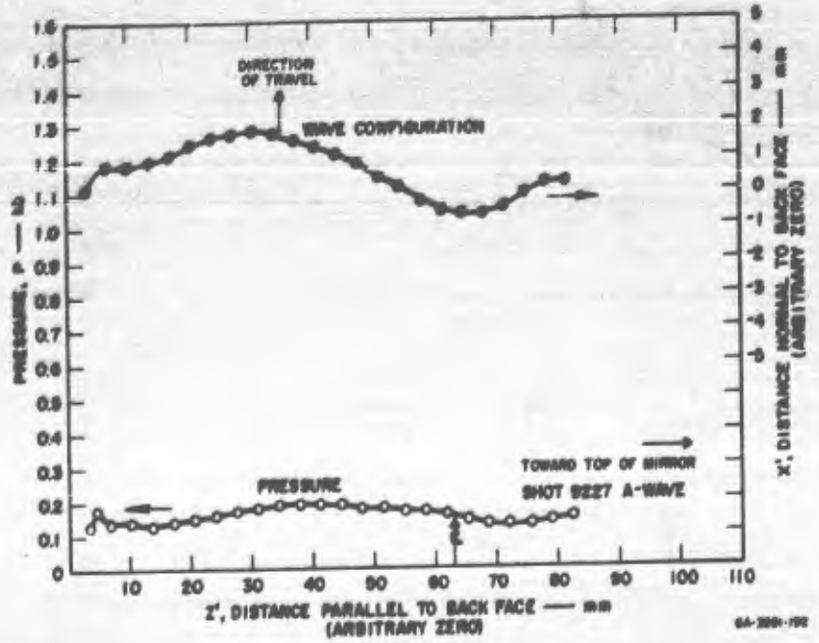

FIG. 51 PRESSURE DISTRIBUTION AND WAVE CONFIGURATION. ELASTIC WAVE IN ANVIL, SHOT 9227 (U)

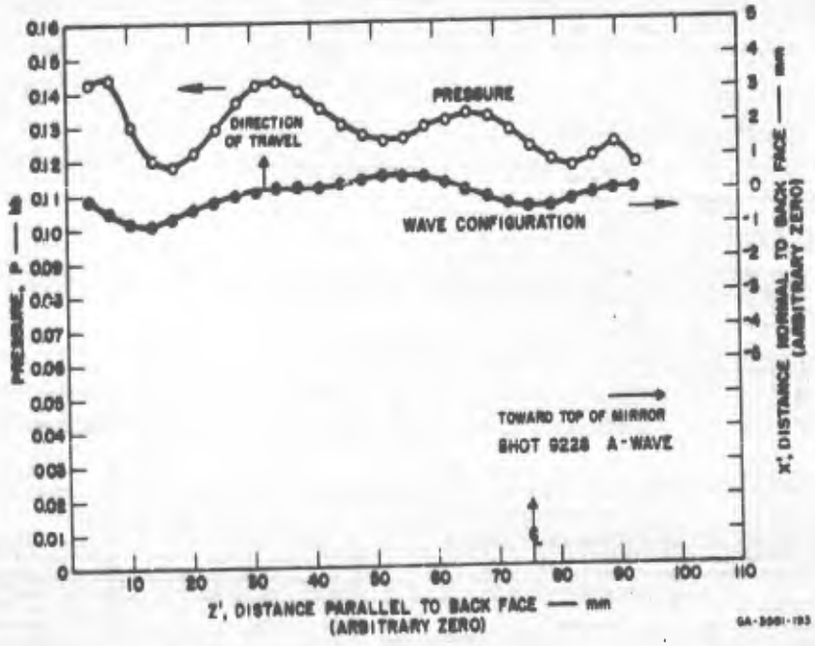

FIG. 52 PRESSURE DISTRIBUTION AND WAVE CONFIGURATION, ELASTIC WAVE IN ANVIL, SHOT 9228 (U)

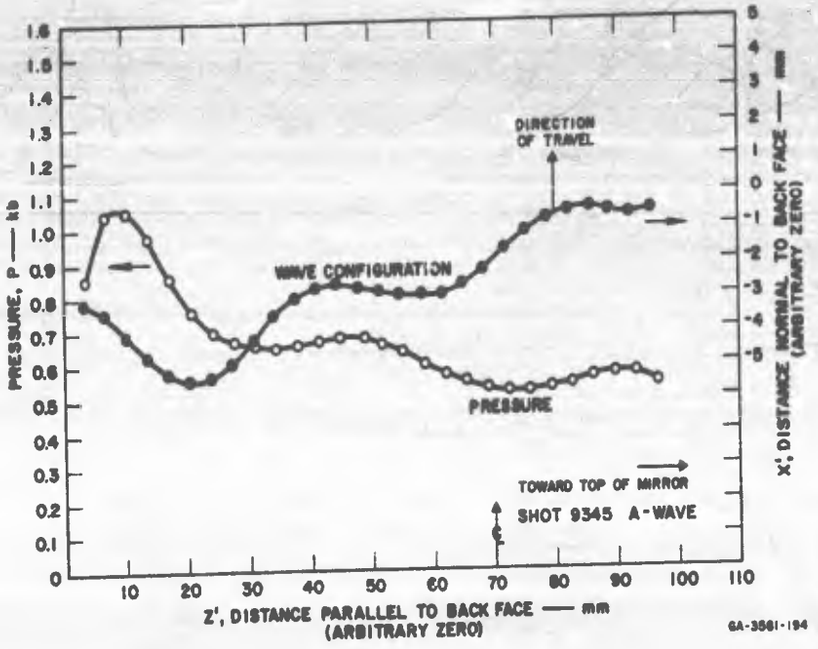

FIG. 53 PRESSURE DISTRIBUTION AND WAVE CONFIGURATION, ELASTIC WAVE IN ANVIL, SHOT 9345 (U)

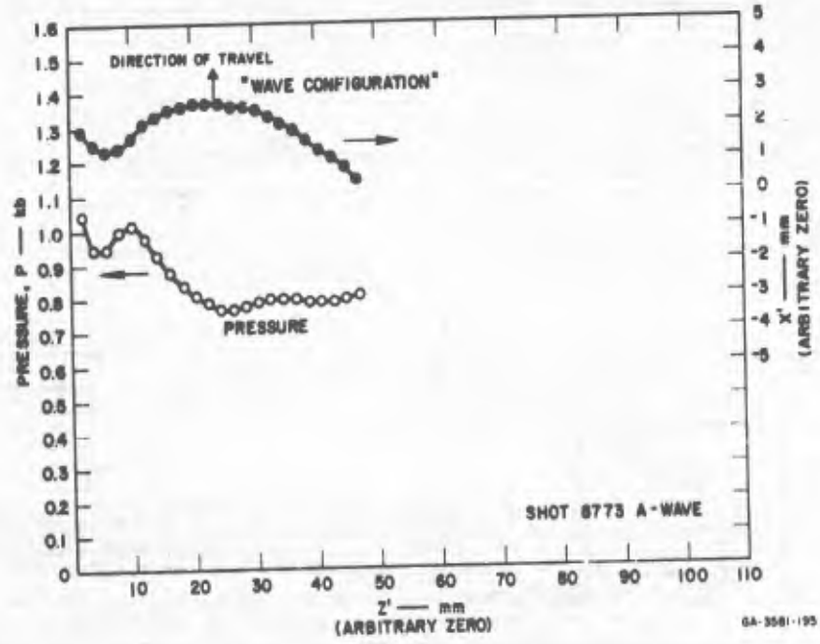

FIG. 54 PRESSURE DISTRIBUTION AND "WAVE CONFIGURATION," ELASTIC WAVE IN ANVIL, SHOT 8773 (U)

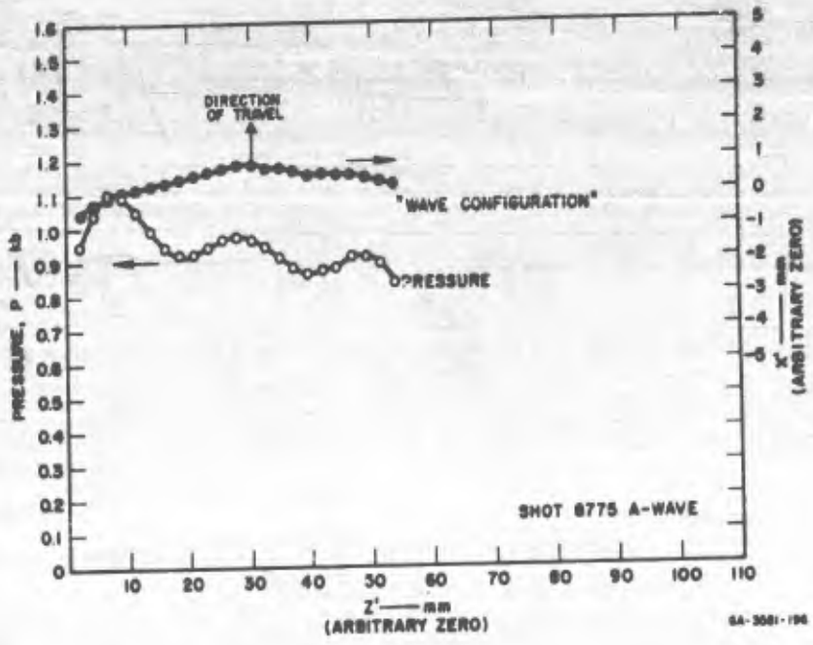

FIG. 55 PRESSURE DISTRIBUTION AND "WAVE CONFIGURATION," ELASTIC WAVE IN ANVIL, SHOT 8775 (U)

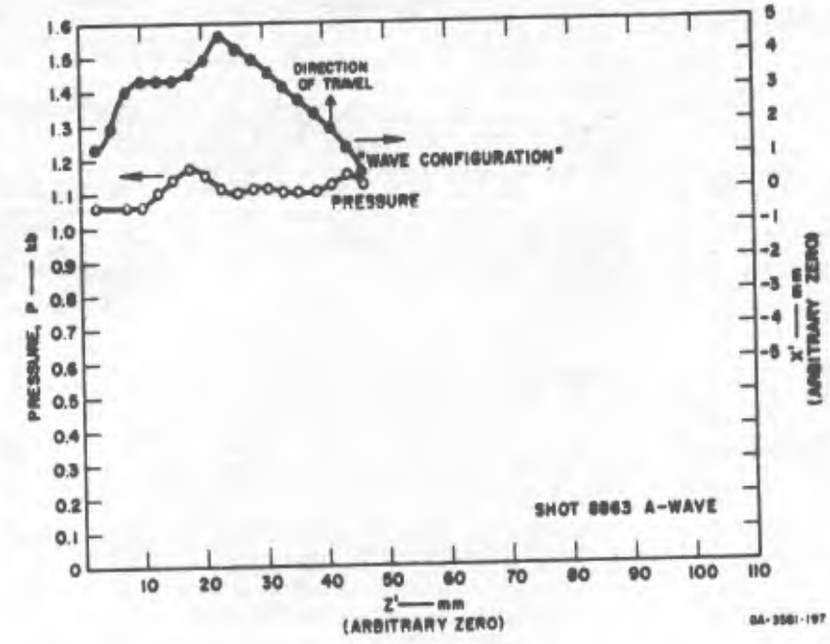

FIG. 56 PRESSURE DISTRIBUTION AND "WAVE CONFIGURATION," ELASTIC WAVE IN ANVIL, SHOT 8863 (U)

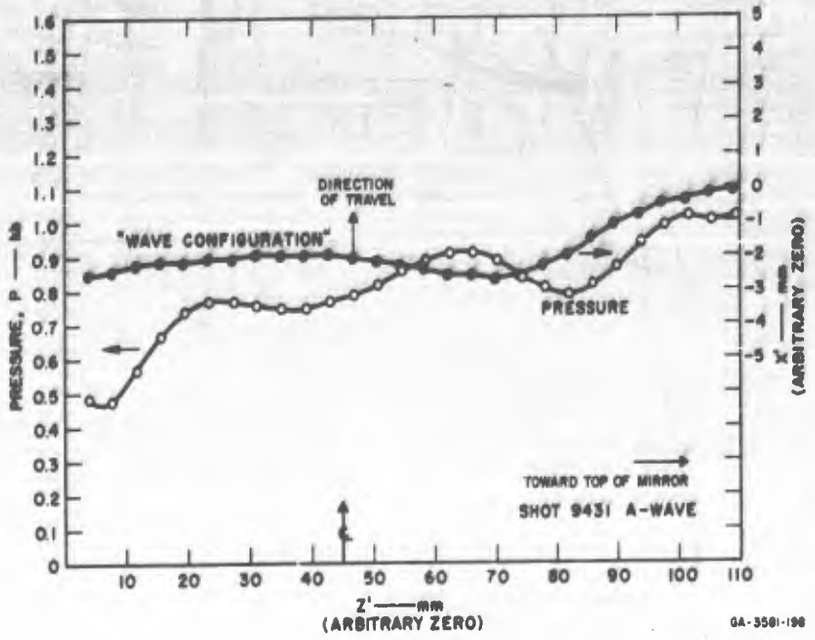

FIG. 57 PRESSURE DISTRIBUTION AND "WAVE CONFIGURATION," ELASTIC WAVE IN ANVIL, SHOT 9431 (U)

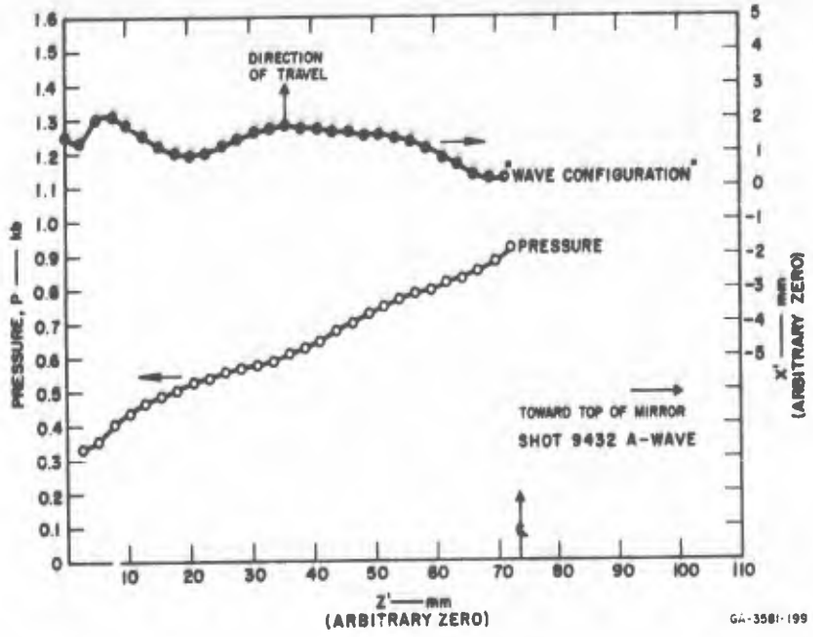

FIG. 58 PRESSURE DISTRIBUTION AND "WAVE CONFIGURATION," ELASTIC WAVE IN ANVIL, SHOT 9432 (U)

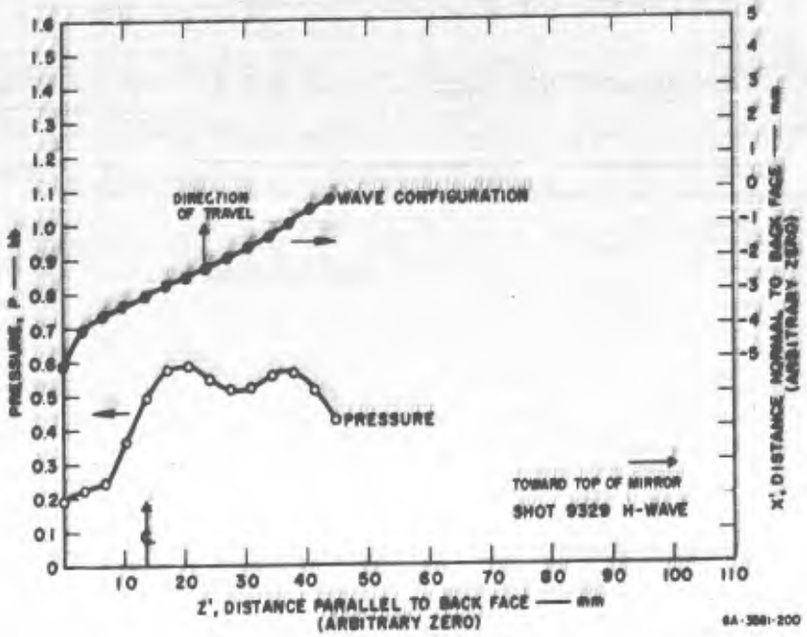

FIG. 59 PRESSURE DISTRIBUTION AND WAVE CONFIGURATION, H-WAVE IN ANVIL, SHOT 9329 (U)

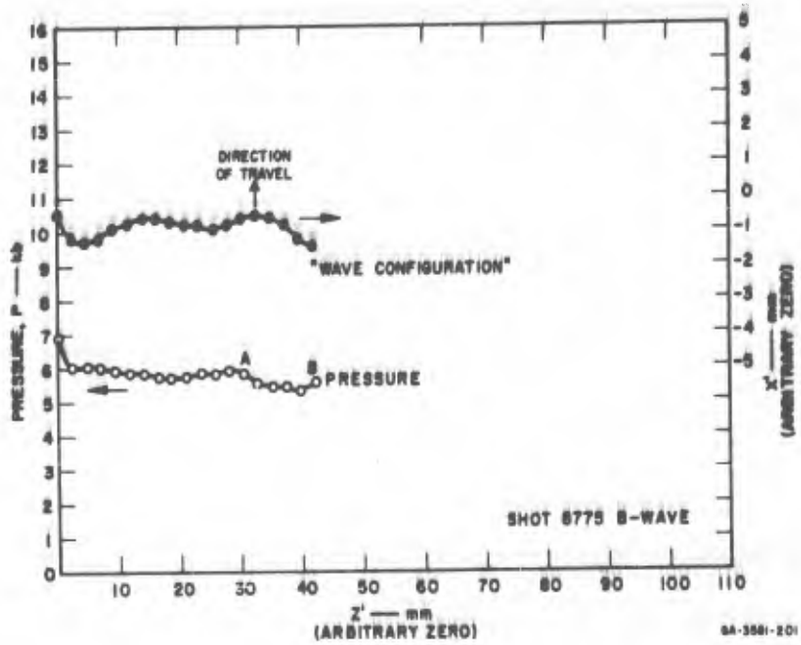

FIG. 60 PRESSURE DISTRIBUTION AND "WAVE CONFIGURATION," PLASTIC WAVE IN ANVIL, SHOT 8775 (U)

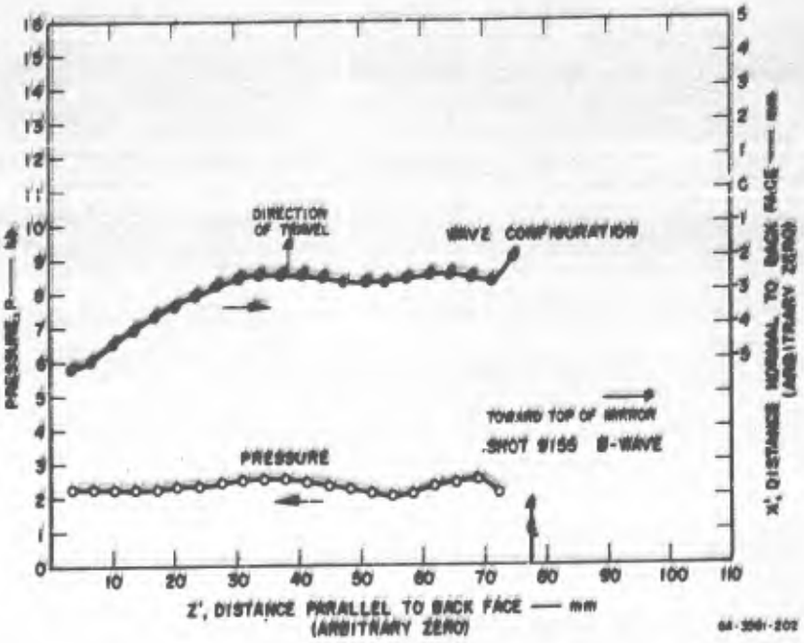

FIG. 61 PRESSURE DISTRIBUTION AND WAVE CONFIGURATION, PLASTIC WAVE IN ANVIL, SHOT 9155 (U)

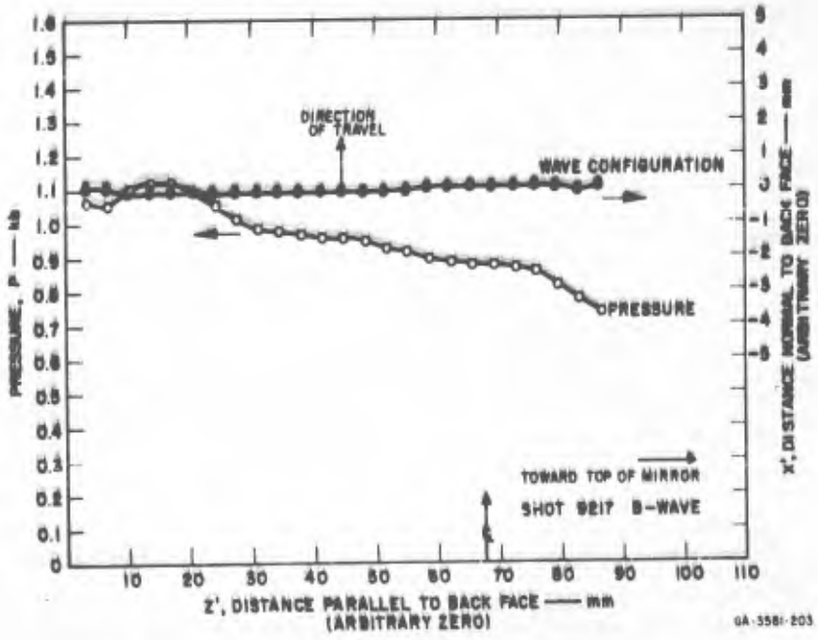

FIG. 62 PRESSURE DISTRIBUTION AND WAVE CONFIGURATION, PLASTIC WAVE IN ANVIL, SHOT 9217 (U)

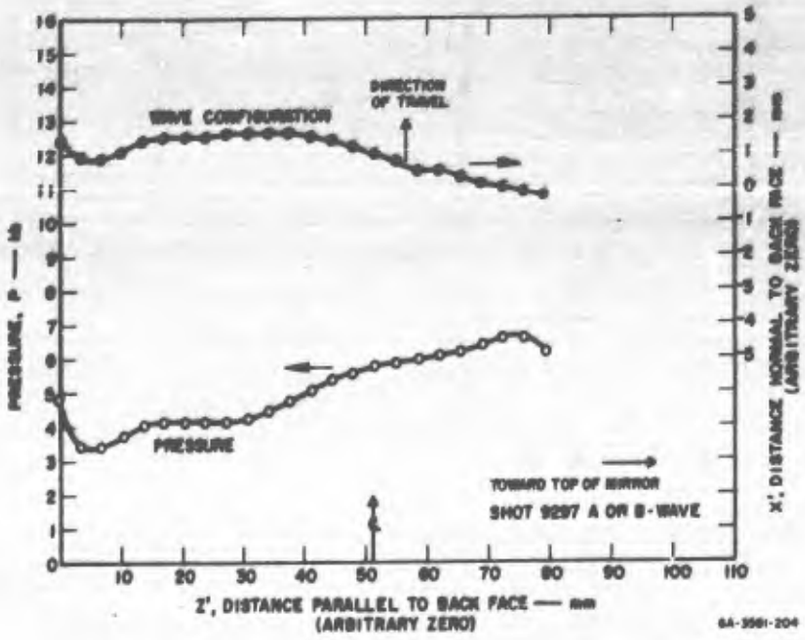

FIG. 63 PRESSURE DISTRIBUTION AND WAVE CONFIGURATION, PLASTIC WAVE IN ANVIL, SHOT 9297 (U)

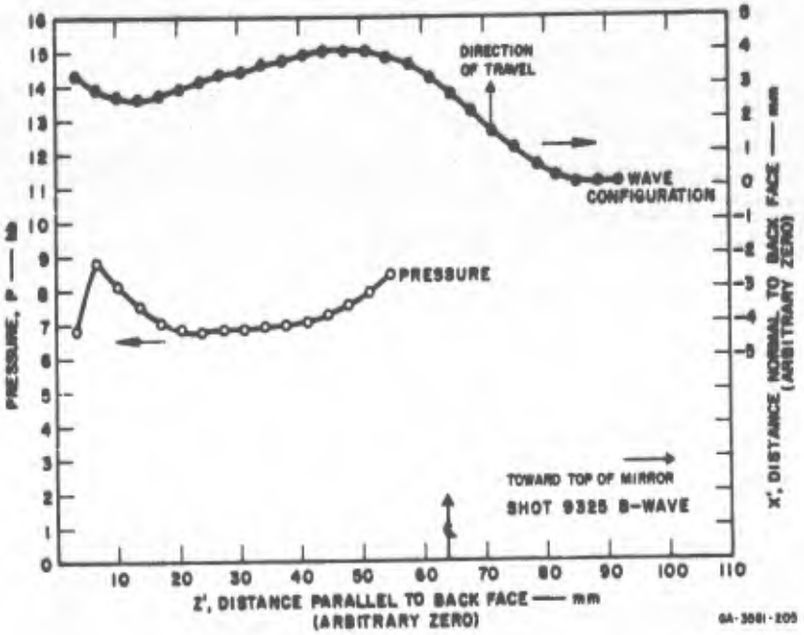

FIG. 64 PRESSURE DISTRIBUTION AND WAVE CONFIGURATION, PLASTIC WAVE IN ANVIL, SHOT 9325 (U)

The same argument can be applied perhaps more successfully to Fig. 48, where from sections $A'B'$ and $C'D'$ we read the pressure in the first wave as 0.96 kb. Shots 9216 and 9217 (Figs. 49 and 50, respectively) yield pressures of 1.35 and 1.1 kb, respectively. In these observations of the first or A-wave in 42 lb/ft^3 polyurethane, there is no well-established correlation between stress and foam or flyer thickness, and for the time being we regard the variation in our values of stress as a measure of experimental error.

In Figs. 47 through 50 and Fig. 53 regions of high pressure correspond roughly to areas of condensing wave front, and low pressures are fairly closely related to a diverging wave. Perhaps it should be kept in mind that we placed an electric timing switch (Fig. 40) between the foam and the anvil in Shot 9345, the center of which fell about 30 mm to the left of $\mathcal{C}_L$ along the abscissa of Fig. 53; this is just the region from which we have taken the value of A-wave pressure, 0.65 ± 0.05 kb.

The small trace movements associated with the first wave in 20 lb/ft^3 polyurethane are more difficult to read consistently; consequently, Figs. 51 and 52 show considerably more confusion than those just discussed. (We had to smooth the film readings by eye before fitting the polynomials.) We have found by averaging the stress over the entire mirror 0.16 ± 0.02 kb in Shot 9227 and 0.13 ± 0.01 kb in Shot 9228. Wave configurations shown in Figs. 51 and 52 are spread over less distance normal to the back face of the anvil than those computed from experiments with other target materials; this may be a result of the more drastic smoothing procedures.

We can apply the calculations of subsection A above to the two-dimensional experiments, Shots 8773, 8775, 8863, 9341, and 9342, with interesting results. Since during these shots we photographed only those parts of the mirror free of edge effect or the effect of "start-up," calculated "wave configuration" should reflect changes of detonation speed and/or changes of wave speed in the foam. Instantaneous apparent speed U_a can be found from wave shape by the formula:

$$U_a \simeq \bar{U}_a \left(1 + \frac{\Delta x'}{\Delta z'}\right)$$

where $\bar{U}_a$ is average apparent speed, and $\Delta x'$ and $\Delta z'$ are coordinate changes between two neighboring points in the front. (In computation for Shots 8773,

8775, and 8863 we arbitrarily chose $\bar{U}_e$ to be assumed detonation speed, i.e., 7.3 mm μsec for EL5061 and 7.8 mm μsec for composition B-3.)

The "wave configurations" from the two-dimensional experiments (Figs. 54 through 59) imply apparent speed variations over the mirrors of less than 5%, which we can attribute perhaps to experimental error and to actual changes in detonation speed. We may in the same way regard the pressure distributions for the two-dimensional experiments in which the wave passed through a uniform thickness of foam to reach the mirror (Figs. 54 through 56). Shot 9432, however, showed a strong pressure change in the A-wave of a more serious nature; there stress gradually falls from 0.90 kb at the top to under 0.4 kb at the bottom (Fig. 58). Stress in Shot 9431 (Fig. 57) also shows a downward trend of smaller magnitude. Because of the larger wedge angle the wave in Shot 9432 passed through more foam to reach the bottom of the mirror than in Shot 9431; that is, the effects of attenuation, if it exists, should be more severe in Shot 9432 than in 9431.

This is the evidence, referred to in the Summary, that rarefactions moving at sound speed may be able to overtake and weaken the supposedly constant A-wave.

Information concerning the first wave from Shot 9296 is fragmentary, and we conclude from it only that the A-wave has approximately the same strength found in other observations of 20 lb/ft^3 polyurethane. Similarly, because only a small part of the wave appears on the record of Shot 9329 (0.74 g/cm^3 Al), the deduced value of first wave stress, 0.55 kb, must be considered only approximate (Fig. 59).

C. PRESSURE DISTRIBUTION IN THE ANVIL DUE TO SECOND OR B-WAVE

When impacts are either one- or two-dimensional, the area of observation of the second wave is more limited than that of the first. We have discussed the weakening of the second wave in the wedge by the edge effect of the first (for example, Fig. 26). The plane mirrors of Shots 8775 and 8863 are similarly affected; the influence of the top edge is clearly seen in the photographs, Figs. 6 and 7, and the weakening due to rarefactions from the bottom appears in the calculated pressure distribution, Fig. 60 (in the segment between the letters *A* and *B*). This must be, of

course, a weakening that takes place while the wave is in the foam. We might expect the relatively slow moving second wave to be influenced for considerable distance up the mirror by sound signals trailing behind the first wave. In the case of Shot 8773 we would also expect that the B-wave is weakened in the foam by the rarefaction reflected by the A-wave from the mirror surface; in Shots 8775 and 8863 the B-wave presumably arrives at the foam-anvil interface before the arrival of the mirror rarefaction there and is not weakened by it in the foam. One or more of the later reverberations in the smear record of Shot 8773 is probably an elastic radiation from the locked mass of foam stimulated by the relief of stress carried by the reflection of the A-wave at the mirror.

We read second wave pressure in the mirror from Fig. 60 as 5.85 ± 0.07 kb. We believe the 0.050-inch-thick EL506D explosive layer introduced about 3.2×10^4 dyne-sec cm^{-2} of momentum into the foam. Effective foam thickness was only slightly greater than 0.5 inch or 12.7 mm because of the oblique impact.

Two of the flyer-plate impacts produced good measurements of second or B-wave strength, Shots 9155 (Fig. 61) and 9217 (Fig. 62), both of which used 42 lb/ft^3 polyurethane targets. In Shot 9325 (1.1 g/cm^3 silica, Fig. 64) the B-wave may have over run the elastic wave and left a fairly intelligible record on the film; analysis of Shot 9297 in 60 lb/ft^3 polyurethane is presented in Fig. 63. In many others the B-wave influenced only a small part of the record, and the calculation of stress is doubtful: Shots 9216 in 42 lb/ft^3 polyurethane, 9329 in 0.74 gm/cm^3 Al, and 9345 in 1.1 gm/cm^3 silica. Table IV contains our conclusions as to true wave strength in all of these experiments. In Table IV for Shot 9329 the I- and J-wave strengths are listed separately. These waves are defined in Fig. 38. The weak second-occurring wave in Shot 9345 (Fig. 36) is ignored and the larger fragmentary disturbance is regarded as the B-wave. Table IV also shows some values of minimum foam thickness in which we have observed the suppression of the B-wave.

V STATIC PROPERTIES OF FOAM

A. COMPRESSION TESTS AND MEASUREMENT OF SOUND SPEEDS

With compression and tensile testers* arranged to apply compressive force to a cylinder of foam encased in a lubricated steel jacket, we derived quasi-static stress-strain curves for most of those distended materials we have subjected to impact loading (Figs. 65, 66, 67, 68, 69, 70). (We explored briefly the effect of variation of strain-rate over the very small range available in the testing machines without finding any noteworthy dependence. Fig. 66.) We also measured sound speed† in the same specimens before compression in the tester and have entered these values in the figures. Because we had used our supplies we were unable to compress a sample of the 1.5 g/cm^3 graphite; we tested 1.04 g/cm^3 material instead (Fig. 71).

Stress is the simple kind of function of strain described in the Introduction except in the case of the heavy aluminum foam (Fig. 69), that is, each curve but one has a low-stress region which, if the shock Hugoniot followed the quasi-static stress-strain curve, would predict the possibility of a forerunning elastic wave. When the undisturbed material is at rest, points (P, V) of a shock Hugoniot in the pressure-volume plane are related to the initial or unshocked state (P_o, V_o) and the shock speed U by:

$$U^2 = V_o \frac{P - P_o}{\frac{V_o - V}{V_o}} \quad .$$

Since for the elastic wave $U = U_e$ and $P_o = 0$:

$$U_e^2 = V_o \frac{P}{\frac{V_o - V}{V_o}} \quad .$$

*Instron, model TTOL/M1.6, tensile tester; Baldwin Press, model MAIH.

†By comparing transit times of a single, narrow pressure pulse induced by a PZT transducer through sample and through a mercury column of accurately known length.

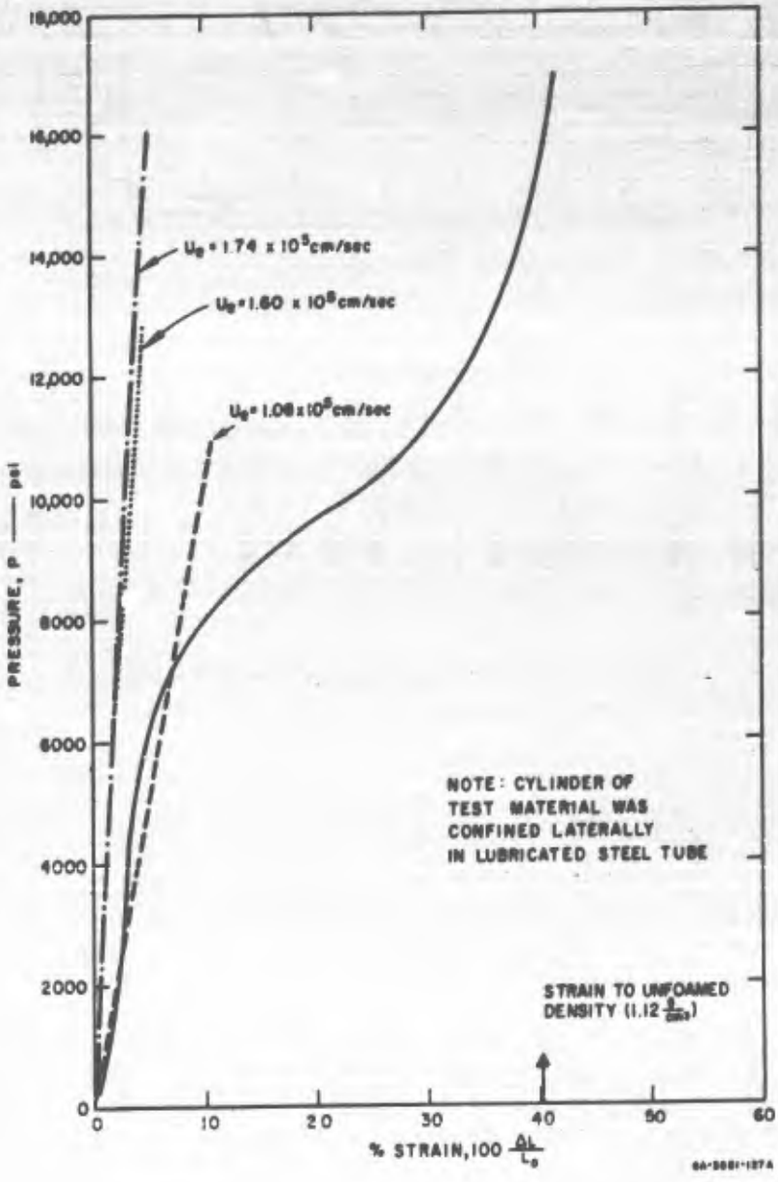

FIG. 65 QUASI-STATIC COMPRESSION OF 42 lb/ft^3 POLYURETHANE FOAM

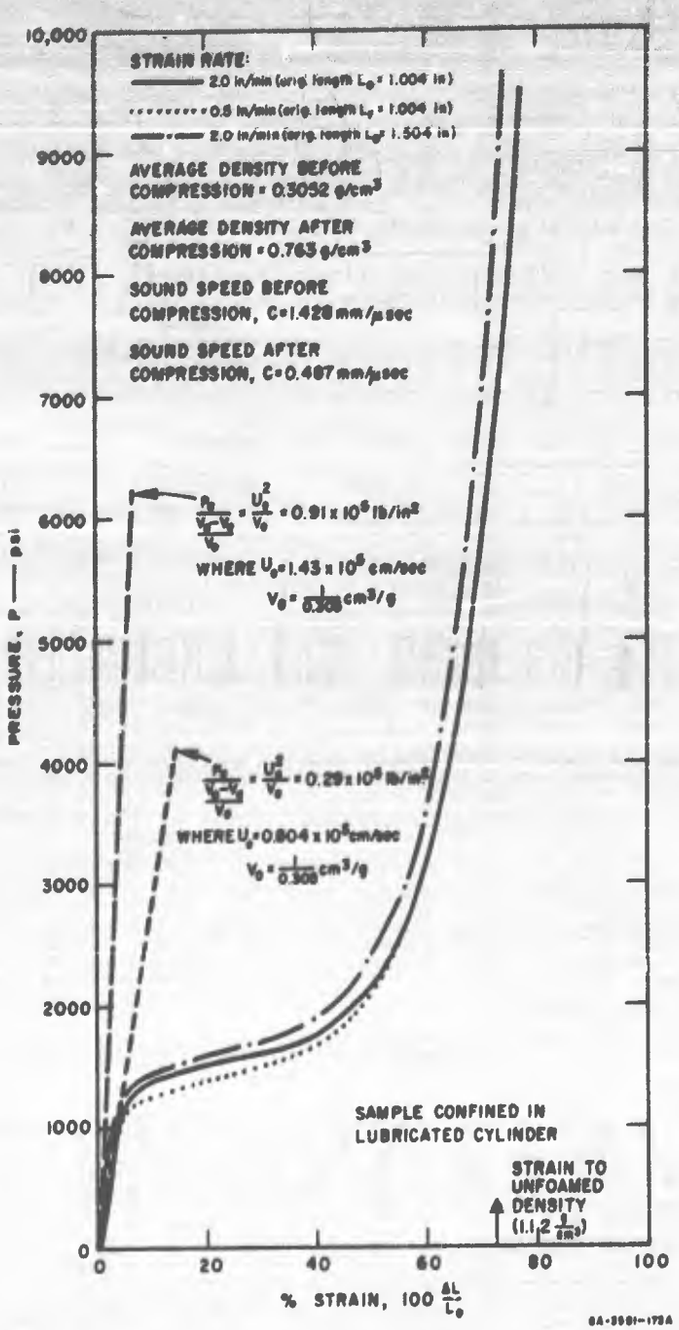

FIG. 66 QUASI-STATIC COMPRESSION OF 20 lb/ft³ POLYURETHANE FOAM (U)

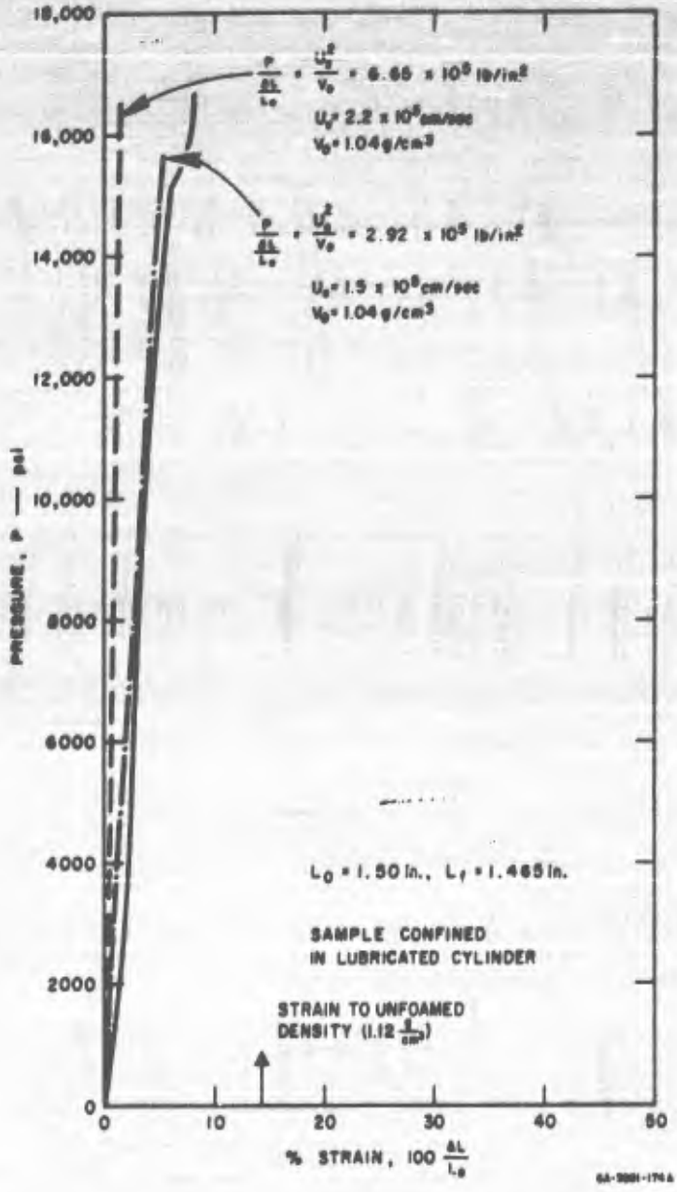

FIG. 67 QUASI-STATIC COMPRESSION OF
60 lb/ft^3 POLYURETHANE FOAM (U)

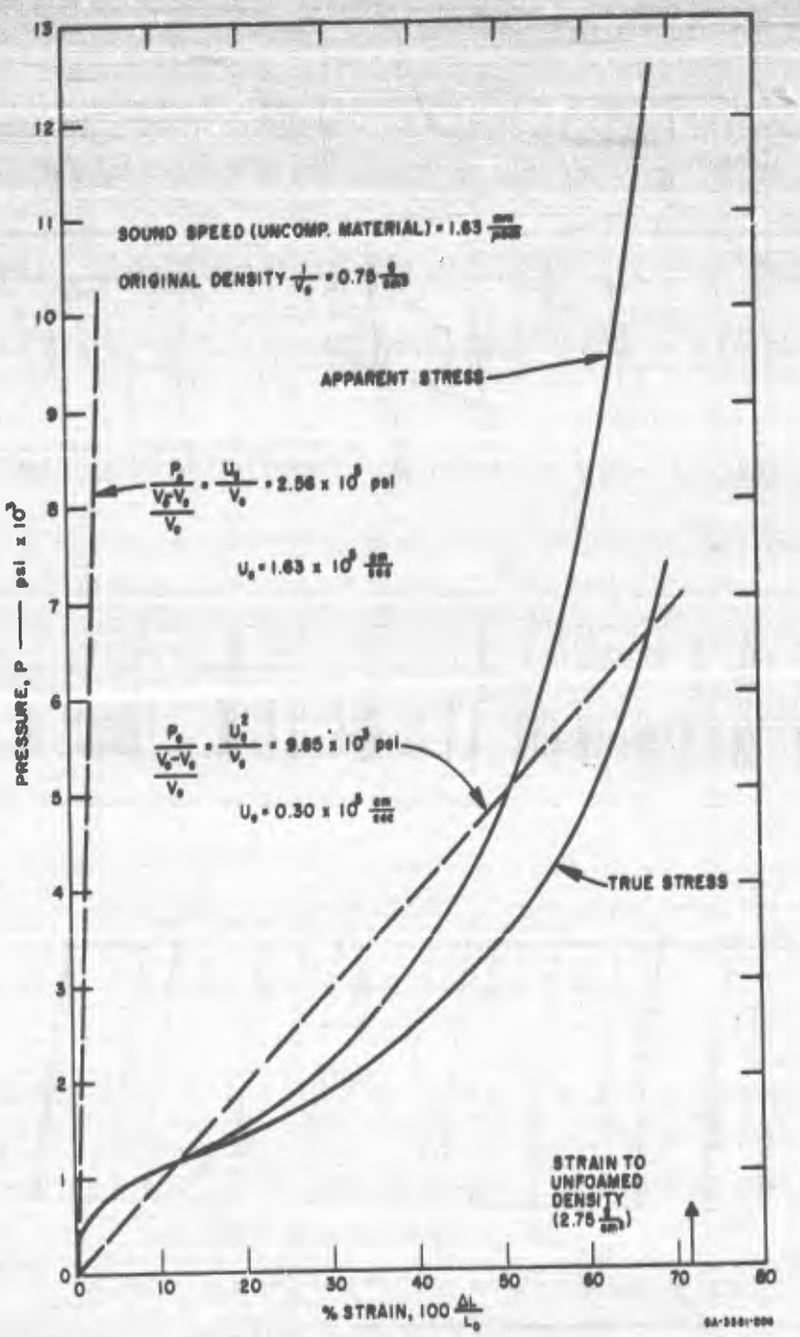

FIG. 68 QUASI-STATIC COMPRESSION OF OPEN CELL 0.74 g/cm^3 ALUMINUM FOAM (U)

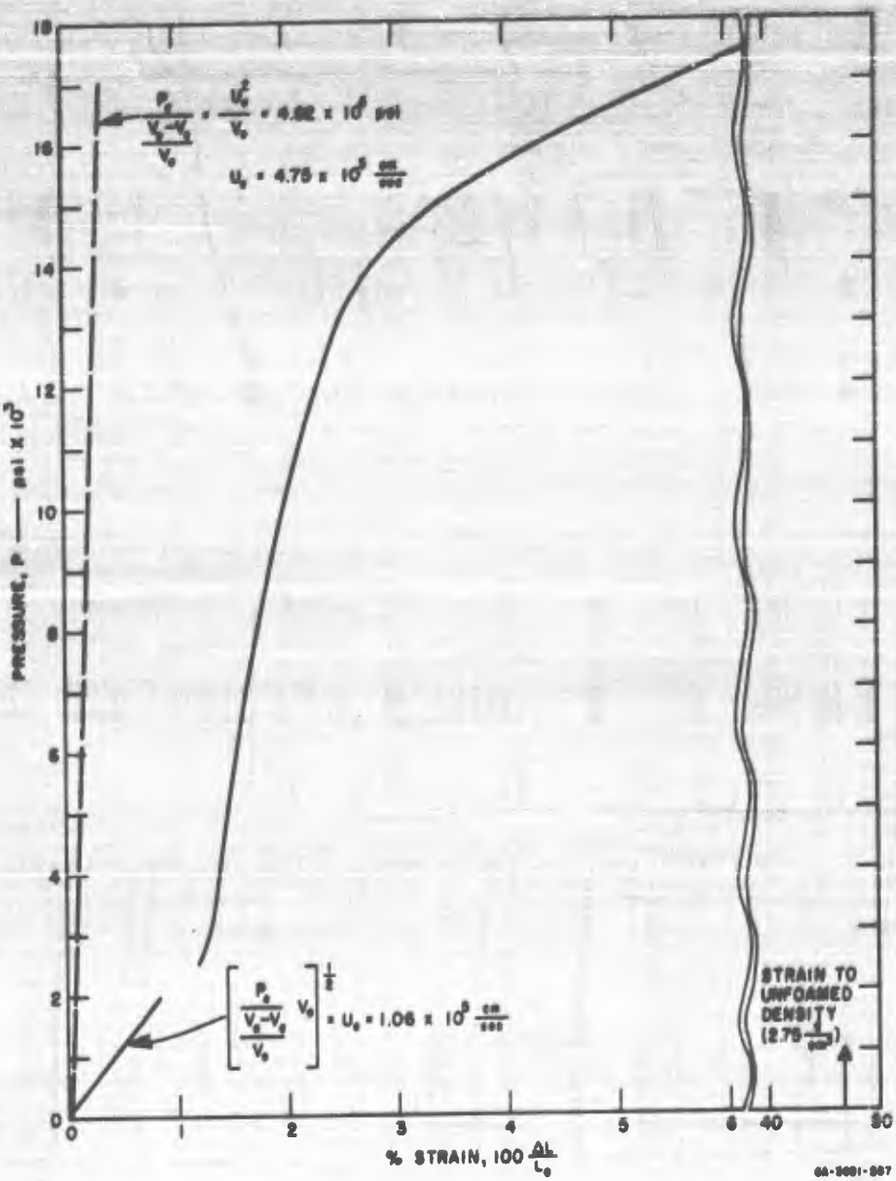

FIG. 69 QUASI-STATIC COMPRESSION OF CLOSED CELL 1.5 g/cm^3 ALUMINUM FOAM (U)

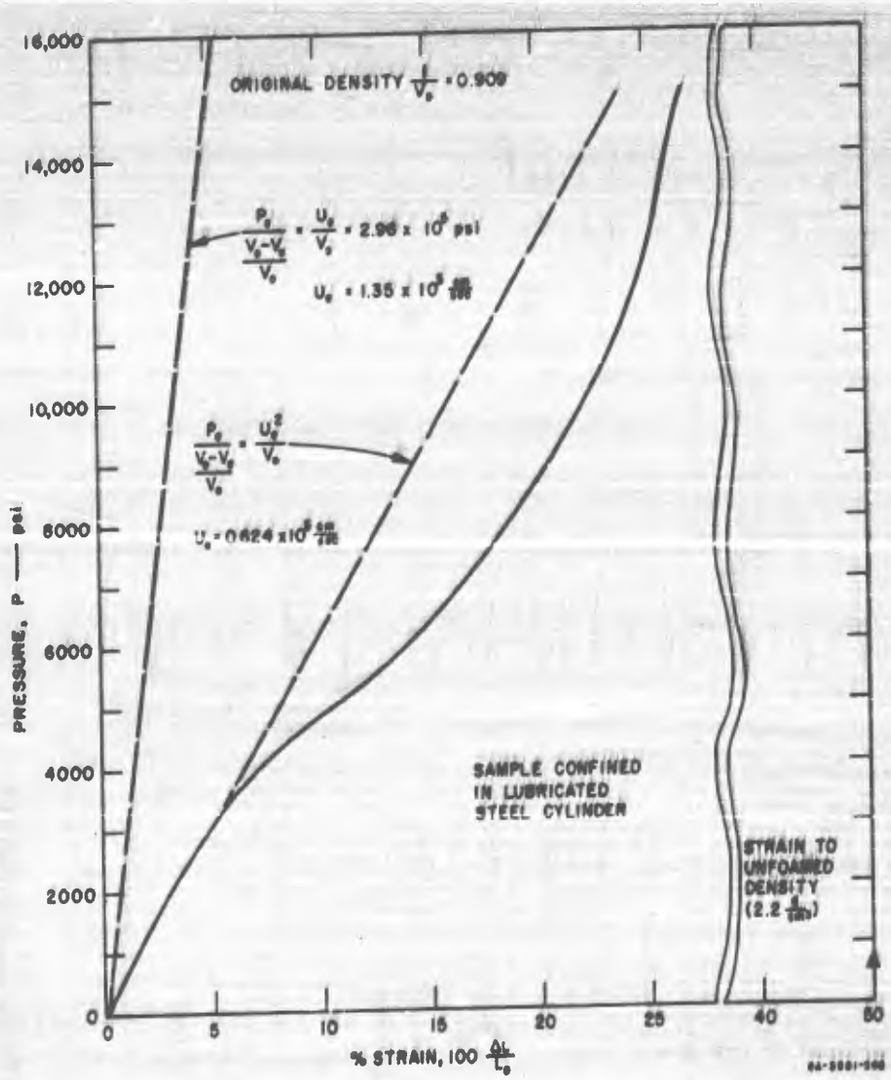

FIG. 70 QUASI-STATIC COMPRESSION OF 1.1 g/cm^3 SILICA FOAM (U)

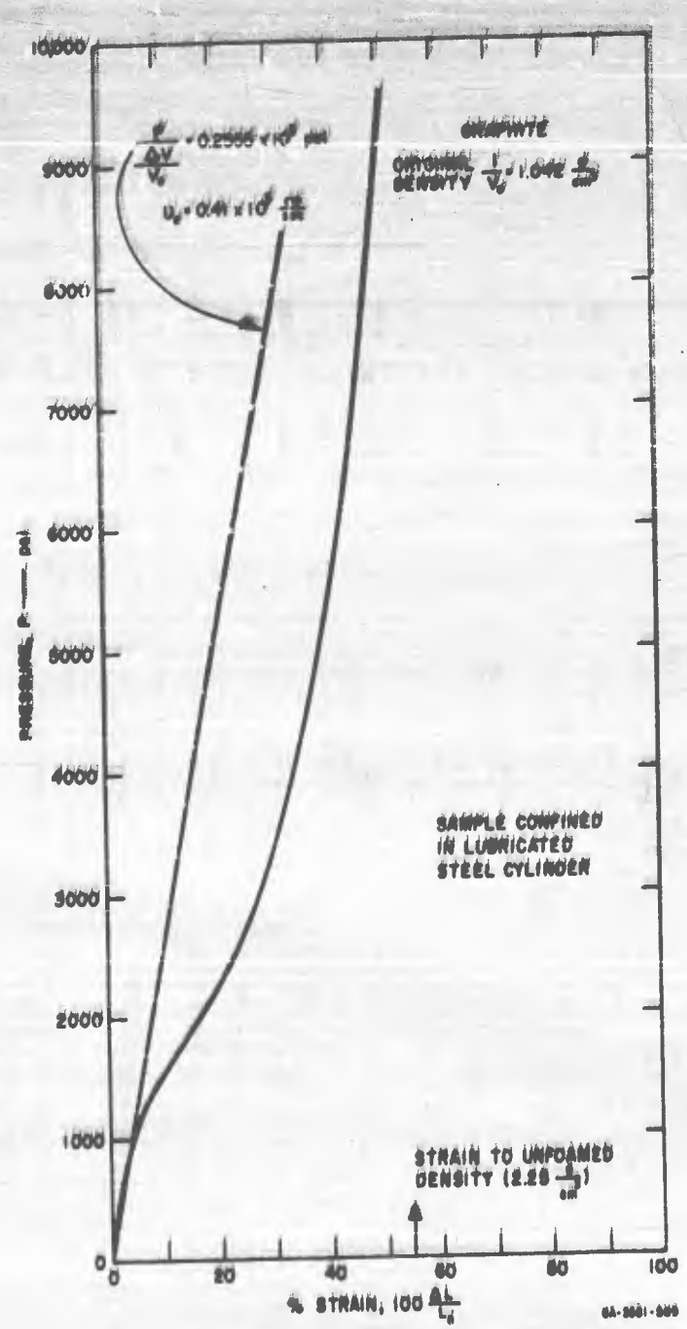

FIG. 71 QUASI-STATIC COMPRESSION OF 1.04 g/cm^3 GRAPHITE FOAM (U)

but the quantity $(V_o - V)/V_o$ is just the abscissa and P the ordinate of the stress-strain curves measured in our tests. Thus, on each figure there are at least two straight lines drawn through the origin; one has a slope, $P/[(V_o - V)/V_o] = PV_o/(V_o - V)$, computed by assuming measured sound speed $C = U_e$ and the other is drawn roughly to parallel the low pressure section of the compression curve. From the second a shock speed is predicted.

Also, along the abscissae are arrows marking the strain necessary to reach normal density of the material of which the foam is made.

In Fig. 65, the stress-strain curve for 42 lb/ft^3 polyurethane, neither the slope corresponding to sound speed ($U_e = 1.74 \times 10^5$ cm/sec) nor that based on the A-wave speed measurements of Shots 9431 and 9432 ($U_e = 1.60 \times 10^5$ cm/sec) is near the actual slope of the curve ($U_e \cong 1.1 \times 10^5$ cm/sec). In this case we accept $U_e = 1.60 \times 10^5$ cm/sec as most nearly correct for the forerunning waves occuring in our impact experiments.

In silica the divergence between the slope based on sound speed and that of the static compression curve is striking (Fig. 70). As will be explained later (Section VI B) the evidence from measurements of time intervals in the flyer plate experiments points toward and A-wave speed considerable less than sound speed, *i.e.*, more nearly like that implied by the compression curve.

In no case is a sharp yielding at the elastic limit seen in static compression. The best we can hope for is to be able to identify a zone of yielding.

B. MEASUREMENT OF DENSITY UNIFORMITY

Fluctuation of initial density throughout a foam target could lead to erratic behavior of the shock waves and to incorrect deduction of foam properties. Since we do not manufacture any foam in this laboratory, we have accurately measured densities of random samples of target material.

From our experiments last year and this, we had several scraps of various foamed materials left over, all marked with the nominal densities of the large specimen from which they were cut. All polyurethane foam came from one supplier and all aluminum foam from another, but the scraps probably represented fairly widely spaced sampling from one or more batches.

From each kind and density of material we machine-cut eight test cylinders, all 1.0 to 1.5 inches long and about 1.12-inches in diameter. The diameter and length of each were measured to an accuracy of ±0.0005 inch and we weighed each to ±0.0005 gram. The accuracy of the density measurement then is between 1 and 2%. We computed the average density and standard deviation of a single measurement of density for each category and found the latter to be about 1 to 2% of the average in most cases. The range of variation in density in those cases is about the same. One material, 32 lb/ft^3 polyurethane, showed much less uniformity in density. (We have not used any of this material in the present program.) Some of these results are collected in Table IX.

Table IX

SOME RESULTS OF DENSITY MEASUREMENTS OF FOAMS

MATERIAL	AVERAGE DENSITY (gm cm^{-3})	RANGE OF DENSITIES (%)	STANDARD DEVIATION OF A SINGLE MEASUREMENT (%)
20 lb/ft^3* polyurethane	0.305	±1.0	2.0
32 lb/ft^3* polyurethane	0.517	-2.3 +9.0	4.3
40 lb/ft^3* polyurethane	0.670	-0.93 +2.4	0.96
Al-foam† closed cell	1.455	+0.93 -1.1	0.74

*Eight samples

†Four samples only

VI SIMPLE THEORY OF THE SHOCK BEHAVIOR OF FOAMS

LIST OF SYMBOLS USED IN SECTION VI

SYMBOL	DEFINITION
x	distance
x_s	distance coordinate of shock front
x_b	distance coordinate of boundary at which pressure is applied
x_e	distance coordinate of elastic precursor front
x_{sc}, x_{bc}	critical value of x_s or x_b for which single shock front splits into two fronts
x_s^*, x_b^*	critical value of x_s or x_b for which amplitude of second shock reduces to zero
x_r	distance coordinate of sound wave in rarefaction fan
t	time
t_c	critical time at which single shock front splits into two fronts
t^*	critical time at which amplitude of second shock reduces to zero
η	reduced distance ($\eta = x - x_e$) subscripts refer to corresponding values of x above
τ	reduced time ($\tau = t - t_e$) subscripts refer to corresponding values of t above
V	specific volume
V_0	initial or distended specific volume
V_e	specific volume in elastic precursor
V_1	specific volume of locked foam
ρ	density ($\rho = 1/V$)
p	pressure

SYMBOL	DEFINITION
P_c	critical pressure at which single shock front splits into two fronts
P_2	peak pressure delivered to solid boundary upon reflection of first shock in foam
P_1	pressure in left-hand locked mass of foam
P_{10}	pressure at rear boundary of foam at moment of impact
P'_{10}	trial value of P_{10}
U, U_s	shock wave velocity
u	particle velocity (subscripts refer to values corresponding to pressure-volume states above)
I_0	momentum delivered to foam
μ	mass per unit area of foam and flyer between flyer free surface and locking shock front
μ_c	value of μ corresponding to x_{1c} above
μ^*	value of μ corresponding to x_1^* above
μ_0	mass per unit area of flyer

A. EXPOSITION

Fowles and Curran[20] have given approximate equations of motion within an elastic-rigid locking solid, which they define as a material possessing the particularly simple shock Hugoniot represented in Fig. 72.

To avoid use of the concept of instantaneous transfer of flyer momentum to the target slab, we have changed the equations derived by Fowles and Curran. We now assume that the flyer is not slowed immediately by the impact on the target, but that the adjacent elements of the target instantaneously accelerate to flyer speed. We retain the assumption that all the material behind the locking wave moves with the same velocity. This material now includes the flyer plate. Momentum is transferred to the target through the advance of a shock wave, as before.

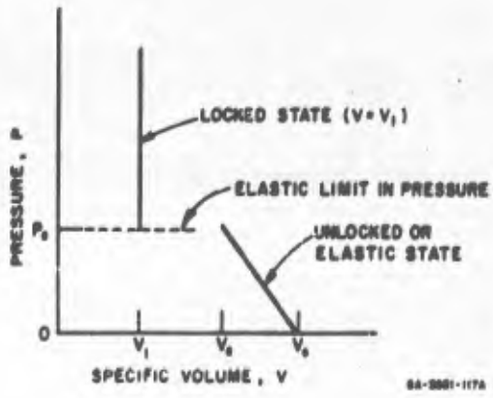

FIG. 72 POSSIBLE EQUATION OF STATE OF LOCKING SOLID WITH ELASTIC REGION (U)

We add to the terminology of Fowles and Curran by defining two new quantities:

μ_o = mass per unit area of flyer

$P'_{10} = \dfrac{u_{10}^2}{V_o - V_1}$ — a trial initial pressure.

The modified equations are derived almost exactly as the originals:

$$u_{10} = \frac{I_o}{\mu_o} \quad .$$

If $P'_{10} > P_e$, then there is one wave until time $t = t_c$, and $P_{10} = P'_{10}$. We will call this Case I.

$$x_s = V_o\left[\mu_o^2 + \frac{2I_o}{V_o - V_1}\,t\right]^{1/2} - V_o\mu_o \quad , \quad o \le t \le t_c \quad ,$$

$$t_c = \left[\frac{I_o^2}{P_e} - \mu_o^2(V_o - V_1)\right]\frac{1}{2I_o} \quad ,$$

$$u_1 = \frac{I_o}{\left[\mu_o^2 + \frac{2I_o}{V_o - V_1}\,t\right]^{1/2}} \quad , \quad o \le t \le t_c \quad ,$$

$$P_1 = \frac{u_1^2}{V_o - V_1} \quad , \quad o \le t \le t_c$$

$$\mu_c = \frac{I_o V_o}{V_c(V_o - V_1)}$$

$$x_{sc} = V_o(\mu_c - \mu_o) \quad .$$

If $P_e < P'_{10} \le P_c$ then $t_c = x_c = o$ and two waves appear simultaneously at the receiving face of the target. This is Case II.

Again,

$$u_{10} = \frac{I_o}{\mu_o} \quad ,$$

but

$$P_{10} = P_e + \frac{(u_{10} - u_e)^2}{V_e - V_1}$$

and

$$\mu_e = \mu_o \quad .$$

It can be easily shown that if $P'_{10} < P_e$ then

$$P_e + \frac{(u_{10} - u_e)^2}{V_e - V_1} < P_e \quad .$$

For $t \geq t_e$ the derivations in both Cases I and II are unchanged except the equation

$$\mu_e = \frac{I_e V_e}{U_e (V_e - V_1)}$$

is replaced with

$$\mu_e = \frac{x_{se}}{V_e} + \mu_e \quad .$$

Instead of Eq. (52) of AFSWC-TDR-62-22, we write

$$\eta_b - u_e \tau = (V_e - V_1)\left(-\mu_e + \left\{\mu_e^2 + 2\left[\frac{I_e - u_e \mu_e}{V_e - V_1}\tau - \frac{u_e^2 \tau^2}{2(V_e - V_e)(V_e - V_1)}\right]\right\}^{1/2}\right)$$

and Eq. (53) becomes

$$u_1 - u_e = \frac{I_e - \mu_e P_e^{1/2}(V_e - V_e)^{1/2} - P_e \tau}{\left\{\mu_e^2 + 2\left[\frac{I_e - \mu_e P_e^{1/2}(V_e - V_e)^{1/2}}{V_e - V_1}\right]\tau - \frac{P_e}{V_e - V_1}\tau^2\right\}^{1/2}}$$

Other equations become:

$$\tau^* = \frac{I_e - \mu_e P_e^{1/2}(V_e - V_e)^{1/2}}{P_e} = \frac{I_e - \mu_e u_e}{P_e}$$

$$\eta_e^* = U_e \tau^*$$

$$\eta_b^* = u_c\tau^* + (V_c - V_1)\left(-\mu_c + \left\{\mu_c^2 + 2\left[\frac{I_o - u\mu_c}{V_c - V_1}\tau^* - \frac{u_c^2\tau^{*2}}{2(V_o - V_c)(V_c - V_1)}\right]\right\}^{1/2}\right)$$

$$\eta_s^* = \frac{1}{V_c - V_1}\{V_c\eta_b^* - V_1 u_c\tau^*\}$$

$$\mu^* = \frac{1}{V_1}(x_s^* - x_b^*) + \mu_o \quad .$$

There is also a Case III, *i.e.* $P'_{10} \leq P_c$, when there is never more than one wave. In this case

$$P_{10} = P'_{10} \quad .$$

$$u_{10} = \frac{I_o}{\mu_o} \quad .$$

and

$$t_c = x_c = \tau^* = \eta_s^* = \eta_b^* = o \quad \text{and} \quad \mu^* = \mu_c = \mu_o \quad .$$

Qualitatively the prediction made by the simple theory of foam response to one-dimensional shock is unchanged by the modifications outlined above, except that the forerunner may now (but not necessarily) appear simultaneously with flyer arrival (Case II) and reflections off the wall must interact with a metal layer. In general the structures expected in the foam are sketched in Fig. 73; abacissae x are distances normal to the infinite foam faces measured from the original foam free surface, and coordinates t are times measured from the moment of impact of flyer and foam. All waves moving in the same direction along straight lines have the same speed.* Since $x_c \neq 0$, $t_c \neq 0$, the situation shown in the figure is Case I. The interval between waves of rarefaction, appearing for $t > t^*$, is arbitrarily chosen and should be as small as convenient. When the first rarefaction, traveling from (x_s^*, t^*), meets the locked-mass at the wall, pressure is relieved slightly at the wall

* All elastic compressional and rarefactional fronts travel toward the wall with speed V_c, but the speed of the elastic reflections from the wall must be set equal to:

$$V_c[1 - 2(V_c/V_o)]$$

which is slightly smaller in magnitude than V_c for most foamed materials.

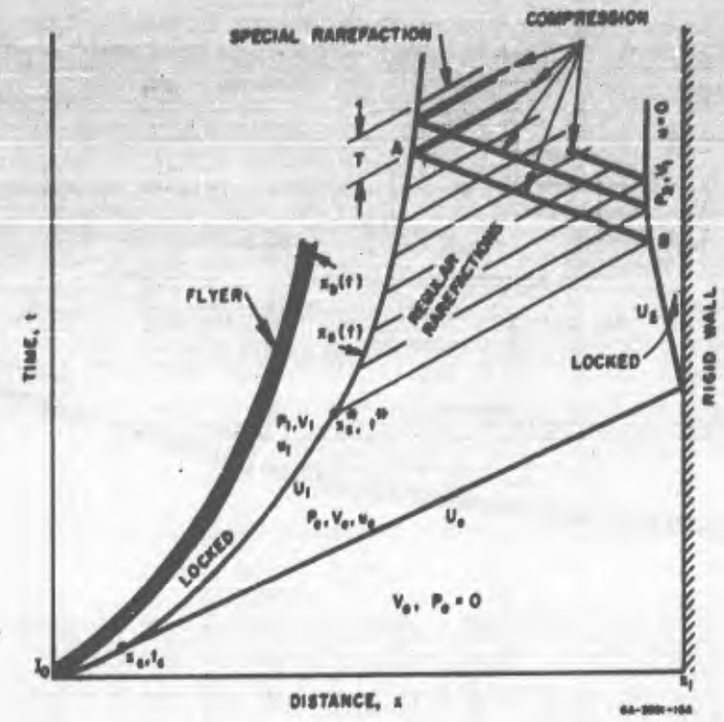

FIG. 73 FOAM WAVE STRUCTURES IN (x-t) PLANE (U)

and the advance of the locking wave toward the flyer is slowed; also, if pressure at the wall and in the locking wave remains above P_e after the relief, an elastic wave starts toward the flyer carrying stress P_e. When it reaches point A, however, pressure behind it is only slightly above local pressure since it has interacted with a series of rarefactions from the left-hand locked mass. The influence of the successive rarefactions and the leftgoing elastic wave upon each other is found by addition and subtraction of stress differences. Later rarefactions arouse a similar response at the right-hand locking wave until pressure in the latter falls to P_e and it ceases its advance. Subsequent rarefactions reflect from the right-hand locked mass as rarefactions.

The following quantitative description of the interaction of the regular relief waves and the right-hand locked mass is based on the designation of states shown in Fig. 74. First, particle speed u_ϵ in the reflected compressional wave carrying state ϵ is computed from:

$$(u_a - u_\epsilon)^2 = (P_\epsilon - P_a)(V_a - V_\epsilon) \quad , \qquad (2)$$

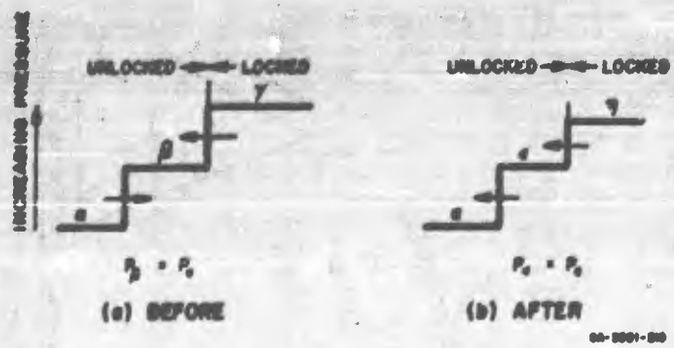

FIG. 74 INTERACTION OF REGULAR RAREFACTIONS AND RIGHT-HAND LOCKED MASS (U)

then we compute the new stress P_η in the locked mass:

$$P_\eta - P_e = \frac{(u_e)^2}{V_e - V_1} .$$

In the collision at point B (Fig. 73) pressure P_a is related to the particle speed u_a by the formula:

$$P_e - P_a = \frac{(u_e - u_a)^2}{V_a - V_e}$$

and u_a is a certain arbitrarily chosen amount smaller than u_e, particle speed in the wave at the elastic limit; but for later similar collisions the wave bringing state a is the result of one or more elastic encounters between two waves, all of which tend to reduce the rightward particle speed in state a. The pressure P_a, however, is not reduced by these encounters; in fact the decrements of particle speed of the left-hand collapsed material will usually be chosen so that successive values of P_a brought to right-hand locked mass will be equal. Clearly, then, the time will come in our calculation when we can find no positive (*i.e.*, rightward) value of u_e to satisfy Eq. (2) above. At this point growth of the right-hand collapsed layer will stop and the pressure difference across the right locked-unlocked interface will disappear. The right-hand locked mass will be at pressure P_e and be covered by a growing motionless layer of unlocked material at the same pressure. The next relief wave to

reach the right-hand locked layer will bring a left-going particle velocity and be reflected from the compacted layer as a left-going rarefaction carrying zero particle speed. The stress in the right-hand locked mass will fall accordingly; that is, we assume that pressure in compacted foam is relieved without any change in specific volume or particle speed.

This process of relief of pressure at the wall will continue until stress there reaches zero, when further rarefactions lead to tension and probably rupture and separation of the foam at the right-hand locked-unlocked interface. The momentum in the foam detached from the wall by this action is left-going and represents "bounce-off."

We treat the interactions of the reflections at the left-hand locked mass, such as the impact at point A in Fig. 73, only approximately correctly. A thin, hard layer of high shock impedance on the surface of a semi-infinite soft slab will reflect a compressional front from the slab in the form of an oppositely-going compressional front allowed by a series of rarefactions which eventually lower the stress to zero at the hard-soft interface. In other words, the effect of the hard layer when struck by a wave of constant stress and infinite duration is to reflect into the soft slab a compressional pulse of a certain length which carries just enough momentum to balance the oppositely going momentum in the hard layer. The layer, of course, reaches a final speed equal to the speed the free surface of the soft material would have attained immediately upon reflection of the original wave, if the layer had been absent. The length and magnitude of the compressional pulse depends upon the shock impedance (or the reverberation speed) in the hard layer contrasted to the impedance in the soft layer. We simplify the reaction at point A considerably by treating the locked material as rigid, that is, we assume it has infinite impedance. If no locking mechanism were present, the pressure jump in the reflected front would always equal that in the impacting front. However, in our model no stress greater than P_ϵ can be transmitted elastically so the interaction at point A may provoke renewed growth of the left-hand locked mass. Figure 75 is a diagram of the situation. In Alternative I the reflected pressure P_η is less than P_ϵ, and the interface between locked and unlocked material moves at particle speed which is the same on both sides of the boundary. The change in particle speed introduced into the unlocked material by the state γ is removed by a single wave which carries the state η, i.e., $u_\epsilon = u_\eta = u_\alpha = u_\beta$. Alternative II presents the possibility

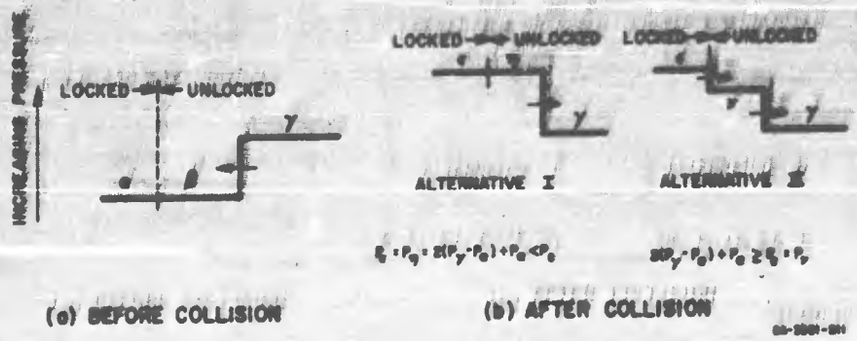

FIG. 75 INTERACTION OF A COMPRESSION WAVE AT THE LEFT-HAND LOCKED MASS (U)

of a two stage return to original particle speed; here again $u_\epsilon = u_\alpha = u_\beta$ but

$$(u_\nu - u_\gamma)^2 = (P_\epsilon - P_\gamma)(V_\gamma - V_\epsilon) \quad .$$

Under Alternative II the reflected pressure P_ϵ is not, in general, equal to $P_\alpha + 2(P_\gamma - P_\alpha)$ as under Alternative I, but rather

$$P_\epsilon - P_\epsilon = \frac{(u_\alpha - u_\gamma)^2}{V_\epsilon - V_1} \quad .$$

If the left-hand locked mass and the flyer plate had not been present at the point A, it would have been reasonable to assume the reflection into the unlocked foam of a rarefaction jump of strength $P_\gamma - P_\alpha$ from the point A. Such a rarefaction would require a change in particle speed Δu behind it equal in magnitude to the quantity:

$$\Delta u = \sqrt{(P_\gamma - P_\alpha)(V_\beta - V_\gamma)}$$

and of such a sign as to increase the material speed leftwards. Instead, under Alternative I we consider the left-hand locked mass and the flyer to have gained during a time interval of length T leftward momentum of amount

$$M_1 = \left(\frac{x_a - x_b}{V_1} + \mu_0 \right) \Delta u = \overline{\mu} \Delta u$$

or under Alternative II of amount

$$M_{II} = \left(\frac{x_j - x_\beta + \frac{1}{2} t'_{\alpha\beta} \dot{T}}{V_j} + \mu_\beta \right) \Delta w = \left(\mu + \frac{1}{2} t'_{\alpha\beta} \dot{T} \right) \Delta w$$

where

$$t'_{\alpha\beta} = V_j \left(\frac{P_\alpha - P_\beta}{V_\alpha - V_\beta} \right)^{\frac{1}{2}} + u_\beta \quad .$$

x_j, x_β and μ are functions of time and should be evaluated in these equations at the time of the interaction at point A. The interval $\dot{T}$ (which begins with the collision at point A) is then found from the formulae:

$$2(P_\gamma - P_\alpha)\dot{T} = M_I$$

and

$$(P_\zeta - P_\alpha)\dot{T} = M_{II} \quad .$$

After the elapse of time $\dot{T}$, a right-going relief wave is introduced at the left-hand locked-unlocked interface, the effect of which is to increase the leftward speed of the left-hand locked mass by an amount Δw and, of course, reduce the pressure in the left-hand locked mass. During the interval $\dot{T}$ the regular rarefactions[4] continue to appear at the interface and the left-hand locked mass continues to slow its rightward motion in steps. If we imagine that the "after-collision" conditions indicated in Fig. 75 change during $\dot{T}$ to certain similar states designated by primes, then at the end of $\dot{T}$ further changes are introduced which may be signalled by double primes:

$$u_\zeta' - u_\zeta'' = \Delta w \quad .$$

If $P_\zeta' \leq P_\zeta$, Alternative I can give rise to only one new situation, that called Alternative IA in Fig. 76. Here $P_\zeta' = P_\eta'$ and a new rarefaction

[4] These begin at time $\dot{T}$ and are associated with the slowing of the rightward motion of the flyer and the compacted layer in contact with it. If we make the decrement in particle velocity (and pressure) the same across each rarefaction front, then the time intervals separating the waves increase with increasing time of origin. See Eq. (58) AFSWC-TDR-62-22. In Fig. 73 these time intervals are drawn approximately equal so the successive rarefaction jumps would not in that case carry equal decrements.

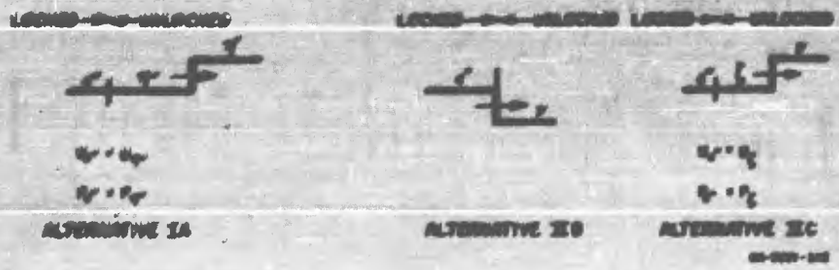

FIG. 76 RELIEF WAVES APPEARING AT THE LEFT-HAND LOCKED MASS AFTER REVERBERATION TIME T (U)

front carries pressure $P_{\eta''}$ into the elastically strained material:

$$P_{\epsilon''} - P_{\eta'} = \frac{(\Delta u)^2}{V_{\eta'} - V_{\eta''}} \quad .$$

There are three possibilities from Alternative II: (A) regular rarefactions reduce the overpressure in the left-hand locked mass so that $P_{\epsilon'} = P_{\nu'} \leq P_{\nu}$, $u_{\epsilon'} = u_{\nu'} \leq u_{\nu}$; (B) neither regular rarefactions nor the relief at time T lower stress in the left-hand locked mass below the value P_{ϵ}; (C) at time T the reverberation relief wave reduces pressure in the left-hand locked mass below P_{ϵ} for the first time after point A. Alternative IIA is essentially the same as IA. Alternative IIB is possible only if one or more additional compressional waves meet the left-hand locked mass during the interval T, in which case $P_{\epsilon'} > P_{\epsilon}$, and

$$P_{\epsilon''} - P_{\epsilon} = \frac{(\Delta u)^2}{V_{\epsilon} - V_1} \quad .$$

For Alternative IIC:

$$P_{\rho} - P_{\epsilon} = \frac{(\Delta u)^2}{V_{\epsilon} - V_{\rho}} \quad .$$

If under Alternative I a left-going compressional wave intervenes during time T, an Alternative IB, i.e., $P_{\epsilon'} > P_{\epsilon}$, may be possible, which of course is essentially the same as Alternative IIB or IIC.

In all the foregoing formulae, of course, pressures P are related to specific volumes V through an assumed equation of state typified by Fig. 72.

We can with a little effort avoid the possibility of Alternative II at any one collision, such as that at point A, by choosing the frequency of the regular rarefactions so high that the left-going compressional wave which meets the left-hand locked mass in that collision must cross the trajectories of two or more regular relief waves. The pressure jump in the left-going compression is, of course, equal to the pressure decrement in one rarefaction; hence the compression reflected from the left in a case such as that described must be too small to bring the stress above P_φ. Because as time goes on after t^* pressure in the left-hand locked mass may accumulate from repeated impacts with compressional reflections, it is not evident that we can always avoid Alternative II altogether.

If the two locked layers move together until they collide we must drop the assumption of rigidity in the collapsed material; we have not treated this case (except very approximately in subsection B following).

B. COMPARISON WITH EXPERIMENTS

In our flyer plate experiments we have not been able to watch the foam target for longer than about 8 to 10 μsec after the passage of the first wave through it, so we have not compared the predictions of the calculation outlined above with the actual behavior of the foam for times much greater than t^*. In fact in many of our experiments the two locked masses meet before t^*. We have, therefore, mainly tried to compare arrival times of the various structures at the wall as predicted and as observed. In this study it is enough to calculate arrivals at the receiving surface of the wedge anvil, *i.e.*, at the wall, since passage of waves through the anvil to the mirror can not change any time intervals between them significantly.

Since extensive impact data exist only for polyurethane of approximate density 40 lb/ft^3, we limit our test of the calculations to this material for the present.

Targets in the polyurethane impact experiments were 42 lb/ft^3 material; in the wave speed measurements (Shots 9431 and 9432),

39 lb/ft^3 foam. Therefore in the calculational simulation of the flyer plate experiments we shall use a first (A-) wave speed $U_e = 1.65 \times 10^5$ cm sec^{-1} instead of the 1.60×10^{-5} value measured. Initial specific volume V_0 is about 1.48 cm^3 g^{-1} when density is 42 lb/ft^3. I_0, input momentum, is 1.15×10^6 (dyne-sec/cm^2) and μ_0, flyer mass per unit area, 0.140 g cm^{-2}, for the 0.020 inch thick flyer and twice those values when the 0.040 inch flyer is used. We found the mean value of the first wave strength in the anvil to be about 1.0 kb. The elastic strength P_e in the foam required to produce such a wave in the anvil is less than this and depends upon the behavior parameters of the foam according to the following formula:

$$P_e = \frac{P_e(V_0 - V_1)}{V_0 - V_1 + P_e\left(\frac{V_0}{U_e}\right)^2}$$

where P_e = observed stress in anvil. Since we do not under shock loading observe final specific volume V_1 directly, we give V_1 various values, calculate corresponding values of P_e above, and for each V_1 make the computational simulations of foam behavior to compare with the four polyurethane experiments (Shots 9155, 9180, 9216, and 9217).

In all the four shots except 9180 the first (or A-) wave is sharp; in every one the B-wave is gradually rising and the E-locus very sharply defined. In the simple theory all fronts are complete discontinuities. Therefore we define the time arrival A-B between the first and second smear record waves in two ways: from the start of A to the start of B and from the start of A to the completion of the rise in B. We can then nearly match these observations with two separate calculations, the first based on $V_1 = 1.05$ cm^3 g^{-1} and the second using $V_1 = 0.90$ cm^3 g^{-1}. Calculated trajectories for these two cases are shown in Figs. 77 and 78. These figures contain tracks of the driver-(or E-) wave but because of the uncertainty in the difference between flyer and driver arrival times at the plane of the original foam surface and in the E- wave speed in the foam, such tracks are rough estimates only. In Figs. 77 and 78 the treatment of foam behavior after collision of the two locked layers is also very approximate; the possibility of rebound or "bounce-off" before driver impact is not considered. (This also increases the doubt concerning the location of the E-wave arrivals.)

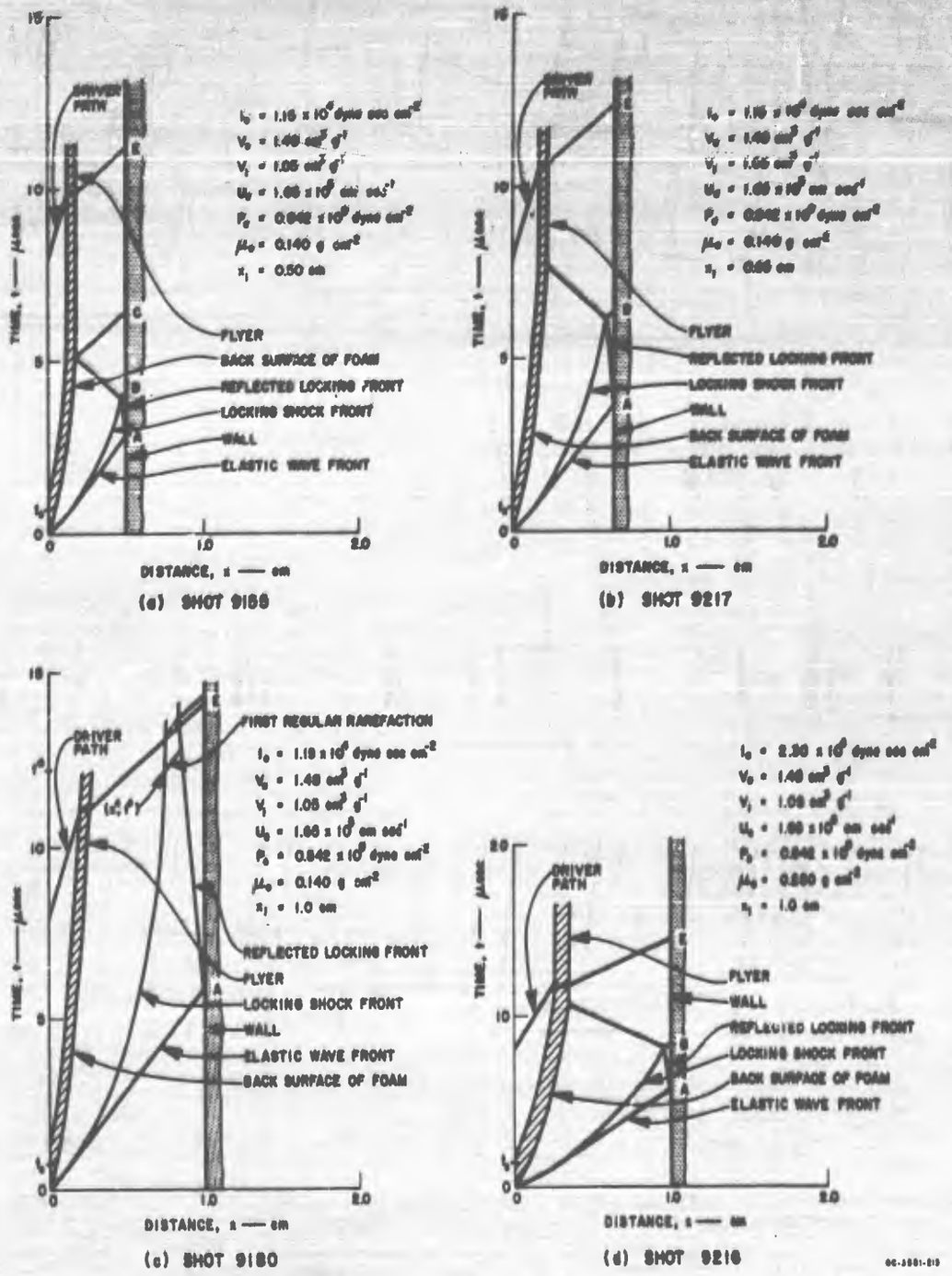

FIG. 77 CALCULATIONAL SIMULATION OF EXPERIMENTS IN 42 lb/ft^3 POLYURETHANE BY THE SIMPLE THEORY BASED ON V_1 = 1.05 cm^3/g (U)

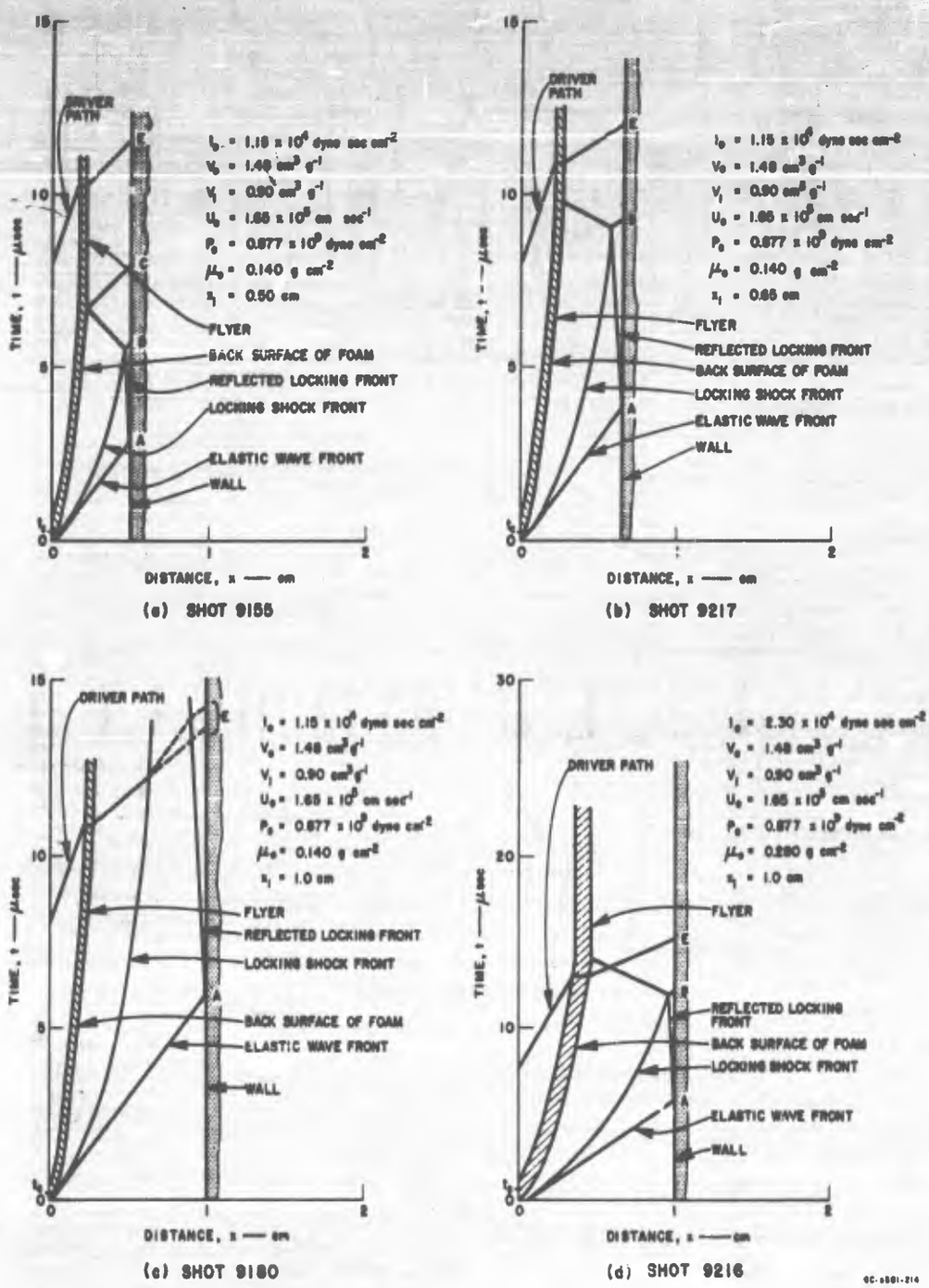

FIG. 78 CALCULATIONAL SIMULATION OF EXPERIMENTS IN 42 lb/ft^3 POLYURETHANE BY THE SIMPLE THEORY BASED ON V_1 = 0.90 cm^3/g (U)

Table X

COMPARISON OF CALCULATED AND OBSERVED TIME INTERVALS
(μsec)

	A-B	A-E
Shot 9155		
Calc. 1	1.2	8.1
Calc. 2	2.6	8.5
Observed	1.7 to 2.6	8.0
Shot 9180		
Calc. 1	B-wave stops short	8.3 to 8.5
Calc. 2	B-wave stops short	7.5 to 8.0
Observed	B-wave stops short	9.5
Shot 9216		
Calc. 1	2.6	9.8
Calc. 2	6.2	9.2
Observed	2.6 to 4.9	3.6
Shot 9217		
Calc. 1	2.7	8.7
Calc. 2	5.5	8.3
Observed	3.0 to 4.9	8.65
Calculation 1 based on $V_1 = 1.05$ cm^3 g^{-1} Calculation 2 based on $V_1 = 0.90$ cm^3 g^{-1} Other parameters: $I_0 = 1.15 \times 10^4$ dyne sec cm^{-2} except Shot 9216 when $I_0 = 2.30 \times 10^4$ $\mu_0 = 0.140$ g cm^{-2} except Shot 9216 when $\mu_0 = 0.280$ $V_0 = 1.48$ cm^3 g^{-1} $P_e = 1.0 \times 10^9$ dyne cm^{-2} $U_e = 1.65 \times 10^5$ cm sec^{-1}		
Shot 9325		
Calculated	0.80	5.3
Observed	~0.2	3.7
Shot 9345		
Calculated	4.7	4.2
Observed	4.8 to 5.7	3.3
Calculation based on values: $V_0 = 0.909$ $V_1 = 0.50$ $U_e = 0.624 \times 10^5$ $P_e = 0.485 \times 10^9$		

From Figs. 77 and 78 and from the smear photographs we have taken the data for Table X which compares observed and calculated time intervals (observed intervals are distances along the time axis of the smear record between the loci of breaks corresponding to two waves). In Fig. 77 the observed interval *A-C* during Shot 9155 corresponds to a wave speed in locked foam of about 1.5 mm/μsec but the same speed from Fig. 78 appears to be near 2.5 mm/μsec. Since the pressure behind the driver wave must be very high, we have used the speed 2.5 mm/μsec to plot *E*-wave trajectories in the figures.

When V_1 = 1.05 and 0.90 $cm^3\ g^{-1}$, final strain is 29 and 39%, respectively. These values of V_1 suggest that the explosively-induced compression may take appreciable time.

Shock heating of the foam would tend to prevent collapse to a density expected at the same stress reached statically. Our static measurements do show a final strain above 39% at stresses much less than the 3 kb achieved in the shock, but uncertainty in the calculated simulation of shock behavior forbids conclusions concerning the magnitude of shock heating.

The calculations also yield values of stress P_1 and particle speed u_1 in the locking (or B-) wave just before impact with the right-hand locked layer in the simulations of Shots 9155, 9217 and 9216. For the foam characteristics used in Fig. 78, for the target thickness of Shot 9155 and for the input momentum $I_0 = 1.15 \times 10^4$, these values are $P_1 = 1.2 \times 10^9$ (dyne-sec/cm^2) and $u_1 = 0.21 \times 10^9$ cm sec^{-1}. If we consider the shock Hugoniot of locked polyurethane to be a straight line of slope

$$\frac{P_1}{V_1} = \frac{2.5 \times 10^5}{0.90} = 2.77 \times 10^5 \text{ gm cm}^{-2}\text{sec}^{-1}$$

then the stress transmitted to the anvil by the main wave in the foam should be 7.1 kb or the stress difference between A- and B-waves in the anvil should be 6.1 kb. We observe a wave of about half this strength (Table IV).

Similar computations for Shots 9217 and 9216 predict stress jumps in the B-wave in the anvil of 3.3 and 5.4 kb, respectively. Again measured values are smaller, *i.e.*, 1.0 and 3.0 kb, respectively (Table IV).

We have no measurements of elastic speed in silicia foam comparable to those made in the 39 lb/ft^3 polyurethane by the optical lever. Inferences of this speed based on sound velocity and on the compression curve are at sharp variance with each other (Fig. 70). If we choose sound speed, *i.e.*, let $U_e = 1.35 \times 10^5$ cm/sec and take anvil stress of the elastic wave $P_e = 0.65$ kb (Fig. 53), we can get fair agreement between the prediction and observation (Shots 9325 and 9345) of the A-B wave interval when $V_1 = 0.50$ cm^3/g, *i.e.*, if we assume about 45% final strain (Fig. 41).

This is more ultimate strain than seems likely from Fig. 70 although the value of P_e corresponding to these choices (8900 psi) is reasonable. However, predicted *A-E* intervals are so far in error we are led to try the elastic speed based on the slope of compression curve (Fig. 70), 0.624×10^5 cm/sec; this choice is more successful as can be seen in Fig. 79, a plot of the predicted trajectories for the case $U_e = 0.624 \times 10^5$ cm/sec and $V_1 = 0.50$ cm^3/g, and in Table X. Figure 80 is the prediction for the case $U_e = 1.35 \times 10^5$ cm/sec for comparison.

The simple theory based on $V_1 = 0.50$ cm^3/g and $U_e = 0.624 \times 10^5$ cm/sec requires a shock wave speed in locked silica foam of about 1.0×10^5 cm/sec to predict the observed value of *B*-wave strength in the anvil during Shot 9345.

The electronic measurements read from the raster oscilloscope seem to make little contribution to our understanding of wave speeds in foam. As pointed out earlier they do, however, confirm the value of flyer speed measured optically.

For Shots 9325 and 9345, both in 1.1 g/cm^3 silica foam, transit times of the disturbances which activated the two switches on opposite foam faces were 2.40 and 2.98 μsec, respectively; average speeds were then 1.73 and 1.54 mm/μsec, respectively. The actual *E*-wave appeared much too soon for these switch closures to be due to any of the wave motions we have discussed.

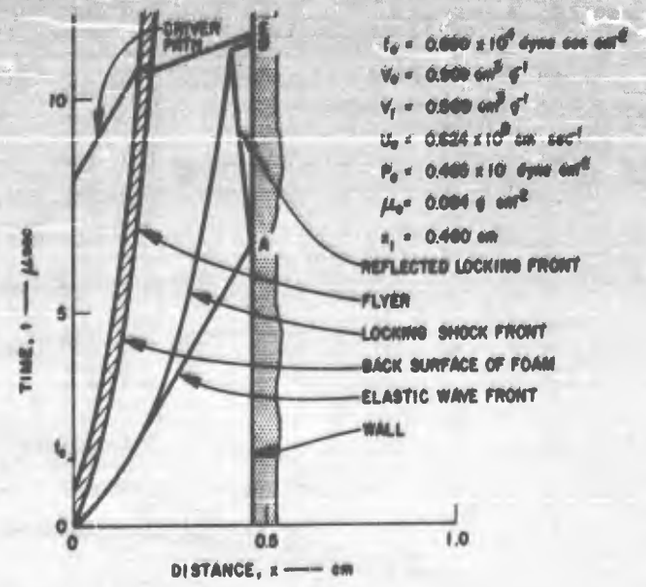

(a) SHOT 9345

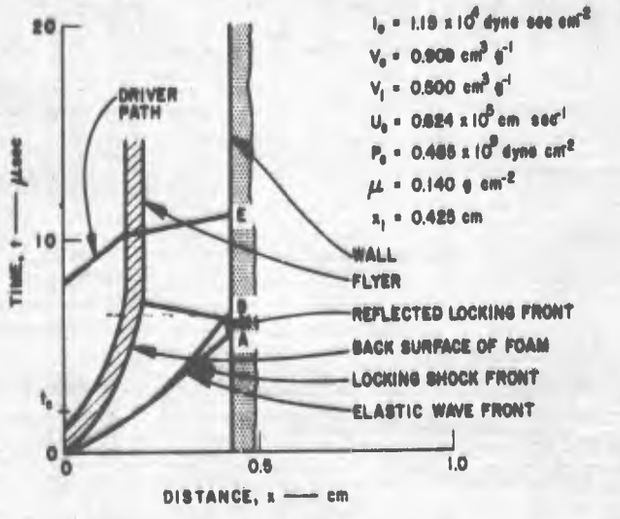

(b) SHOT 9325

FIG. 79 CALCULATIONAL SIMULATION OF EXPERIMENTS IN 1.1 g/cm^3 SILICA BY THE SIMPLE THEORY BASED ON ELASTIC SPEED AS DEDUCED FROM COMPRESSION CURVE (U)

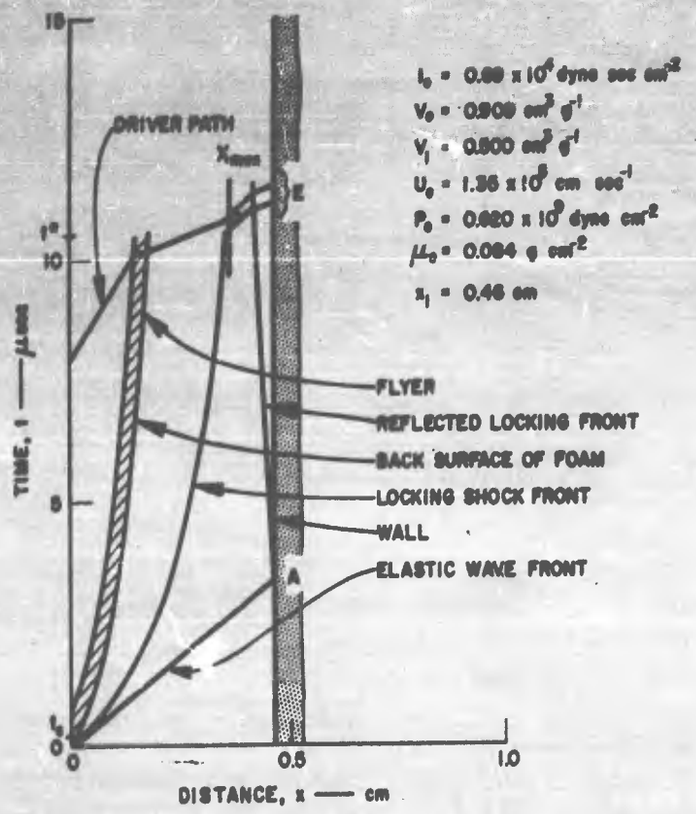

(a) SHOT 9345

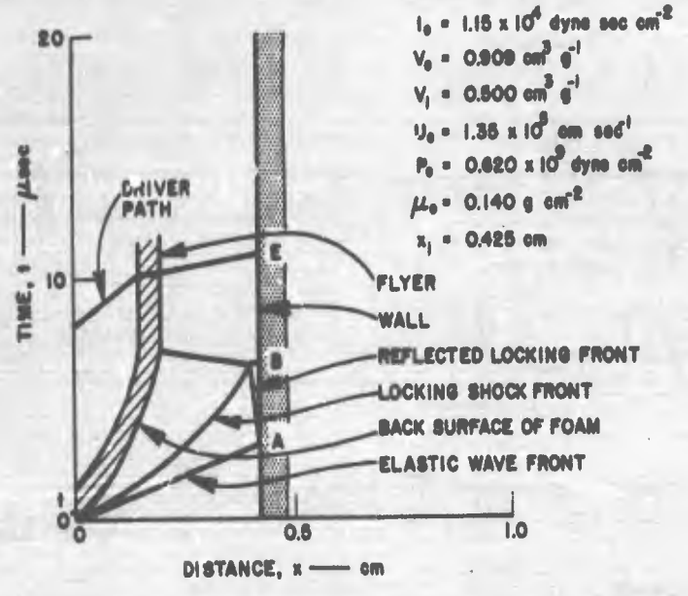

(b) SHOT 9325

FIG. 80 CALCULATIONAL SIMULATION OF EXPERIMENTS IN 1.1 g/cm³ SILICA BY THE SIMPLE THEORY BASED ON ELASTIC SPEED EQUATED TO SOUND SPEED (U)

VII APPLICATION OF THE METHOD OF ARTIFICIAL VISCOSITY

Von Neumann[1] and Richtmyer[2] have given a numerical method for closely approximating flow in and through shock waves and avoiding discontinuities. They write the Lagrangian hydrodynamic equations in difference form and add to the pressure a pseudo-viscous term

$$q(x,t) = \frac{l^2}{V}\left(\frac{\partial u}{\partial x}\right)^2 \quad \text{if} \quad \frac{\partial u}{\partial x} < 0$$

$$= 0 \quad \text{if} \quad \frac{\partial u}{\partial x} \geq 0$$

where l is an adjustable constant; V is specific volume; $u(x,t)$, particle speed; and x and t the Lagrangian spatial and time coordinates, respectively. Quantity q is insignificant over most of the flow region but has the effect of producing a gradual instead of discontinuous change of the flow parameters through regions where shocks would be expected to appear.

We have adapted this technique to the collision of two flat plates by choosing the proper boundary and initial conditions and also provided for an immovable wall to simulate the anvil. The equation of state we use for polyurethane foam is a pressure-volume relation of the form discussed earlier (*cf.* Fig. 72) except the locked material is no longer considered to be rigid but to obey an equation of state of the form:

$$P = \frac{a^2(V_1' - V)}{[b(V - V_1') + V_1']^2}$$

and V_1', a and b are constants. V_1' is slightly larger than V_1 and represents the specific volume of the locked material when relieved to zero stress.

VIII CONCLUSIONS AND RECOMMENDATIONS

Although more study is needed to confirm our conclusion for arbitrary examples of foam loading, we believe that the simple theory with the static compression curve will probably be capable of broadly classifying foams on the basis of countermeasure effectiveness. It is quite clearly not able to predict accurately maximum pressures or impulses in the face of change of wave shape or attenuation of the elastic wave, which seem to be common phenomena in thick samples, and in any case its use for accurate prediction is complicated by the ambiguities of choosing the elastic limit and the locked density.

The simple theory may, however, help our understanding of foam behavior. For example, we can by calculation match the observed wave intervals in 40 lb/ft^3 polyurethane by adjusting the value of final specific volume, V_1, over a small range. Perhaps this adjustment has a real counterpart within the shock wave. The seeming failure of the theory to foretell the main wave strength may be misleading since the equation of state of the locked foam is not known. For example, we could interpret the A-C interval of Shot 9155 to imply a shock speed in compacted material of 1.5 mm/μsec, (instead of 2.5 mm/μsec) which would lead to a second shock strength of nearly the observed value.

We believe that the value of elastic speed to be used in an accurate calculational simulation can come only from separate measurements during actual shock loading. Acoustic speed or the velocity deduced from static compression may be a good first estimate, but neither is necessarily the same as the speed of the forerunner stimulated by impact. If forced to choose one or the other though, we would at the present use the deduced quantity. Our attempt to measure this speed with electronic devices has not succeeded; optical methods should be more successful because arrival times and strengths can be observed simultaneously and the identity of the wave producing the signal made certain.

Static compression of foams provides reliable limits between which the forerunning wave strength will be found. We saw good evidence of decay of this strength in one experiment (Shot 9432) when the distance

travelled by the *A*-wave in 39 lb/ft^3 polyurethane foam was unusually long (greater than one inch). The existence of an elastic speed lower than sound speed for this material appears to provide a simple mechanism for attenuation of the forerunner, however.

Final strain reached through a shock may not be as great as that achieved slowly during compression tests. The arguments for this conclusion (presented mainly in Figs. 77 and 78) are not decisive partly because of uncertainties in the values of experimental parameters (such as I_o, P_o, and V_o), but mainly because they assume model foam behavior which has not been confirmed. However, the fact of increasing rise-time with increasing distance travelled is well established for the *A*-front and probably for the *B*-disturbance as well. Certainly the time needed to collapse the cells, neglected completely by the simple theory, is a very important element of any detailed description of shocks in foam.

Of the distended materials tested, 40 lb/ft^3 polyurethane can reduce the pressure delivered to an enclosed structure by an impulse in the neighborhood of 10^4 dyne-sec/cm^2 to 1 kb with the least weight (about 0.5 g/cm^2) of added material. Twice this weight in silica may reduce peak transmitted pressure to 0.6 kb.

Behavior of the 0.75 g/cm^3 open cell aluminum foam is strange but the material is promising as a countermeasure and merits further study.

If observation time in the anvil mirror were doubled, present experimental techniques would probably be adequate for such further study of shock loading of foams, although the lack of flyer planarity is a serious hindrance to increased accuracy. More effective use could probably be made of the simple two-dimensional method (as illustrated in Fig. 4) for rapid exploration of foam properties than has been during the present effort. When all wave speeds in the foam are much less than explosive detonation speeds, we can with this method easily find *A*-wave strength and with a series of such experiments find the minimum foam thickness needed to suppress the *B*-wave.

REFERENCES

1. Fowles, G. R. and D. R. Curran, AFSWC-TDR-62-22, 1962.
2. *Ibid.*, p. 31.
3. Fowles, G. R., *J. Appl. Phys.*, 32, 1475 (1961).
4. Fowles, G. R. and D. R. Curran, *op. cit.*, pp. 58-64.
5. Pressman, Z., Poulter Labs. Tech. Rpt. 009-60, Stanford Research Institute, Menlo Park, California.
6. Bancroft, D., E. L. Peterson, and S. Minshall, *J. Appl. Phys.*, 27, 291 (1956).
7. Fowles, G. R. and D. R. Curran, *op. cit.*, pp. 51-53.
8. *Ibid.*, pp. 66-67.
9. Ewing, W. M., W. S. Jardetzky, and F. Press, *Elastic Waves in Layered Media*, McGraw-Hill, Inc., N.Y., 1957, p. 15.
10. Fowles, G. R. and D. R. Curran, *op. cit.*, pp. 22-44.
11. Von Neuman, J. and R. D. Richtmyer, *J. Appl. Phys.*, 21, 232 (1950).
12. Richtmyer, R. D., *Difference Methods for Initial-Value Problems*, Interscience Publishers, Inc., N.Y., 1957, especially Sections 9 through 12, Chap. X.

DISTRIBUTION

No. cys

HEADQUARTERS USAF

1 Hq USAF (AFRDP), Wash, DC 20546
1 Hq USAF (AFRST), Wash, DC 20546
1 Hq USAF (AFRNE-B), Wash, DC 20546
1 Hq USAF (AFTAC), Wash, DC 20546
1 AFOAR (RROSP, Lt Col Atkinson), Bldg T-D, Wash, DC 20333
1 AFOSR, Bldg T-D, Wash, DC 20333

MAJOR AIR COMMANDS

AFSC, Andrews AFB, Wash 25, DC
1 (SCT)
1 (SCT-2)
1 (SCLT, Col P. F. English)

SAC, Offutt AFB, Nebr
1 (OA, Dr. E. A. Jackson)
1 (OAWS)
1 AUL, Maxwell AFB, Ala 36112
1 USAFIT (Usaf Institute of Technology), Wright-Patterson AFB, Ohio 45433

AFSC ORGANIZATIONS

ASD, Wright-Patterson AFB, Ohio 45433
1 (ASNXRR)
1 (ASRMDS-1), ATTN: Mr. Janik
1 (ASRCMC, Capt Wilson)
1 RTD (RTN-W, Maj Munyon), Bolling AFB, Wash 25, DC
1 BSD (BSR), Norton AFB, Calif
1 SSD (SSTR), AF Unit Post Office, Los Angeles 45, Calif
1 RADC (Document Library), Griffiss AFB, NY 13442

KIRTLAND AFB ORGANIZATIONS

1 AFSWC (SWEH), Kirtland AFB, NM 87117

AFWL, Kirtland AFB, NM 87117
1 (WLRS)
1 (WLA)
1 (WLAV)

DISTRIBUTION (cont'd)

No. cys	
	AFWL, Kirtland AFB, NM (continued)
1	(WLRPT, Capt Atkins)
1	(WLRPT, Capt Niles)
1	(WLRPA, Lt Mauldin)
20	(WLL)
	OTHER AIR FORCE AGENCIES
	Director, USAF Project RAND, via: Air Force Liaison Office, The RAND Corporation, 1700 Main Street, Santa Monica, Calif
1	(RAND Library)
1	(Dr. Olen Nance)
1	(Mr. Jack Whitener)
	ARMY ACTIVITIES
1	US Army Materiel Command, Harry Diamond Laboratories, (ORDTL 06.33, Technical Library), Wash 25, DC
1	Commandant, US Army Ordnance School, ATTN: Dr. Coy Glass, Aberdeen Proving Ground, Md
	Commanding Officer, Picatinny Arsenal, Samuel Feltman Ammunition Laboratories, Dover, NJ
1	(SMVPA-VA6)
1	(Mr. Murray Wienstien)
1	Director, Army Research Office, Arlington Hall Sta, Arlington, Va
1	Director, US Army Engineer Research & Development Laboratories, ATTN: Tech Documents Center, Ft Belvoir, Va
	NAVY ACTIVITIES
1	Chief of Naval Research, Department of the Navy, Wash 25, DC
1	Commander, Naval Ordnance Laboratory, ATTN: Dr. Rudlin, White Oak, Silver Spring, Md
1	Director, Special Projects, Department of the Navy, Wash 25, DC
1	Office of Naval Research, Wash 25, DC
	OTHER DOD ACTIVITIES
1	Chief, Defense Atomic Support Agency, ATTN: Lt Col Singer, Wash 25, DC

DISTRIBUTION (cont'd)

No. cys	
1	Director, Weapon Systems Evaluation Group, Room 1D-847, The Pentagon, Wash 25, DC
1	Director, Advanced Research Projects Agency, Department of Defense, The Pentagon, Wash 25, DC
1	Office, Director of Defense Research & Engineering, The Pentagon, Wash 25, DC
20	Hq Defense Documentation Center for Scientific and Technical Information (DDC), Cameron Sta, Alexandria, Va 22314
	AEC ACTIVITIES
2	Sandia Corporation (Info Distribution Div), Sandia Base, NM 87115
1	Sandia Corporation (Technical Library), P.O. Box 969, Livermore, Calif
2	University of California Lawrence Radiation Laboratory (Tech Info Div), P.O. Box 808, Livermore, Calif
2	Director, Los Alamos Scientific Laboratory (Helen Redman, Report Library), P.O. Box 1663, Los Alamos, NM 87554
1	Brookhaven National Laboratory, Upton, Long Island, NY
1	Argonne National Laboratory (Tech Library), Argonne, Ill 60440
1	Oak Ridge National Laboratory (Tech Library), Oak Ridge, Tenn
	OTHER
1	OTS, Department of Commerce, Wash 25, DC
1	Institute for Defense Analysis, Room 2B257, The Pentagon, Wash 25, DC THRU: ARPA
1	Battelle Memorial Institute, 505 King Avenue, Columbus, Ohio
1	University of Michigan, Institute of Science and Technology, ATTN: BAMIRAC Library, P.O. Box 618, Ann Arbor, Mich
1	General Electric Company - MSD, ATTN: Dr. F. A. Lucy, Rm M9505, P.O. Box 8555, Philadelphia 1, Pa
	Aerospace Corporation, P.O. Box 95085, Los Angeles 45, Calif
1	(Dr. Domenic Bitondo)
1	(Dr. George Welch)
1	(Dr. Robert Cooper)
1	(Mr. H. C. Sullivan)

DISTRIBUTION (cont'd)

No. cys	
1	Physics International, 2229 4th Street, Berkeley 10, Calif
1	AVCO Corporation, Research and Advanced Development, ATTN: Dr. D. T. Morgan, 201 Lowell Street, Wilmington, Mass
1	Kaman Aircraft Corporation, Nuclear Division, ATTN: Dr. David Williams, Colorado Springs, Colo
1	Philco Corporation, Aeronutronic Division, ATTN: Dr. R. G. Allen, Ford Road, Newport Beach, Calif
1	E. H. Plesset Associates, Inc., ATTN: Dr. Harris Mayer, Union Bank Bldg., 2444 Wilshire Blvd., Santa Monica, Calif
	Stanford Research Institute, Menlo Park, Calif
1	(ATTN: Dr. Duvall)
1	(ATTN: Dr. Fowles)
1	Space Technology Labs, ATTN: Dr. Herman Lear and Mr. Jackson Maxey, P.O. Box 95001, Los Angeles 45, Calif
1	General Electric Company, Re-entry Systems Department, ATTN: A. Clark, 3198 Chestnut Street, Philadelphia 1, Pa
1	Lockheed Missile and Space Company, ATTN: Department 81-92, W. Rous, Sunnyvale, Calif
1	National Carbon Company, Division of Union Carbide, ATTN: Mr. D. C. Hiler, P.O. Box 500, Lawrencebury, Tenn
1	Official Record Copy (Lt Mauldin, WLRPA)

UNCLASSIFIED